The regulation of Rab13 in endosomal trafficking

Maria Stephanie Ioannou

The Integrated Program in Neuroscience
Montreal Neurological Institute
McGill University

Montréal, February, 2016

A thesis submitted to McGill University in
partial fulfillment of the requirements of the degree of
Doctor of Philosophy in Neurological Science

ABSTRACT

Rab GTPases are critical regulators of membrane trafficking and not surprisingly defects in Rabs contribute to various human diseases. For example, Rab13 is associated with several phenotypes associated with cancer, but the regulation of Rab13 in membrane trafficking is poorly understood. The general objective of this doctoral research was to study the function and regulation of Rab13 in endosomal trafficking. Rabs cycle between an active GTP-bound form and an inactive GDP-bound form. Upon activation by guanine nucleotide exchange factors, Rabs associate with membranes where they recruit effector molecules to mediate their downstream response. However, the spatio-temporal activation of Rab13 was unknown. Furthermore, the DENN-domain is an evolutionarily conserved protein module that functions enzymatically as guanine nucleotide exchange factors for Rabs. Here, we identified the DENN containing protein DENND2B as guanine nucleotide exchange factor for Rab13 and uncover a mechanism whereby activation of Rab13 by DENND2B in a complex with the Rab13 effector MICAL-L2 at the cell periphery drives cancer cell migration, invasion, and tumor metastasis. Furthermore, active Rabs typically anchor to membranes using a hydrophobic prenyl modification and dissociate from membranes upon inactivation. Here we discovered that Rab13 traffics on vesicles in its inactive form as part of a protein complex independent of prenylation. Therefore, in this doctoral thesis we have provided a detailed characterization of the regulation of Rab13 in endosomal trafficking.

RÉSUMÉ

Les protéines de type Rab GTPases sont des régulateurs essentiels dans le trafic intracellulaire membranaire. Il n'est donc pas surprenant de constater que leur mauvais fonctionnement puisse causer différentes pathologies chez l`humain. À titre d'exemple, Rab13 est associée à plusieurs phénotypes observés dans les cancers mais son fonctionnement dans le trafic cellulaire n'est toujours pas élucidé. L'objectif de cette thèse de doctorat était de mettre en lumière la fonction et la régulation de Rab13 dans le trafic endosomal. Les protéines de type Rab oscillent entre une forme active liée au nucléotide GTP et une forme inactive liée au nucléotide GDP. Après avoir été activées par les facteurs d'échange du nucléotide guanine, les Rabs s'associent aux membranes d'où elles recrutent d'autres molécules effectrices afin d'initier leur réponse cellulaire. Toutefois, la réponse spatio-temporelle de Rab13 était jusqu'à maintenant inconnue. Nous avons découvert la protéine DENND2B comme étant le facteur d'échange guanidique pour Rab13. De plus, nous également révélé un mécanisme d'activation par lequel Rab13 et DENND2B en complexe protéique avec la protéine MICAL-L2 favorise la migration des cellules cancéreuses, l'invasion et le processus métastatique. De plus, les formes actives des protéines Rabs se lient aux membranes par leur modification hydrophique de type prénylique pour ensuite s'en dissocier lors de leur inactivation. Nos travaux démontrent que Rab13 trafique sur les vésicules membranaires dans leur forme inactive de façon non-tributaire de la prénylation. Cette thèse de doctorat nous a donc permis de mettre en lumière un mécanisme clair et détaillé concernant la régulation de la protéine Rab13 dans le trafic endosomal.

ACKNOWLEDGEMENTS

First and foremost I would like to thank my supervisor, Dr. Peter McPherson. While surfing the internet instead of writing this very thesis, I stumbled across a quote that could not be more fitting. “Don’t pick a job. Pick a Boss. Your first boss is the biggest factor in your career success. A boss who doesn’t trust you won’t give you opportunities to grow” (William Raduchel). Peter, you have provided me with an endless number of opportunities to develop as a scientist. You challenged me to grow yet you were patient when I needed it. You have equipped me with the skills to be a successful scientist and I will forever be grateful.

To the members of my committee, Dr. Heidi McBride and Dr. Keith Murai, thanks for your helpful insight and guidance and sticking with me throughout my entire PhD. Thank you for the additional mentorship from Thomas Stroh and Hiroshi Tsuda. And thank you to Louis Hodgson for providing me with a unique training opportunity in New York that was not only successful but lots of fun!

A special thanks to Andrea L. Marat and Martine Girard for supporting me not only scientifically when I didn’t understand my results, but with all of my personal struggles as well. Thank you to my fellow labmates both past and present; Jacynthe, Maryam, Jason, Jie, Andrea S., Nadya, Brigitte, Hatem, Patrick, Mathilde, Gopinath, Chanshuai, Vincent, Mark and Carl as well as my friends from the Fon lab GG, Matt and Tom and the one and only Ravitar, we certainly had some fun and I will miss you all. Thank you to my parents for supporting and always encouraging me. Lastly, to Jesse, thank you for all of your patience and support, and thank you setting the bar so high, you inspire me to be a better scientist.

DEDICATION

I dedicate this thesis to my late παππού Christopher Laoumzis. You moved our family to Canada for a better life because of your friendship with a Canadian doctor named Wilder Penfield. How serendipitous it is that I am now getting a doctorate degree from the very institute that he founded and directed.

LIST OF ABBREVIATIONS

ΔC	C-terminal deletion
ACAP2	ankyrin repeat and PH domain 2
ACC	adrenocortical carcinoma
AF	alexafluor
ANOVA	analysis of variance
AP2	adaptor protein 2
APC	adenomatous polyposis coli
Arf	ADP-ribosylation factor
AS160	Akt substrate 160
ATP	adenosine-5'-triphosphate
BROAD	The Broad Institute
c-abl	c-Abelson murine leukemia
CCLE	cancer cell line encyclopedia
CD1	connecdenn1 (DENND1A)
CD3	connecdenn3 (DENND1C)
cp	circular permutation
CRIB	Cdc42/Rac1 interactive binding domain
DENN	differentially expressed in normal and neoplastic cells
EEA1	early endosomal antigen 1
EGF	epidermal growth factor
EGFR	epidermal growth factor receptor
EmGFP	emerald green fluorescent protein
ER	endoplasmic reticulum
ERK	extracellular-signal-regulated kinase
FL	full length
FRET	Förster resonance energy transfer
GAP	GTPase-activating protein
GDI	GDP dissociation inhibitor
GDP	guanosine-5'-diphosphate
GFP	green fluorescent protein
GBM	glioblastoma multiforme
GDP	guanosine triphosphate
GDF	GDI-displacement factors
GTP	guanosine-5'-triphosphate
GTPγS	guanosine 5'-3-*O*-(thio)triphosphate
GEF	guanine-nucleotide exchange factor
GLUT4	glucose transporter type 4
Grb2	growth factor receptor-bound protein 2
GST	glutathione *S*-transferase
GTP	guanosine triphosphate
H&E	Hematoxylin and eosin stain
Hsc70	heat shock cognate 70 kDa protein
HVD	hypervariable domain
LFA-1	lymphocyte function-associated antigen 1
MADD	MAP-kinase activating death domain protein
mCer3	monomeric Cerulean3

mCh	monomeric Cherry
mVen	monomeric Venus
MDCK	Madin-Darby canine kidney
MEF	mouse embryonic fibroblasts
MICAL-L1	molecule interacting with CasL 1-like1
MICAL-L2	molecule interacting with CasL 1-like2
MICH	Michigan
MSKCC	Memorial Sloan Kettering Cancer Center
Mst1	mammalian Ste20-like 1
N-term	N-terminal
OCRL	oculocerebrorenal syndrome of Lowe
PAK	p21-activated kinase
pap	papillary cell carcinoma.
PFA	paraformaldehyde
PI(3)P	phosphatidylinositol-3-phosphate
PI(4)P	phosphatidylinositol-4-phosphate
$PI(3,4)P_2$	phosphatidylinositol-3,4-biphosphate
PKA	protein kinase A
PKC	protein kinase C
PKD	protein kinase D
Rab	Ras-related in brain
RBD	Rab binding domain
REP	Rab escort protein
RFP	red fluorescent protein
RGGT	Rab geranylgeranyl transferase
RME	receptor-mediated endocytosis
SD	standard deviation
SEM	standard error of the mean
SM	starting material
SNARE	soluble N-ethylmaleimide-sensitive factor attachment protein receptor
ST5	Suppression of Tumorigenicity 5
squ	squamous cell carcinoma
TBC	Tre-2/Bub2/Cdc16
TCGA	The Cancer Genome Atlas
TGN	trans-Golgi network
TPA	12-O-tetradecanoylphorbol-13-acetate
TRAPP	transport protein particle
VASP	vasodilator-stimulated phosphoprotein
VEGF	vascular endothelial growth factor
VEGFR	vascular endothelial growth factor receptor
WT	wild type
YIP	Ypt-interacting proteins

TABLE OF CONTENTS

Abstract 2
Acknowledgements and dedications 4
Abbreviations 6
Table of contents 8
List of figures and tables 10
Author contributions 11

CHAPTER 1.1: INTRODUCTION TO RAB GTPASES 13
1.1.1 Endosomal trafficking 13
1.1.2 Rab GTPases 13
1.1.3 Rab structure 15
1.1.4 Rab post-translational modifications 16
1.1.5 Rab activation by GEFs 18
1.1.6 The DENN domain 20
1.1.7 DENN domain structure 21
1.1.8 Rab deactivation by GAPs 22
1.1.9 TBC domain structure 23
1.1.10 Effectors 23
1.1.11 Targeting Rabs 25
1.1.12 Rab cascades 27

CHAPTER 1.2: RAB13 AND THE REGULATION OF CANCER CELL BEHAVIOR 30
1.2.1 Introduction to Rab13 31
1.2.2 The biology of Rab13 31
1.2.3 Regulation of Rab13 expression 33
1.2.4 Rab13 in cell metabolism 35
1.2.5 Rab13 in cell proliferation 36
1.2.6 Rab13 in cell-cell adhesion 37
1.2.7 Rab13 in cell migration and scattering 39
1.2.8 Rab13 in cell migration and angiogenesis 42
1.2.9 Conclusions 43
1.2.10 Figure 44

Preface to Chapter 2 49
CHAPTER 2: DENND2B ACTIVATES RAB13 AT THE LEADING EDGE OF MIGRATING CELLS AND PROMOTES METASTATIC BEHAVIOR 50
2.1 Abstract 51
2.2 Introduction 51
2.3 Results 54
2.4 Discussion 63
2.5 Tables and figures 69
2.6 Supplemental figures 87
2.7 Supplemental videos 95
2.8 Materials and methods 97
2.9 Supplemental table 111
2.10 Acknowledgements for Chapter 2 113

Preface to Chapter 3 114
CHAPTER 3: RAB13 TRAFFICS ON VESICLES INDEPENDENT OF PRENYLATION 115
3.1 Abstract 116
3.2 Introduction 116
3.3 Materials and methods 117
3.4 Results and discussion 121
3.5 Tables and figures 130
3.6 Acknowledgements for Chapter 3 146

CHAPTER 4: DISCUSSION AND GENERAL CONCLUSIONS 147
4.1 Summary of original contributions to scientific knowledge 147
4.2 Discussion 149
4.2.1 Rab13 in exocytosis 149
4.2.2 Rab13 in trafficking cascades 152
4.2.3 Rab13 in cell proliferation 153
4.2.4 Rab13 in neuronal function 155
4.2.5 Cycling inactive Rab13 on membranes 156
4.3 General conclusions 158
4.4 Figures 160

REFENCES 162

LIST OF FIGURES AND TABLES

List of Figures

Figure 1.1 Amplification of Rab13 in human cancers 44
Figure 1.2 Rab13 levels correlate with poor patient prognosis 45
Figure 1.3 Rab13 promotes GLUT4 recycling in response to insulin 46
Figure 1.4 Rab13 regulates tight junction disassembly 47
Figure 1.5 Rab13 promotes integrin recycling to enhance cell migration 48
Figure 2.1 DENND2B is a GEF for Rab13 69
Figure 2.2 Rab13 and DENND2B promote epithelial cell invasion 71
Figure 2.3 Rab13 co-localizes with DENND2B at the cell's leading edge 73
Figure 2.4 Active Rab13 accumulates at the cell's leading edge 75
Figure 2.5 Rab13 activation occurs at the leading edge of migrating cells 76
Figure 2.6 DENND2B C-terminal region is required for the morphological transformation of MCF10A cells 78
Figure 2.7 DENND2B C-term interacts with MICAL-L2 79
Figure 2.8 Rab13 knockdown reduces migration of breast cancer cells 81
Figure 2.9 Rab13 knockdown reduces invasiveness and growth of breast cancer cells 83
Figure 2.10 Rab13 knockdown reduces tumor growth and migration *in vivo* 85
Supplemental Figure 2.1 DENND2B binds Rab13 87
Supplemental Figure 2.2 Rab13 and DENND2B promote epithelial cell invasion 88
Supplemental Figure 2.3 Optimization and validation of a Rab13 biosensor 90
Supplemental Figure 2.4 Rab13 knockdown limits growth and metastasis of tumors *in vivo* 93
Figure 3.1 Inactive Rab13 traffics on vesicles 131
Figure 3.2 Rab13 is found on vesicles with multiple endosomal origins 133
Figure 3.3 Rab13 resists membrane extraction by GDI 135
Figure 3.4 Inactive Rab13 traffics on vesicles following deletion of the prenylation motif 137
Figure 3.5 Rab13 associates with membranes via protein-protein interactions in cells 139
Figure 3.6 Rab13 associates with membranes via protein-protein interactions in tissue 142
Figure 3.7 Rab13 associates in a protein complex independent of nucleotide status 144
Figure 4.1 Rab13 is activated locally at the plasma membrane 160
Supplemental Figure 4.1 DENND2B activates Rab13 to induce neurite outgrowth in PC12 cells 161

List of Videos

Video 2.1. Active Rab13 drives MCF10A cell invasion into collagen matrix 95
Video 2.2. Wild-type Rab13 traffics on vesicles to the cell periphery and accumulates on the plasma membrane 95
Video 2.3. Vesicles carrying wild-type Rab13 fuse with the plasma membrane 95
Video 2.4. Active Rab13 traffics on vesicles to the cell periphery and accumulates on the plasma membrane at the leading edge of a migrating cell 96
Video 2.5. Inactive Rab13 traffics on vesicles to the cell periphery but does not appear on the plasma membrane 96
Video 2.6. Rab13 is activated at the leading edge during cell migration 96

List of Tables

Supplemental Table 2.1: Oligonucleotides used in Chapter 2 111
Supplemental Table 3.1: Oligonucleotides used in Chapter 3 130

AUTHOR CONTRIBUTIONS

Chapter 1:

Rab13 and the Regulation of Cancer Cell Behavior

Maria S. Ioannou[1] and Peter S. McPherson[1]
[1]Department of Neurology and Neurosurgery, Montreal Neurological Institute, McGill University, Montreal, Quebec H3A 2B4, Canada

Modified from ©Ioannou & McPherson, 2016.
Originally published in The Journal of Biological Chemistry
doi: 10.1074/jbc.R116.715193

MSI Wrote the manuscript and made all the figures.
PSM Wrote the manuscript

Chapter 2:

DENND2B activates Rab13 at the leading edge of migrating cells and promotes metastatic behavior

Maria S. Ioannou[1], Emily S. Bell[2], Martine Girard[1], Mathilde Chaineau[1], Jason N.R. Hamlin[1], Mark Daubaras[1], Anie Monast[2], Morag Park[2], Louis Hodgson[3], Peter S. McPherson[1]
[1]Department of Neurology and Neurosurgery, Montreal Neurological Institute, McGill University, Montreal, Quebec H3A 2B4, Canada, [2]Department of Biochemistry, Goodman Cancer Centre, McGill University, Montreal, Quebec H3G 0B1, Canada, [3]Department of Anatomy and Structural Biology, Gruss-Lipper Biophotonics Center, Albert Einstein College of Medicine, New York, NY, 10461 USA

©Ioannou et al., 2015.
Originally published in The Journal of Cell Biology.
doi 10.1083/jcb.201407068.

MSI Designed all the experiments, performed experiments (related to Figure 2.1 D-I, Figure 2.2 A-C and G-H, Figure 2.3 A-G, Figure 2.4 A-C, Figure 2.5 A, E and F, Figure2.6 A-D, Figure 2.7 A-B and D-F, Figure 2.8 A-F, Figure 2.9 A-D, Figure 2.10 D-E, Supplemental Figure 2.2 B-E, Supplemental Figure 2.3 H and J, Supplemental Figure 2.5 and Videos 2.1-2.6) and wrote the manuscript.
EB Designed the experiments, performed experiments (Figure 2.2 D-F, Figure 2.9 E and F, Figure 2.10 A-D, F and G and Video 2.1) and helped write sections of the manuscript related to cancer cell proliferation and in vivo mouse model of cancer.
MG Performed experiments (Figure 2.1 A-C and Supplemental Figure 2.1 A-B)
MC Produced valuable reagents for the experiments and gave helpful advice on the project.
JH Performed experiments (Figure 2.7 C and Supplemental Figure 2.2 A)
MD Produced reagents valuable for the experiments.
AM Performed experiments related to in vivo mouse model of cancer (Figure 2.10 A-D, F and G, Supplemental Figure 2.4)
MP Designed the experiments related to in vivo mouse model of cancer.
LH Designed the experiments, performed experiments (Figure 2.5 B-D and Supplemental Figure 2.3 A-G and J) and helped write sections of the manuscript related to the FRET-based Rab13 biosensor.
PSM Designed all the experiments and wrote the manuscript.

Chapter 3:

Rab13 traffics on vesicles independent of prenylation

Maria S. Ioannou, Martine Girard, & Peter S. McPherson
Department of Neurology and Neurosurgery, Montreal Neurological Institute, McGill University, Montreal, Quebec H3A 2B4, Canada

Originally published in The Journal of Biological Chemistry
doi: 10.1074/jbc.M116.722298

MSI Designed the experiments, performed experiments (all figures) and wrote the manuscript
MG Performed experiments
PSM Designed all the experiments and wrote the manuscript.

1.1.1 Endosomal trafficking

Eukaryotic cells are highly compartmentalized into distinct membrane bound organelles. In order for the cell to function, these organelles must communicate with each other via the transport of various lipids and proteins in a highly regulated fashion. This is often achieved by the formation of small vesicle carriers that transport material from one membrane to another, as well as the transport and fusion of entire organelles. Each step of these trafficking pathways is regulated by several proteins and lipids in order to ensure high fidelity communication between compartments in cells. The specific steps to be regulated include cargo selection, the budding and scission of vesicles from the donor membrane, assembly and disassembly of various coat proteins on the vesicles, association of vesicles with molecular motors and the cytoskeleton, tethering to the correct target membrane, and finally fusion with the acceptor membrane. In addition, mechanisms are required to ensure that each organelle retains its own unique identity and function given the high flux of material into and out of each compartment.

1.1.2 Rab GTPases

The Rab (Ras-related in brain) family of GTPases are critical regulators of membrane trafficking. In fact, they play a role in all the steps of membrane trafficking listed above. Rabs act as molecular switches to control membrane trafficking. As with other GTPases, they are activated by guanine-nucleotide exchange factors (GEFs) that interact with the GDP-bound form of the Rab and catalyze the exchange of GDP for GTP. In the active GTP-bound configuration, Rabs interact with the cytosolic face of the membrane and recruit effector molecules. Hydrolysis of GTP to GDP is catalyzed by GTPase-activating proteins (GAPs). Because GTP hydrolysis can occur in the absence

of a GAP, albeit at a slower rate, it is thought that GEFs play a more crucial role in regulating Rab GTPases (Barr and Lambright, 2010). Inactive GDP-bound Rabs dissociate from membranes and effectors, and bind to Rab GDP dissociation inhibitors (GDIs) that hold the Rab soluble and prevent re-activation until interacting with the appropriate GEF.

The Rab family of GTPases are an evolutionarily conserved family with approximately 70 members in humans. The genes for Rabs are found dispersed on different chromosomes and are present in all eukaryotes (Bock et al., 2001). The majority of yeast Rabs have one or more human homolog illustrating their importance in eukaryotic biology (Stenmark and Olkkonen, 2001;Bock et al., 2001). In mammals, the number of Rabs is thought to have expanded by gene duplication giving rise to 39 highly related (75-95% sequence identity) sub-families with overlapping functions (Bock et al., 2001;Pereira-Leal and Seabra, 2000;Moore et al., 1995). Each Rab is localized predominantly to a specific intracellular organelle or vesicle (Zerial and McBride, 2001). Several mammalian Rabs exhibit cell-type specific expression where they function in specialized trafficking pathways (Grosshans et al., 2006). Not surprisingly, functional impairment of Rabs are associated with numerous human diseases (Stenmark, 2009). For example, mutations in Rab7 cause the peripheral neuropathy Charcot-Marie Tooth disease (Verhoeven et al., 2003); accumulation of cholesterol due to impaired trafficking by Rab9 leads to Niemann-Pick type C disease (Narita et al., 2005); and altered expression of Rab25 is found in several cancer types (Agarwal et al., 2009). Moreover, several bacterial pathogens exploit Rabs in order to colonize host cells during infection (Brumell and Scidmore, 2007). For example, *Mycobacterium tuberculosis* replicates in a phagosome/early endosomal compartment. The mycobacterium containing phagosome retains Rab5 to facilitate the delivery of iron by fusion with early and recycling endosomes (Kelley and Schorey, 2004;Sturgill-Koszycki et al., 1994). However, these compartments actively exclude Rab7 preventing the

maturation of the phagosome to a late endosome and subsequent degradation (Clemens and Horwitz, 1995;Deretic et al., 1997). *Legionella pneumophila* replicates in an endoplasmic reticulum (ER) derived vacuole that avoids fusion with the default secretory pathway by recruiting the ER-to-Golgi apparatus regulator Rab1 (Brumell and Scidmore, 2007;Derre and Isberg, 2004;Derre and Isberg, 2005). Thus, the abundance of pathologies associated with impaired Rab trafficking pathways highlights their importance in cell physiology and need to better understand how Rabs function.

1.1.3 Rab Structure

Structural analysis of Rabs by X-ray crystallography shows that Rabs share a fold common to all small GTPases of the Ras superfamily (Stenmark and Olkkonen, 2001;Dumas et al., 1999;Ostermeier and Brunger, 1999;Chattopadhyay et al., 2000;Milburn et al., 1990). The fold is made up of a six-stranded β sheet (five parallel and one antiparallel) surrounded by five α helices. Rabs bind to guanine nucleotides and Mg^{2+} through five loops that connect the α helices and β strands within this fold. This Mg^{2+} ion is required for both the high affinity nucleotide binding as well as the hydrolysis of GTP. The amino acid residues that contact the bound-nucleotide and Mg^{2+} are highly conserved across the Ras superfamily (Stenmark and Olkkonen, 2001). Rabs adopt two distinct conformations depending on whether they are bound to GDP or GTP (Stroupe and Brunger, 2000). The major conformational difference is found in two regions denoted switch I and switch II (Schlichting et al., 1990;Milburn et al., 1990). A serine or threonine in switch I contacts the terminal phosphate of GTP and is coordinated by Mg^{2+} when the Rab is active. Switch II stabilizes the Mg^{2+} ion through an aspartate residue, binds the terminal phosphate via a glycine residue, and uses a glutamine residue to catalyze the intrinsic hydrolysis of the GTP (Vetter and Wittinghofer, 2001;Lee et al., 2009). These residues are highly conserved across GTPases and are often mutated to create constitutively active or inactive Rabs to study Rab functions. The catalytic glutamine is substituted

for leucine to abolish GTP hydrolysis, rendering the Rab GTP-locked. The serine/threonine can be substituted with asparagine to disrupt Mg^{2+} binding thereby reducing the affinity for GTP by 100-fold without affecting the affinity for GDP, and consequently rendering the Rab GDP-locked (Farnsworth and Feig, 1991;Nuoffer et al., 1994). The switch regions are also important for nucleotide specific protein interactions. For instance, the Rab3 effector rabphilin-3a binds to both switch regions specifically when Rab3 is GTP-bound, whereas Rab35 contacts its GEF, DENND1B through both switch regions when it is in its GDP-bound form (Wu et al., 2011b).

1.1.4 Rab post-translational modifications

The most notable post-translational modification of small GTPases is prenylation; the addition of a farnesyl or geranylgeranyl pyrophosphate to the C-terminal cysteine residue via a thioether linkage (Casey and Seabra, 1996). This lipid modification is required to anchor the GTPase to the cytoplasmic leaflet of membranes or interact with certain proteins (Leung et al., 2006). The necessity of this lipid anchor for proper GTPase function is highlighted by the discovery that oncogenic Ras requires prenylation in order to transform cells (Willumsen et al., 1984). Therefore, prenylation and the mechanisms to inhibit prenylation have been widely studied (Basso et al., 2006). While other small GTPases are prenylated by type I farnesyl transferase and geranylgeranyl transferase type I, Rabs are exclusively prenylated by type II Rab geranylgeranyl transferase (RGGT) (Casey and Seabra, 1996;Lane and Beese, 2006). Unlike type I prenyl transferase, RGGT on its own does not bind short peptides containing the C-terminal cysteine residue nor the Rab alone (Seabra et al., 1992;Anant et al., 1998). Instead RGGT recognizes a second protein, Rab escort protein (REP) when bound to a Rab (Andres et al., 1993). RGGT adds the geranylgeranyl moieties while in complex with REP and Rab (Thoma et al., 2001b;Alexandrov et al., 1994). REP can then escort the newly prenylated Rab to its target membrane, though whether RGGT remains associated at this step is

unclear (Thoma et al., 2001a;Thoma et al., 2001b;Alexandrov et al., 1994). Most Rabs contain two cysteine residues and are doubly prenylated making this significantly more hydrophobic than singly prenylated Rabs containing a single cysteine. However, like doubly prenylated Rabs, singly prenylated Rabs, such as Rab8 and Rab13 remain preferentially modified by RGGT (Wilson et al., 1998;Joberty et al., 1993). Interestingly, Rabs with a single cysteine or CXC motif but not CC motif undergo additional post-translation modification in that they are carboxyl methylated (Smeland et al., 1994;Leung et al., 2006). However the function of carboxyl methylation of Rabs is unclear as the absence of methylation does not affect Rab localization (Bergo et al., 2001). It has been proposed to strengthen the association of the Rab with the negatively charged membrane by reducing the repulsive negative charge of the carboxy terminus (Shahinian and Silvius, 1995).

Another post-translational modification of Rabs that is often underappreciated is phosphorylation. Several Rabs can be phosphorylated in an activity dependent manner. For example, Rab3B, Rab6 and Rab8 are phosphorylated in platelets following thrombin treatment (Karniguian et al., 1993). Phosphorylation of Rab6 increases its affinity for GTP by 3-fold yet failed to alter its GTPase activity (Fitzgerald and Reed, 1999). However, phosphorylated Rab6 by protein kinase C (PKC) redistributes Rab6 to the cytosol and therefore may play an important role in the targeting of Rab6 (Scheper et al., 2004). Rab4 is phosphorylated by the mitosis inducing protein $p34^{cdc2}$ (Bailly et al., 1991). This phosphorylation event has no effect on the affinity for guanine nucleotides. However, phosphorylation during mitosis results in the redistribution of Rab4 entirely into the cytosol (Bailly et al., 1991). Interestingly, the phosphorylated Rab4 in the cytosol is in its active GTP-bound form (Gerez et al., 2000). Therefore $p34^{cdc2}$ may perturb membrane trafficking pathways during mitosis by altering Rab localization. In contrast to the serine/threonine phosphorylation of several Rabs, Rab24 is the only Rab known to be phosphorylated on a tyrosine residue (Ding et al., 2003). However,

phosphorylated Rab24 also accumulates in the cytosol, predominately in its GTP-bound form (Overmeyer and Maltese, 2005). These studies suggest that redistribution of active Rabs to the cytosol may be a general function of phosphorylation, however further studies are needed to understand the physiological consequences of these findings.

During infection, bacteria post-translationally modify Rabs in order to control membrane-trafficking pathways. One modification is reversible adenylation, the attachment of an AMP group from ATP (Itzen et al., 2011). The *Legionella pneumophila* protein DrrA/SidM adenylates Rab1b while SidD reverses this reaction (Mukherjee et al., 2011). The adenylation occurs on a tyrosine residue in the switch II region and selectively interferes with interactions with GAPs rendering the protein constitutively active (Muller et al., 2010;Muller et al., 2012). *Legionella pneumophila,* known to cause Legionnaires disease, also modifies Rab1 and Rab35 by phosphocholination. Phosphocholine is transferred from CDP-choline by the enzyme AnkX and catalyzed by Lem3 and can also be reversed by the enzyme Ipg0696 (Tan et al., 2011;Goody et al., 2012). This phosphocholination also occurs in the switch II region and interferes with Rab activation by GEFs as well as GDI and effector binding (Goody et al., 2012). While these post-translational modifications by bacteria represent important mechanisms for hijacking the host cells trafficking pathways, it remains elusive whether adenylation or phosphocholination occur in uninfected cells.

1.1.5 Rab Activation by GEFs

The precise spatial and temporal activation of Rabs is critical for their ability to regulate membrane trafficking. Activation of Rabs is achieved by various proteins harbouring enzymatic GEF activity that facilitate the exchange of GDP for GTP. As the number of Rabs has evolved to perform specialized roles in membrane trafficking, so to have the GEFs that activates them. In fact, several

large and diverse families of Rab GEFs have been described. In yeast, the multisubunit TRAPP complexes function as Rab GEFs in the secretory pathway. TRAPP-1 activates the yeast Rab Ypt1p to facilitate tethering of Golgi-derived vesicles with the ER (Jones et al., 2000;Wang et al., 2000;Sacher et al., 2008). TRAPP-II also regulates post-Golgi trafficking by activating both Ypt1 and Ypt31-32p (Morozova et al., 2006;Barr and Lambright, 2010). In contrast to other GEFs, the catalytic residues of the TRAPP complex are located on its multiple subunits (Kim et al., 2006). While TRAPP-II exists in higher eukaryotes, it harbours no GEF activity for Rab11, the most closely related Rab to Ypt31-32p (Barr and Lambright, 2010). Instead, TRAPP-II activates Rab1 and tethers COPI-coated vesicles to cis-Golgi membranes (Yamasaki et al., 2009). Thus, in higher eukaryotes, where Rab11 evolved to mediate trafficking from the TGN to the plasma membrane, the TRAPP complex remained associated with early secretory trafficking events (ER to/from Golgi apparatus).

Another family of GEFs for the Rab5 subfamily (Rab5, Rab17, Rab21 and Rab22) functioning in early endocytic trafficking are Vsp9-domain proteins (Barr and Lambright, 2010). Vsp9 domain proteins are widely conserved in eukaryotes with at least 9 identified proteins in mammals (Carney et al., 2006). The most well studied being Rabex-5 that activates Rab5 and is required for the fusion of plasma membrane derived vesicles with early endosomes (Horiuchi et al., 1997;Lippe et al., 2001). Another example of a Vps9 protein is Ras interaction/interference (Rin). Rin1 activates Rab5 and associates with both epidermal growth factor receptor (EGFR) and Ras (Tall et al., 2001;Barbieri et al., 2003;Han and Colicelli, 1995). In fact, binding to activated Ras enhances Rin's GEF activity (Tall et al., 2001), and like Ras, both Rin1 and Rab5 facilitate EGFR endocytosis (Tall et al., 2001;Barbieri et al., 2003). Thus, Rin1 acts downstream of Ras to promote endocytosis of EGFR through Rab5 activation (Carney et al., 2006).

1.1.6 The DENN domain

The largest family of GEFs for Rab GTPases are the DENN domain containing proteins. The DENN (differentially expressed in normal and neoplastic cells) domain is an evolutionarily conserved protein module that is present in species from the fission yeast *Schizosaccharymyces pombe*, all the way to high eukaryotes like humans (Marat et al., 2011). However, in contrast to other Rab GEFs, DENN domain proteins are entirely absent from the budding yeast *Saccharomyces cerevisiae* and activate Rabs that have no known *Saccharomyces cerevisiae* homologue (Yoshimura et al., 2010). This suggests that the DENN domain proteins evolved alongside the Rabs they activate. The first DENN containing protein identified as a GEF was MAP-kinase activating death domain protein (MADD). MADD was originally discovered as a GEF for Rab3 in brain (Brown and Howe, 1998;Wada et al., 1997). However, the first demonstration that the isolated DENN domain is sufficient to activate a Rab was of connecdenn1/DENND1A (Allaire et al., 2010). Connecdenn 1/DENND1A was originally discovered in a proteomic analysis of clathrin-coated vesicles (Girard et al., 2005a;Allaire et al., 2006). Connecdenn 1 is targeted via direct binding to clathrin heavy chain and the clathrin adaptor AP-2 to clathrin coated structures that mature into early endosomes (Allaire et al., 2006) . Mutations in the *C. elegans* ortholog of connecdenn, RME-4, led to defects in the clathrin-mediated endocytosis of yolk protein in oocytes (Sato et al., 2008). More specifically, connecdenn/RME-4 mutations led to the accumulation of yolk protein receptor in early endosomes suggestive that connecdenn/RME-4 plays a role in recycling the yolk receptor back to the plasma membrane rather than directly controlling clathrin-mediated endocytosis (Sato et al., 2008). The Rab35 ortholog, RME-5 is also present on early endosomes, and mutations in Rab35/RME-5 phenocopied that of connecdenn/RME-4 (Sato et al., 2008). Furthermore, connecdenn/RME-4 interacts with Rab35/RME-5 preferentially in its inactive GDP-bound form, common to GEFs (Sato et al., 2008). These initial studies were highly suggestive that connecdenn is a GEF for Rab35 and

indeed the isolated DENN domain of connecdenn was shown to have robust GEF activity toward Rab35 (Allaire et al., 2010). Furthermore, these initial studies suggested that all DENN proteins may harbour GEF activity for Rabs.

Based on protein sequence alignments, there were initially 18 identified DENN domain proteins organized into eight families (Levivier et al., 2001;Marat et al., 2011). Indeed, each of these DENN family members harbours GEF activity for a unique Rab or subset of Rabs (Yoshimura et al., 2010). The DENN domain is often found alongside other protein domains which may or may not be conserved across family members, while outside of the DENN domain, different DENN families have very low sequence homology (Marat et al., 2011). However, solving the structure of the DENN domain along with sophisticated bioinformatics has identified additional DENN containing proteins, bringing the total number to 26 (Levine et al., 2013;Zhang et al., 2012).

1.1.7 DENN Domain Structure

Our understanding of the DENN domain was further advanced by solving the crystal structure of the isolated DENN domain of connecdenn 2/DENND1B in a complex with Rab35 (Wu et al., 2011b). Unlike the tripartite domain structure originally predicted by primary sequence analysis, the DENN domain is a bi-lobed structure (Levivier et al., 2001;Wu et al., 2011b). The N-terminal lobe folds into a longin module composed of five antiparallel β-strands sandwiched between three α helices (Tochio et al., 2001;Wu et al., 2011b). The longin domain is an evolutionarily conserved protein module found in several proteins critical for membrane trafficking events such as vesicle budding, tethering and fusion (Filippini et al., 2001;Martinez-Arca et al., 2003;Rossi et al., 2004). The N-terminal longin module is connected to the C-terminal lobe by a long random coiled linker (Wu et al., 2011b). The C-terminal lobe, composed of a core five stranded β sheet flanked by several α helices and while

both lobes contact the Rab, the C-terminal lobe forms the primary binding surface for the Rab substrate (Wu et al., 2011b).

1.1.8 Rab Deactivation by GAPs

Deactivation of Rabs by hydrolysis of GTP back to GDP is catalyzed by GTPase activating proteins (GAPs). Thus, GAPs can spatially and temporally restrict Rab activity within the cell (Barr and Lambright, 2010). This helps to prevent the accumulation of Rabs on specific subdomains and/or refine compartment boundaries. For example, constitutively active Rab5 mutants stimulate membrane fusion and accumulate on enlarged early endosomes (Stenmark et al., 1994). The majority of Rab GAPs contain a conserved Tre2/Bub2/Cdc16 (TBC) domain. The TBC domain family represents the largest family of Rab regulators containing 44 members (Gabernet-Castello et al., 2013). Approximately half of the known TBC domain proteins have an identified Rab substrate (Frasa et al., 2012). However, given the abundance of Rabs relative to number of TBC proteins, it is not surprising that several TBC proteins can act on multiple Rabs. For example, TBC1D10A targets Rab27 and Rab35 while TBC1D4 targets Rab2, Rab8, Rab10 and Rab14 (Fukuda, 2011). The specificity of these TBC proteins for their Rab substrate can be influenced by their localization and association with other co-factors (Barr and Lambright, 2010). At least one non-TBC domain GAP has been identified, that is Rab3GAP which acts on Rab3 (Nagano et al., 1998). Consistent with the regulation of synaptic vesicle exocytosis by Rab3, mutations in Rab3GAP cause Martsolf and Warburg syndromes, which include neurological defects such as mental retardation (Aligianis et al., 2005;Aligianis et al., 2006).

1.1.9 TBC domain structure

TBC domains are composed of an entirely helical structure and most catalyze the hydrolysis of GTP using a dual-finger mechanism whereby the catalytic arginine and glutamine residues are used as the 'fingers' (Rak et al., 2000;Frasa et al., 2012). The dual-finger mechanism was first discovered for the TBC domain of Gyp1p in complex with Rab33 (Pan et al., 2006). Similarly, GAPs for Ras and Rho stabilize the transition of the GTPase using the catalytic arginine finger, however, unique to the TBC domain is the use of the catalytic glutamine residue (Pan et al., 2006). This glutamine residue substitutes for the glutamine found in the Switch II region of the Rab that is responsible for GTP hydrolysis (Pan et al., 2006). While the structure of the non-TBC GAP Rab3GAP has not been elucidated, it appears to use an arginine finger mechanism similar to GAPs for other Ras GTPase (Clabecq et al., 2000).

1.1.10 Effectors

Rab effectors are proteins that mediate one or more of the downstream effects of that Rab (Grosshans et al., 2006). They interact selectively with the active GTP-bound Rab and subsequently dissociate once the Rab is inactivated. One commonly used method to identify Rab effectors is the yeast two-hybrid system to screen proteins that bind preferentially to GTP-bound Rabs (Fukuda et al., 2008). Given that effectors perform the downstream function of Rabs, it is not surprising that Rab effectors have been shown to play a role in all steps of membrane trafficking (Grosshans et al., 2006). For example, the Rab9 effector TIP47 is required for the formation of vesicles carrying mannose 6-phosphate receptors back to the TGN from late endosomes (Grosshans et al., 2006;Pfeffer et al., 1995;Carroll et al., 2001;Diaz and Pfeffer, 1998). The Rab27 effector melanophilin links Rab27a-containing melanosomes to the actin motor myosin-Va (Fukuda et al., 2002). Tethering of ER-derived vesicles to the Golgi apparatus requires the Golgi-associated complex GM130/GRASP65

and the vesicle-associated protein p115 (Sztul and Lupashin, 2006;Grosshans et al., 2006). Active Rab1 interacts with both tethers and is required for successful fusion of these vesicles with the Golgi apparatus (Allan et al., 2000;Moyer et al., 2001). Finally, the Rab5 effector EEA1 interacts with the t-SNARE, syntaxin-13, and is required for the fusion of early endosomes (McBride et al., 1999). Given the numerous functions of Rabs in membrane trafficking, it is perhaps not surprising that individual Rabs can interact with multiple effectors to mediate different functions. For instance, Rab35 interacts with at least six different effectors (Chaineau et al., 2013). During cell division, Rab35 recruits Oculocerebrorenal syndrome of Lowe protein (OCRL), to the intracellular bridge and where it hydrolyzes $PI(4,5)P_2$ allowing the bridge to pinch and the cells to separate (Dambournet et al., 2011;Chaineau et al., 2013). At the cell periphery, Rab35 recruits the actin-bundling protein fascin to induce filapodia formation in cells and mechanosensory bristle formation in *Drosophila* (Zhang et al., 2009;Chevallier et al., 2009). Rab35 recruits the effector ArfGAP with coiled-coil, ankyrin repeat and PH domain 2 (ACAP2) to endosomes where it inactivates Arf6 to enhance recycling of E-cadherin to the plasma membrane while reducing delivery of β-integrin (Allaire et al., 2013;Kobayashi and Fukuda, 2012). Thus, Rab35 interacts with a variety of effectors that all perform unique functions. As well, some effectors interact with multiple Rabs in order to coordinate trafficking pathways. For instance, Rab35 recruits Molecule Interacting with CasL 1-like 1 (MICAL-L1) to recycling endosomes which subsequently recruits Rab8, Rab13 and Rab36 to these same endosomal compartments (Kobayashi et al., 2014). Thus, the diversity of effectors explains how Rabs are able to mediate a multitude of membrane trafficking steps. Rabs therefore act as spatiotemporal molecular timers regulating when and where the effectors are needed.

1.1.11 Targeting Rabs

As each organelle or vesicle is composed by a distinct Rab or subset of Rabs, one pressing question is how Rabs are targeted to the correct membrane compartment. Early work has shown that membrane targeting requires prenylation and Rab GDIs. While there is a single Rab GDI in yeast, humans express two isoforms GDIα which is enriched in brain and the ubiquitously expressed GDIβ (Alory and Balch, 2001;Nishimura et al., 1994). Thus, Rab GDIs bind to numerous Rabs with little to no specificity (Ullrich et al., 1993). Rab GDIs are important for membrane targeting as they bind to prenylated Rabs in their inactive GDP-bound form (Pfeffer and Aivazian, 2004). GDIs can extract Rabs from membrane upon inactivation and remain bound in the cytosol thereby shielding the prenyl group from associating with incorrect membrane compartments. Once reaching the correct membrane, the GDI is released and the Rab can be activated and re-associate with the membrane. This was evidenced by showing that purified Rab5 in a complex with GDI targets correctly to early endosomes and subsequently releases the GDI into the cytosol (Ullrich et al., 1994). Furthermore, deletion or mutation of the C-terminal cysteine residues to prevent prenylation completely solubilizes Rab4 and Rab5 (Gomes et al., 2003). However, while Rab prenylation and GDI binding is required for membrane association, it does not itself specify localization of the Rab (Chavrier et al., 1991). Several studies have attributed membrane targeting to the hypervariable domain (HVD), the largely unstructured region directly adjacent to the prenylation motif (Chavrier et al., 1991;Li et al., 2014a). The HVD is the most distinct region of Rabs, and protein interactions with this region could presumably dictate Rab localization. Indeed membrane targeting by the HVD is required for several Rabs such as Rab7 and Rab35, but not for Rab1 or Rab5, suggesting that these Rabs rely more heavily on interactions within their switch regions for localization(Ali et al., 2004;Li et al., 2014a). Interactions with GDI-displacement factors (GDF) were proposed to dissociate Rab-GDI complexes and allow for membrane targeting (Pfeffer and Aivazian, 2004). This was originally proposed

following the identification of a proteinaceous factor that could dissociate Rab5, Rab7 and Rab9 from GDI and allow them to associate with membranes (Dirac-Svejstrup et al., 1997). This factor lacks GEF activity and appears specific for endosomal Rabs as it failed to act on endoplasmic reticulum to Golgi-related Rab1 (Dirac-Svejstrup et al., 1997). The genes encoding GDFs were subsequently identified as the Ypt-interacting proteins (Yips) (Yang et al., 1998;Calero and Collins, 2002;Sivars et al., 2003). Yip1 was originally discovered as a GDF for Ypt1 and Ypt31 in yeast, however Yip1 can interact with all yeast Rab homologues (Yang et al., 1998;Calero and Collins, 2002). In mammalian cells, knockdown of Yip3/PRAS1 decreased membrane association of Rab9 (Sivars et al., 2003) however, Yip3/PRAS1 can also interact with several Rab proteins (Martincic et al., 1997;Bucci et al., 1999). Thus, one major weakness in attributing membrane targeting to Yip proteins is their promiscuity in Rab binding.

Another commonly held view is that GEF localization is required for proper Rab targeting. In this model, GEFs could act in place of GDFs. As Rabs are thought to associate with membrane upon activation, they should anchor to membrane compartments containing their specific GEF (Blumer et al., 2013). Indeed in support of this argument, Rab32 fails to localize to ring-like membrane structures in melanosomes following knockdown of its GEF BLOC-3 (Gerondopoulos et al., 2012). However, Rab32 was still present on small punctate structures following BLOC-3 silencing (Gerondopoulos et al., 2012). One potential explanation is that Rab32 associates with vesicles in its inactive form. Or, perhaps there is another GEF for Rab32 present on these structures. Indeed multiple GEFs can act on a single Rab. Such is the case for Rab35 which can be activated on early endosomes by connecdenn 1 and connecdenn 2 while being activated on actin rich structures at the cell periphery by connecdenn 3 (Marat and McPherson, 2010;Marat et al., 2012). Moreover, other factors in addition to GEFs may influence Rab localization. For instance, previously identified

effectors can recruit Rabs to specific compartments. For example, the effector MICAL-L1 recruits Rab8, Rab13 and Rab36 to recycling endosomes in PC12 cells (Kobayashi et al., 2014). Thus, rather than acting as a traditional effector, MICAL-L1 functions as a scaffold to recruit Rabs to a specific endosomal compartments.

Finally, the lipid composition of a membrane can enhance the fidelity of Rab activity on the proper membrane. Specific lipids can recruit GEFs to ensure activation of the Rab on the appropriate membrane. Such is the case in yeast for the GEF Sec2p which is recruited by phosphatidylinositol 4-phosphate [PI(4)P] to secretory vesicles where it activates the Rab Sec4p (Mizuno-Yamasaki et al., 2010). Furthermore, coordination between specific Rabs and lipids may be necessary for the activity of specific effectors. For instance EEA1 requires both activated Rab5 and PI(3)P to associate with early endosomes (Simonsen et al., 1998). This type of coincidence detection would also prevent Rab mediated activity on improper membranes. Thus, the mechanisms targeting Rabs to specific membrane compartments are as diverse as the Rabs themselves and highlight the importance of studying each Rab individually to better understand how they function.

1.1.12 Rab cascades

One important consideration in the membrane trafficking field is how to regulate the progression from one endosomal compartment to another while maintaining the identity of the original compartment. As each compartment is defined by a distinct Rab or subset of Rabs, Rab cascades have been proposed to mediate this process (Stenmark, 2009). One way to coordinate a Rab cascade is through multidomain GEFs that act as scaffolds. In addition to their Rab substrates, some GEFs can interact with GTP-bound Rabs, thereby facilitating a cascade between different Rab trafficking pathways. For example, the transition from early endosomes to late endosomes is marked by the

exchange of Rab5 to Rab7 which is accomplished by the VPS/HOPS complex. As an effector, VPS/HOPS is recruited by GTP-bound Rab5 to early endosomes where it functions as a GEF for Rab7 (Rink et al., 2005). Another example is DENND5 that couples GTP-bound Rab11 on recycling endosomes to the Golgi where it binds Rab6 and acts as a GEF for Rab39 (Miserey-Lenkei et al., 2007;Yoshimura et al., 2010). Effectors themselves can act to coordinate multiple Rabs on a single compartment. As mentioned above, MICAL-L1 recruits Rab8, Rab13 and Rab36 to recycling endosomes (Kobayashi et al., 2014). However, MICAL-L1 is first recruited to these recycling endosomes by activated Rab35 (Kobayashi et al., 2014). Thus, MICAL-L1 coordinates the activity of Rab8 and Rab13 on Rab35-positive recycling endosomes. Finally, the coordination of Rab cascades can also mediate a negative-feedback to ensure that Rab activation remains at appropriate levels (Stenmark, 2009). Mathematical modeling of the conversion of Rab5-positive early endosomes to Rab7-postive late endosomes predicts a 'cut-out switch' whereby Rab7 suppresses further Rab5 signalling (Del Conte-Zerial et al., 2008). Indeed subsequent studies demonstrated that TBC-2 colocalizes primarily with Rab7 and functions as a GAP to inactive Rab5 (Chotard et al., 2010). This type of negative feedback also serves to coordinate Rab activity with other small GTPases such as Arfs. For example, both Rab35 and Arf6 function on early endosomes but with opposing functions (Chaineau et al., 2013). Arf6 activity recycles integrins to the plasma membrane to promote cell migration while Rab35 activity promotes E-cadherin recycling to the plasma membrane to promote cell-cell adhesion (Allaire et al., 2013). Interestingly, Rab35 and Arf6 negatively regulate each other's activity; active Rab35 recruits the Arf6 GAP ACAP2, while active Arf6 recruits the Rab35 GAP TBC1D10 and TBC1D24/Skywalker (Uytterhoeven et al., 2011;Chesneau et al., 2012;Kobayashi and Fukuda, 2012;Egami et al., 2011). Therefore, the communication between different Rabs and other small GTPases is tightly regulated. Furthermore, Rabs can also regulate the maturation of a compartment by modulating its lipid composition. For

example, PI(4,5)P2 is required for clathrin-mediated endocytosis while conversion to PI(4)P is needed for uncoating and cargo sorting. Activation of Rab35 on clathrin-coated vesicles recruits the lipid phosphatase OCRL which facilitates the conversion of PI(4,5)P2 to PI(4)P and subsequent uncoating (Cauvin et al., 2016). Thus the coordination of Rab cascades along with phosphoinositide cascades is crucial for the progression of membrane trafficking pathways.

CHAPTER 1.2

RAB13 AND THE REGULATION OF CANCER CELL BEHAVIOR

Maria S. Ioannou and Peter S. McPherson

Department of Neurology and Neurosurgery, Montreal Neurological Institute,

McGill University, Montreal, QC, H3A 2B4, Canada

Originally published in The Journal of Biological Chemistry

doi: 10.1074/jbc.R116.715193

1.2.1 Introduction to Rab13

As described above, the Rab (Ras-related in brain) family of proteins are master regulators of vesicle trafficking. They are evolutionarily conserved with approximately 70 members in humans, and each Rab is localized predominantly to a specific intracellular organelle or vesicle (Zerial and McBride, 2001). Rabs have been implicated in every step of vesicle trafficking including the formation of cargo laden membrane vesicles and tubules, transport of these carriers on the cytoskeleton, tethering and docking of the carriers at the target membrane, and finally membrane fusion delivering cargo. Not surprisingly, functional impairment of Rab pathways is associated with diseases including immunodeficiencies, neurological disorders and cancer (Stenmark, 2009). One such Rab, Rab13 controls cellular functions that are often altered in cancer and Rab13 is now recognized as an important driver of cancer progression. The purpose of this doctoral thesis was to uncover the basic physiology of Rab13 activation in membrane trafficking as well as how the regulation of Rab13 relates to cancer cell behaviour. Therefore, the remainder of Chapter 1 will focus on the importance of Rab13 in the physiology of cancer and the Rab13 trafficking pathways contributing to tumorigenicity.

1.2.1 The biology of Rab13

As for all small GTPases, Rab13 cycles between an active, GTP-bound state and an inactive, GDP-bound state. Activation of Rab13 is mediated by DENND1C/connecdenn 3, guanine nucleotide exchange factors (GEFs) that interact with GDP-bound Rab13 and facilitate the exchange of GDP for GTP (Nishikimi et al., 2014;Sun et al., 2010). This protein bears a differentially expressed in normal and neoplastic cells (DENN) domain, an evolutionarily ancient protein module that encodes GEF activity for a large number of Rab GTPases (Marat and McPherson, 2010;Allaire et al., 2010;Yoshimura et al., 2010). Rab13 is inactivated by the GTPase-activating protein (GAP) Akt

substrate 160 (AS160)/TBC1D4, which enhances the ability of Rab13 to hydrolyse GTP (Ioannou et al., 2015;Nishikimi et al., 2014;Sun et al., 2010). In its active form Rab13 binds to several effectors including MICAL-L1, MICAL-L2 and PKA (Fukuda et al., 2008;Kohler et al., 2004).

Rab13 is ubiquitously expressed and is thought to have diverged from its closest homologue Rab8, early in the vertebrate lineage (Klopper et al., 2012). Similar to Rab8, Rab13 has been implicated in both biosynthetic and endosomal recycling pathways. Rab13 is found at the trans-Golgi network (TGN), on recycling endosomes and at the plasma membrane (Nokes et al., 2008). Disruption of Rab13 function inhibits the delivery of cargo that reaches the plasma membrane via recycling endosomes from either the biosynthetic or endocytic recycling pathways. Thus, Rab13 is thought to control membrane trafficking at the level of the recycling endosome and Rab13 dysfunction likely alters the cell surface delivery of cargo locally at the plasma membrane, perhaps by playing a role in docking or fusion of membrane carriers derived from recycling endosomes.

There are several proteins implicated in cancer cell behaviour whose trafficking and cellular localization is regulated by Rab13. These include the trafficking of integrins during cell migration, the surface delivery of the glucose transporter GLUT4 in response to insulin signalling, and the trafficking of VEGFR during angiogenesis (Nishikimi et al., 2014;Sun et al., 2010;Wu et al., 2011a). Rab13 is also implicated in regulation of the actin cytoskeleton as its GEF, DENND1C/connecdenn 3 is localized on actin and all of its effectors indirectly promote actin polymerization. Through these activities, Rab13 regulates the integrity of tight junctions and promotes the migratory capacity of cells, pathways important for the behaviour of cancer cells and the progression of the disease.

1.2.3 Regulation of Rab13 expression

Consistent with a role for Rab13 in cancer progression, Rab13 is upregulated in multiple cancer types including diffuse large B-cell lymphoma and glioblastoma (Mahadevan et al., 2005;Li et al., 2014b). In fact Rab13 is significantly amplified in the majority of cancers (Fig. 1.1) (Gao et al., 2013;Cerami et al., 2012) and Rab13 levels inversely correlate with patient prognosis in cancers such as basal type breast cancer (Fig. 1.2) (Gyorffy et al., 2010). Moreover, Rab13 expression levels are elevated in cancer cell lines resistant to radiotherapy compared those that are sensitive to radiotherapy (Kim et al., 2012). Therefore, it is apparent that Rab13 expression correlates with cancer progression.

A key question relates to the mechanisms driving enhanced Rab13 expression in various cancers. p53 is one of the best studied genes in cancer biology and p53 is the most commonly mutated gene in human cancer (Kandoth et al., 2013). Although several cancers have been associated with loss-of-function mutations in p53, several studies identified mutations in p53 that promote oncogenesis in a gain-of-function manner (Muller and Vousden, 2014;Zhou et al., 2014). In fact, mice expressing gain-of-function mutations in p53 have more aggressive and metastatic cancers than p53 null mice (Doyle et al., 2010;Morton et al., 2010). Gain-of-function mutations in p53 have been reported to upregulate multiple genes implicated in cancer progression including key signalling receptors (Weisz et al., 2007). Interestingly, Rab13 is one of several transcriptional targets of p53 and p53 promotes Rab13 expression (Di et al., 2006;Ma et al., 2011). Furthermore, ionizing radiation upregulates Rab13 mRNA in neuroblastoma cells and this upregulation is blocked by inhibiting p53 activation induced by DNA-damage (Bar et al., 2005;Eom et al., 2015). Mutant p53 drives cancer cell invasion in part by promoting recycling of both integrin and epidermal growth factor receptor (EGFR) to the cell surface and as discussed in detail below, Rab13 controls recycling of integrins and was

suggested to do the same for EGFR (Nishikimi et al., 2014;Abou-Zeid et al., 2011;Muller et al., 2009). Therefore, upregulation of Rab13 could contribute to the potent oncogenic effect of gain-of-function p53 mutations in human cancer.

There are multiple mechanisms in addition to p53 mutations that contribute to the upregulation of Rab13 in cancer. For example, Rab13 expression is inhibited by hsa-miR-125b and this microRNA is downregulated in primary hepatocellular carcinoma, correlating with a poor patient prognosis (Li et al., 2008). Up to 15% of all human cancers are associated with inflammation and chronic inflammation is an important risk factor for tumorigenesis (Mantovani et al., 2008;Kuper et al., 2000). Expression of the anti-inflammatory protein annexin A1 is increased in squamous cell carcinoma and treatment of epithelial cancer cells with a recombinant annexin A1 mimetic peptide upregulates levels of Rab13 mRNA (Prates et al., 2015;Calmon et al., 2013). Therefore, inflammation could promote tumorigenesis through its upregulation of Rab13.

The localization of Rab13 translation may also contribute to its role in cancer. Rab13 mRNA is enriched in pseudopodial protrusions in MCF7 and MDA-MB-231 cancer cell lines and migratory fibroblasts (Jakobsen et al., 2013;Mili et al., 2008). The 3'untranslated region of Rab13 is necessary and sufficient to direct Rab13 mRNA to cellular protrusions in response to migratory cues (Mili et al., 2008). This would suggest that localized translation of Rab13 in protrusions promotes invasiveness. However, accumulation of Rab13 mRNA in protrusions is dependent on adenomatous polyposis coli (APC), a tumour suppressor that acts to strengthen cell-cell adhesion (Mili et al., 2008;Faux et al., 2004). While loss of APC prevents recruitment of Rab13 mRNA to protrusions, it does not prevent the formation of protrusions (Mili et al., 2008). Therefore, the function of Rab13

mRNA transport to pseudopodia protrusions and its effect on cell migration and invasion remains elusive.

1.2.4 Rab13 in cell metabolism

Alterations in cell metabolism are an important consideration in cancer progression as cells within a tumour must adapt to various environmental conditions, such as nutrient deprivation, while continuing to proliferate (Cairns et al., 2011). For example, multiple myeloma is one of many cancers with enhanced glucose utilization and multiple myeloma cells exhibit increased glucose sensitivity due to an accumulation of the glucose transporter type 4 (GLUT4) on the plasma membrane (McBrayer et al., 2012). Interestingly, Rab13 functions in the translocation of GLUT4 to the cell surface in response to insulin (Sun et al., 2010). Insulin stimulation increases the pool of active Rab13, which binds to the Rab13 effector MICAL-L2 relieving MICAL-L2 auto-inhibition allowing MICAL-L2 to recruit various actin regulatory proteins including actinin-4 (Sun et al., 2010; Sakane et al., 2010;Nakatsuji et al., 2008). A complex involving Rab13, MICAL-L2 and actinin-4 binds to GLUT4 in an insulin-dependent manner, allowing docking/tethering of GLUT4 vesicles at the cell surface, enabling their fusion (Sun et al. 2015).

Rab13 is inactivated by its GAP, AS160 thereby reducing the plasma membrane pool of GLUT4 (Sun et al., 2010). AS160 itself can be inactivated by phosphorylation thereby enhancing insulin-induced GLUT4 translocation to cell surface (Miinea et al., 2005;Sano et al., 2003;Cheng et al., 2013). Interestingly, Akt is constitutively active in multiple myeloma tumour cells and not surprisingly AS160 is hyper-phosphorylated in myeloma cell lines as well as in breast cancer tumours (Hsu et al., 2001;Jiang et al., 2010). Thus, inhibition of AS160 by phosphorylation in cancer

could enhance Rab13 activity to increase GLUT4 on the plasma membrane, increasing sensitivity to glucose and tumour growth (Figure 1.3).

1.2.5 Rab13 in cell proliferation

Perhaps the key feature of cancer cells is enhanced proliferation. The epidermal growth factor receptor (EGFR) is a well-characterized member of the ErbB family of receptor tyrosine kinases. EGFR is a key factor in tumor growth and activating mutations, gene amplifications and protein overexpression of EGFR have been observed in numerous cancer types (Salomon et al., 1995;Normanno et al., 2006). Rab13 may influence EGFR signalling by regulating EGFR trafficking. Stimulation of EGFR by EGF induces receptor dimerization, internalization into signalling endosomes with eventual sorting to lysosomes for degradation. However, a fraction of EGFR recycles back to the plasma membrane enhancing EGFR signalling (Lenferink et al., 1998). Therefore, increases in EGFR recycling pathways enhance EGFR protein levels, signalling and oncogenic potential. Trafficking of the EGFR is regulated in part by the Rab13 effector protein MICAL-L1. Overexpression of MICAL-L1 results in the accumulation of EGFR in late endosomes while loss of MICAL-L1 increases degradation of EGFR, implying that MICAL-L1 promotes EGFR recycling (Abou-Zeid et al., 2011). The ability of MICAL-L1 to promote EGFR recycling may be mediated by Rab13 as MICAL-L1 recruits active Rab13 to tubular recycling endosomes (Abou-Zeid et al., 2011). Furthermore, intramolecular interaction of MICAL-L1, mediated by binding of the N-terminal calponin homology domain with the C-terminal Rab-binding domain is disrupted by Rab13 binding (Abou-Zeid et al., 2011). Therefore recruitment of active Rab13 could activate MICAL-L1 on tubular recycling endosomes to enhance recycling of EGFR to the plasma membrane. However it is unclear whether this effect is specific to Rab13, as Abou-Zeid et al. (2011) did not test whether Rab13 directly influences EGFR signalling, and MICAL-L1 is known to bind other active Rabs

including Rab8, Rab35 and Rab36 (Kobayashi et al., 2014). Rab35 also regulates EGFR signalling but in the opposite manner; knockdown of Rab35 increases EGFR recycling and downstream ERK signaling (Allaire et al., 2013). It is possible that a Rab cascade exists between Rab13 and Rab35 to regulate EGFR signaling. In fact in PC12 cells, Rab35 recruits MICAL-L1 to endosomes, which in turn recruits Rab13 (Kobayashi et al., 2014). However, Rab35 is known to regulate a 'fast' recycling pathway from early endosomes to the plasma membrane whereas Rab13 is involved in a 'slow' recycling pathway from recycling endosomes and possibly late endosomes. Therefore it is unclear exactly how such a cascade would function to regulate EGFR trafficking and more studies are required to tease apart the details.

1.2.6 Rab13 in cell-cell adhesion

In epithelial and endothelial cells, cell-cell adhesion is initiated by the formation of adherens junctions followed by tight junctions (Nishimura and Sasaki, 2008b). Cadherins and nectins act as cell-adhesion molecules at adherens junctions while claudins and occludins serve as cell adhesion molecules at tight junctions. Loss of cell-cell adhesion is an important component of cell transformation in cancer, as cells must dissociate from each other in order to become more migratory. This is particularly important for single cell metastasis, but also in collective cell migration where cells must detach from the original tissue, and single cells may also detach from the collectively moving cell mass (van et al., 2011). Furthermore, weakening of tight junctions in vascular endothelial cells allows malignant cells to escape the vasculature as part of the metastatic process (Ren et al., 1990;Satoh et al., 1996). Rab13 may promote the invasiveness of cancer cells by negatively regulating the integrity of tight junctions.

One mechanism by which Rab13 inhibits tight junction formation is through regulation of its effector protein kinase A (PKA) (Kohler and Zahraoui, 2005). A notable substrate of PKA is vasodilator-stimulated phosphoprotein (VASP), an actin-binding protein that promotes actin polymerization. Phosphorylation of VASP by PKA abolishes its actin polymerizing activity (Harbeck et al., 2000;Kohler et al., 2004). Yet, phosphorylation of VASP by PKA results in VASP relocation to tight junctions and is required for the establishment of tight junctions (Lawrence et al., 2002). In this way, PKA is proposed to contribute to tight junction recovery by allowing structural relaxation of the cortical actin rim (Lawrence et al., 2002). Consistently, PKA inhibition attenuated tight junction reassembly and epithelial barrier recovery (Lawrence et al., 2002). Interestingly, active Rab13 interacts directly with the α-catalytic subunit of PKA, inhibits PKA-dependent phosphorylation of VASP and prevents VASP association with intracellular junctions (Kohler et al., 2004) (Figure 1.4). Furthermore, activation of PKA by forskolin abolishes the inhibitory effect of active Rab13 on recruitment of phospho-VASP to tight junctions (Kohler et al., 2004). Therefore, active Rab13 inhibits tight junction integrity by negatively regulating PKA and VASP phosphorylation. Given the importance of tight junction disruption in tumorigenicity, it is not surprising that PKA and VASP have been implicated in cancer progression although their roles in this process are complex. For example, PKA activity has been reported to both stimulate and inhibit cancer cell growth (Neary et al., 2004). Similarly, both downregulation and overexpression of VASP results in the loss of contact inhibition and enhanced tumour growth (Liu et al., 1999). The contribution of VASP to tumorigenicity may depend on which of its residues are phosphorylated. Phosphorylation by PKA at Ser239 impairs F-actin bundling while phosphorylation by PKD at Ser157 and Ser322 promotes VASP recruitment and actin bundling at the leading edge of cells (Doppler et al., 2013). VASP phosphorylation on Ser157 by Mst1 is also required for Rab13-dependent transport of LFA-1 to the leading edge in lymphocytes (Nishikimi et al., 2014). Therefore, VASP is an important downstream

target of Rab13 regulation; however, the involvement of VASP in cancer cell behaviour is highly complex.

Another mechanism by which Rab13 regulates tight junctions is through its effector MICAL-L2. Knockdown of Rab13 reduces the levels of both claudin-1 and occludin at the plasma membrane with no effect on E-cadherin while knockdown of MICAL-L2 inhibits transport of all three junctional proteins (Yamamura et al., 2008). As MICAL-L2 is also an effector for Rab8, which regulates surface levels of E-cadherin, MICAL-L2 could regulate the tight and adherens junctions by coordinating Rab13 and Rab8, respectively. Because loss of Rab13 and MICAL-L2 inhibits surface levels of junctional proteins, Rab13 was initially proposed to promote tight junction formation (Yamamura et al., 2008). However, this interpretation is inconsistent with several findings described below that show that Rab13 and MICAL-L2 promote cell migration in part by disrupting cell adhesion. Active Rab13 mutants disrupt claudin-1 and occludin at tight junctions, which suggests that Rab13 activity disrupts tight junction formation whereas studies with inactive Rab13 mutants were conflicting as some studies found defective delivery of claudin-1 to tight junctions while others found no effect (Yamamoto et al., 2003;Morimoto et al., 2005). Therefore, it is clear that Rab13 localizes to and regulates tight junctions, but it remains elusive how it does this. Perhaps Rab13 regulates other small GTPases akin to how Rab35 and Arf6 negatively regulate each other to control whether E-cadherin or integrin is delivered to the surface and whether the cell forms adherens junctions or becomes migratory (Allaire et al., 2013).

1.2.7 Rab13 in cell migration and scattering

Following disruption of cell-cell adhesion, metastatic cells become more migratory as they invade into surrounding tissue. Rab13 is required for the scattering and migration of epithelial cells (Kanda

et al., 2008;Ioannou et al., 2015). A common method for inducing dissociation and scattering of epithelial cells is treatment with 12-O-tetradecanoylphorbol-13-acetate (TPA). TPA-induced cell scattering requires activation of Rab13 and regulation of the actin cytoskeleton by the Rab13 effector MICAL-L2 (Kanda et al., 2008). Active Rab13 relieves MICAL-L2 auto-inhibition, allowing MICAL-L2 to recruit various actin regulatory proteins. Thus, the effect of MICAL-L2 on actin dynamics is highly dependent on the presence of activated Rab13. Not surprisingly, MICAL-L2 is upregulated in ovarian cancer tissue and knockdown of MICAL-L2 supressed the proliferation, migration and invasive capacity of ovarian cancer cells in culture (Zhu et al., 2015). One actin-bundling protein that is recruited by activated MICAL-L2 is filamin. Filamin is responsible for the cytoskeletal changes that occur during cell scattering and migration in epithelial cells (Baldassarre et al., 2009;Sakane et al., 2013). Consistently, filamin levels also correlate with invasiveness of melanoma cell lines and high filamin levels are predictive of poor prognosis in melanoma patients (Zhang et al., 2014).

Interestingly, in the absence of Rab13, MICAL-L2 can promote cell-cell adhesion and supress cell scattering by regulating the actin cross-linking protein actinin-4 (Sakane et al., 2010;Nakatsuji et al., 2008). Actinin-4 is not required for MICAL-L2-induced cell scattering, however knockdown of actinin-4 disrupts MICAL-L2 recruitment to tight junctions and delays tight junction formation (Nakatsuji et al., 2008;Sakane et al., 2013). In the absence of Rab13, MICAL-L2 promotes thick actin bundles at the cell periphery through actinin. However, upon activation of Rab13, autoinhibition of MICAL-L2 is relieved, supressing actinin-4 cross-linking activity (Sakane et al., 2012). Consistently, high levels of actinin-4 are associated with decreased cell motility and inactivation of cytoplasmic actinin by relocation into the nucleus is observed in several cancer cell lines (Gluck and Ben-Ze'ev, 1994;Honda et al., 1998).

Important cargoes for cell migration such as integrin are under the control of Rab13. Integrins are cell surface receptors that mediate adhesion with the extracellular matrix and recycling of integrins to the leading edge of cells is required for cell migration. Thus, integrins play a key role in the ability of cancer cells to metastasize from solid tumors (Desgrosellier and Cheresh, 2010). Rab13 functions in the trafficking of the integrin lymphocyte function-associated antigen 1 (LFA-1) to the leading edge of cells contributing to lymphocyte migration (Nishikimi et al., 2014). Presumably, integrin traffics on vesicles that carry inactive Rab13 and these vesicles likely fuse with the plasma membrane following localized activation of Rab13 at the cell periphery (Ioannou et al., 2015). Enhanced integrin trafficking observed in p53 gain-of-function mutants depends on the activity of diacylglycerol kinase α to tether Rab-coupling protein (RCP) to the tips of invasive protrusions (Muller et al., 2009;Rainero et al., 2012). Perhaps Rab13 regulates the delivery of intergrin-containing vesicles by interacting with RCP.

Rab13 can regulate integrin trafficking through directly interacting with the serine/threonine kinase mammalian Ste20-like 1 (Mst1) (Nishikimi et al., 2014). Mst1 is required for chemokines to active integrins and promote their trafficking to the cell surface to mediate cell migration in lymphocytes (Katagiri et al., 2009). Mst1, an ortholog of *Drosophila* Hippo, controls organ size by regulating cell proliferation during development (Zeng and Hong, 2008) and it functions as a tumor suppressor, since Mst1/Mst2 mutant mice develop multiple large tumours in the liver (Zhou et al., 2009). Mst1 can phosphorylate DENND1C and enhance its GEF activity towards Rab13 (Marat et al., 2012;Yoshimura et al., 2010;Nishikimi et al., 2014). Active Rab13 then facilitates the delivery of the T lymphocyte integrin LFA-1 to the cells leading edge stimulating cell migration (Nishikimi et al., 2014) (Figure 1.5). Consistently, inhibiting Rab13 reduced lymphocyte adhesion and migration

(Nishikimi et al., 2014). However, Mst1 has been reported as a negative regulator of migration in epithelial cancer cell lines as has the Mst1/Hippo ortholog KrsB in *Dictyostelium discoideum* (Attarha et al., 2014;Artemenko et al., 2012). These differences may be attributed to cell type specific regulation of Mst1 and whether Mst1 is acting within the classical Hippo pathway or a Hippo-independent pathway with Rab13 (Rawat and Chernoff, 2015).

1.2.8 Rab13 in cell migration and angiogenesis

Angiogenesis contributes to tumour progression in two notable ways. First, tumors require vascular support in order to grow and survive. Early work demonstrate that anti-angiogenic treatment of mice with islet cell carcinoma reduced tumor growth and increased apoptosis of the tumor cells (Parangi et al., 1996). Secondly, cancer cells require access to blood vessels in order to metastasize to other tissue. Compared to mature blood vessels, tumor angiogenesis creates blood vessels that are immature, highly permeable, have less basement membrane and fewer intercellular junctions (Dvorak et al., 1995). Thus, tumor cells can enter these vessels more easily than mature blood vessels (Dvorak et al., 1995). Angiogenesis requires directional cell migration of endothelial cells in response to chemotactic cues such as vascular endothelial growth factor (VEGF) (Lamalice et al., 2007). Furthermore, anti-angiogenic therapy targeting VEGFR can shrink tumors, albeit only temporarily as tumors inevitably acquire resistance to the drugs and resume growth (Casanovas et al., 2005).

Interestingly, Rab13 controls VEGF-directed cell migration and angiogenesis by regulating the spatiotemporal activation of RhoA (Wu et al., 2011a). Both Rab13 and the RhoA GEF Syx are required for VEGF-induced directional cell migration. VEGF stimulates the recruitment of both RhoA and its GEF Syx onto Rab13 vesicles, which then traffic to the cell's leading edge.

Furthermore, Rab13 indirectly associates with Grb2, an endocytic adaptor protein that binds to activated VEGFR (D'Angelo et al., 1999). Thus, Rab13 positive vesicles carrying RhoA/Syx associate with regions of the plasma membrane containing activated VEGFR inducing the formation of the leading edge (Wu et al., 2011a). Furthermore, Rab13 is required for the angiogenesis and growth of intersegmental vessels in zebrafish (Wu et al., 2011a). Therefore, reducing Rab13 could help limit the growth of tumors by reducing VEGFR-induced cell migration and angiogenesis.

1.2.9 Conclusions

Over the last 25 years, great progress has been made in understanding how defects in Rab GTPases cause disease. Here, we provide a detailed summary of how Rab13 regulates cell behaviours associated with cancer progression. Rab13 functions in the delivery of cargo to the plasma membrane, disruption of cell-cell adhesions and the rearrangement of the actin cytoskeleton coupled to surface delivery of selective proteins to drive cell migration. However, several aspects of Rab13 function remain to be studied and may shed additional insight into the physiology of cancer. For example, future studies should aim to elucidate the mechanisms regulating the fusion of Rab13-positive vesicles with the plasma membrane and determine whether Rab13 works in concert with other Rabs in the form of a Rab cascade. Furthermore a more detailed understanding of how Rab13 regulates cell proliferation will likely prove important in understanding tumour growth. Finally, given the high sequence homology of the Rab GTPase family, it is likely difficult to target Rab13 specifically. However, a thorough understanding of Rab13 regulators and effectors may uncover promising new targets for therapies.

1.2.9 Figures

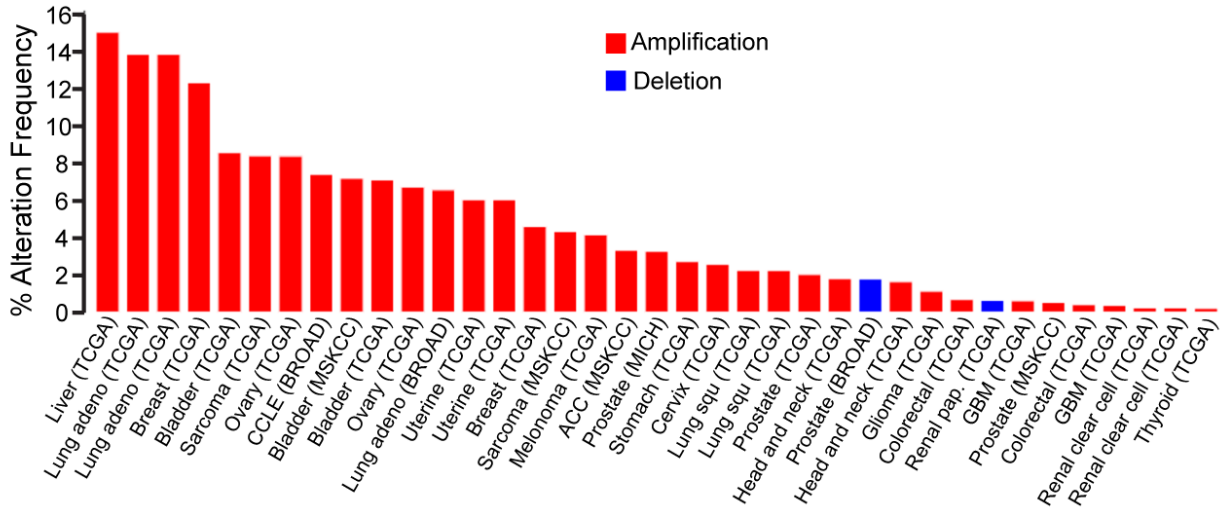

Figure 1.1.

Amplification of Rab13 in human cancers. The copy number alterations of Rab13 in various cancer types. This data was generated using open source data from The Cancer Genome Atlas (TCGA) research network (www.cbioportal.org/). ©Ioannou et al., 2015. Originally published in The Journal of Cell Biology. doi 10.1083/jcb.201407068.

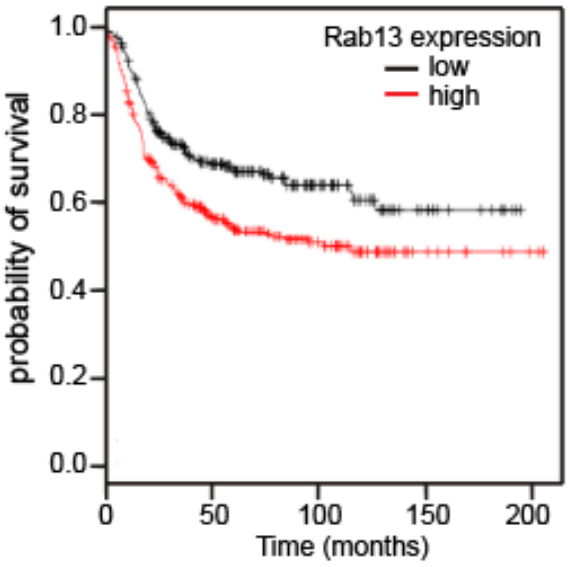

Figure 1.2.

Rab13 levels correlate with poor patient prognosis. Kaplan-Meier analysis of survival of basal-type breast cancer patients using the open source KM plotter (http://kmplot.com/analysis/) where n=668 and p=0.0016 (Gyorffy et al., 2010).

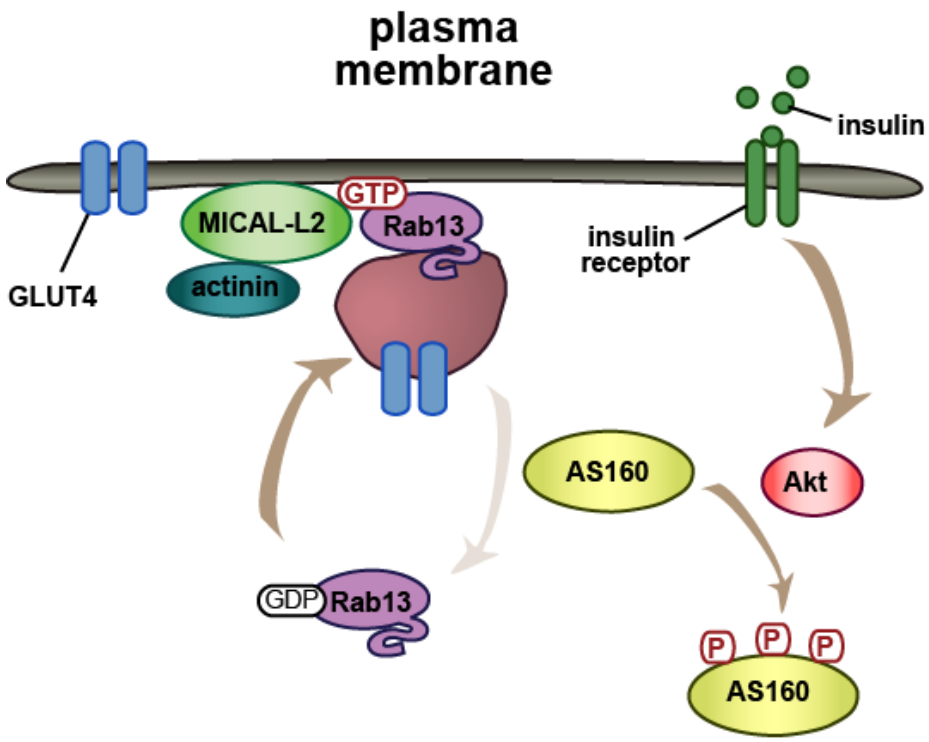

Figure 1.3.

Rab13 promotes GLUT4 recycling in response to insulin. Insulin treatment promotes AS160 phosphorylation by Akt thereby inactivating its GAP activity towards Rab13. This increases the active pool of Rab13 which in turn recruits its effector MICAL-L2 and actinin thereby stimulating the delivery of GLUT4 onto the plasma membrane.

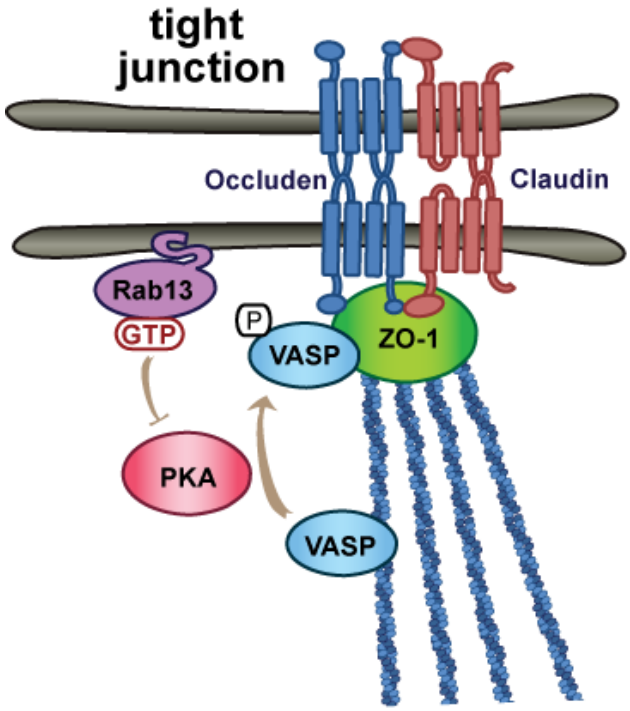

Figure 1.4

Rab13 regulates tight junction disassembly. Protein kinase A (PKA) can phosphorylate the actin binding protein VASP thereby disrupting its ability to bundle actin and promoting its relocation to tight junctions thereby enhancing tight junction formation. However, active Rab13 can bind to and inhibit PKA, prevent VASP phosphorylation and disrupt tight junction assembly.

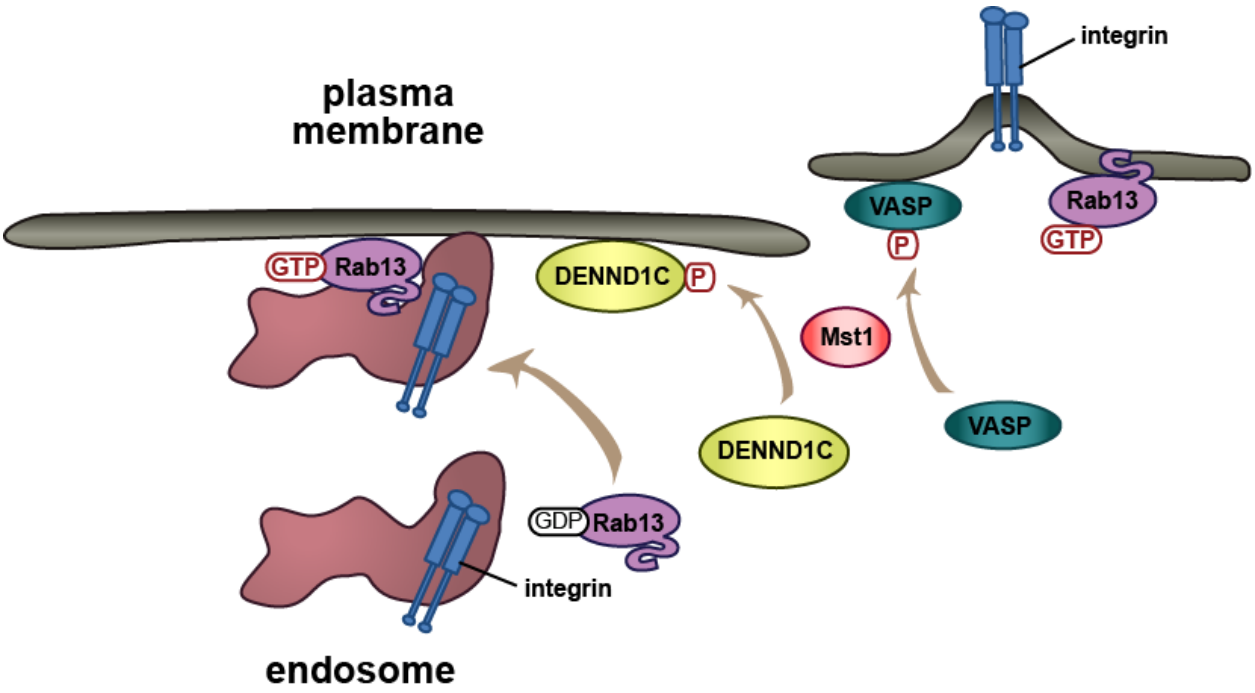

Figure 1.5

Rab13 promotes integrin recycling to enhance cell migration. Mst1 phosphorylates both the actin bundling protein VASP to redistribute it to the cell periphery as well as DENND1C to promote its GEF activity towards Rab13. This coordinates the delivery of integrins to the cell surface with rearrangement of the actin cytoskeleton thereby promoting cell migration.

PREFACE TO CHAPTER 2

Rab GTPases are master regulators of membrane trafficking and impairment of Rab pathways contribute to human diseases including cancer. As introduced in Chapter 1, Rab13 has been implicated in several phenotypes associated with cancer cell behaviour. For example, active Rab13 can disrupt tight junction reassembly and promotes scattering of cultured cells (Kohler et al., 2004;Kanda et al., 2008). However, the mechanisms regulating Rab13 during cancer progression remain incomplete. For instance, what GEF is responsible for activating Rab13 to induce cell scattering? And if Rab13 is localized to multiple subcellular compartments, where is it being activated? Elucidating the localization of activation requires the development of new tools. Therefore in this chapter, we identified DENND2B as a specific GEF for Rab13 and developed a FRET-based activation biosensor to monitor the spatial/temporal dynamics of Rab13 activation in live cells. Finally, all studies to date studied Rab13 in *in vitro* models of cancer, therefore we investigated the role of Rab13 in regulating the growth and metastasis of tumor cells in an *in vivo* model of cancer. Thus in chapter 2, we provide a comprehensive mechanistic understanding of how localized activation of Rab13 by DENND2B in a complex with MICAL-L2 at the cell periphery couples actin dynamics to membrane insertion required for cell migration, invasion, and tumor metastasis.

CHAPTER 2

DENND2B ACTIVATES RAB13 AT THE LEADING EDGE OF MIGRATING CELLS AND PROMOTES METASTATIC BEHAVIOR

Maria S. Ioannou[1], Emily S. Bell[2], Martine Girard[1], Mathilde Chaineau[1], Jason N.R. Hamlin[1], Mark Daubaras[1], Anie Monast[2], Morag Park[2], Louis Hodgson[3], Peter S. McPherson[1]

[1]Department of Neurology and Neurosurgery, Montreal Neurological Institute, McGill University, Montreal, Quebec H3A 2B4, Canada, [2]Department of Biochemistry, Goodman Cancer Centre, McGill University, Montreal, Quebec H3G 0B1, Canada, [3]Department of Anatomy and Structural Biology, Gruss-Lipper Biophotonics Center, Albert Einstein College of Medicine, New York, NY, 10461 USA

Originally published in The Journal of Cell Biology.

doi 10.1083/jcb.201407068.

2.1 Abstract

The small GTPase Rab13 functions in exocytic vesicle trafficking in epithelial cells. Alterations in Rab13 activity have been observed in human cancers, yet the mechanism of Rab13 activation and its role in cancer progression remain unclear. Here we identify the DENN domain protein DENND2B as the guanine nucleotide exchange factor for Rab13 and develop a novel FRET-based Rab biosensor to reveal activation of Rab13 by DENND2B at the leading edge of migrating cells. DENND2B interacts with the Rab13 effector MICAL-L2 at the cell periphery and this interaction is required for the dynamic remodeling of the cell's leading edge. Disruption of Rab13-mediated trafficking dramatically limits the invasive behavior of epithelial cells *in vitro* and the growth and migration of highly invasive cancer cells *in vivo*. Thus, blocking Rab13 activation by DENND2B may provide a novel target to limit the spread of epithelial cancers.

2.2 Introduction

The formation of carcinomas (epithelial cell cancers) involves loss of cell-cell contact, dynamic changes in cell morphology, increased proliferation, and enhanced cell migration and invasion (Goldenring, 2013). Membrane trafficking underlies all of these events. Rab GTPases are master regulators of membrane trafficking controlling the formation of vesicles, vesicle transport via the actin and microtubule cytoskeletons, and vesicle tethering and fusion (Stenmark, 2009). As such, Rabs are key regulators of physiological processes that drive cancer cell biology (Caswell and Norman, 2006;Caswell and Norman, 2008;Mellman and Yarden, 2013).

Enhanced cell migration and the ability to invade through a matrix are perhaps the most obvious manifestations of carcinogenesis. Rab-mediated membrane trafficking controls both normal cell migration, such as that seen in development, and the migratory capacity of invasive carcinomas in at

least two distinct ways (Goldenring, 2013). First, Rabs regulate the delivery of protein cargo required for a balance between cell adhesion and cell migration. For example, Rab35 mediates recycling of cadherins from endosomes and loss of Rab35 function leads to loss of cell-cell contact and enhanced cell migration (Allaire et al., 2013). In addition, cell migration and invasion require a dynamic plasma membrane and the extension of cell protrusions at the migratory leading edge. These processes involve actin assembly, creating protrusive forces to push the membrane forward, coupled with movement of membrane into the growing protrusion to relieve membrane tension (Ridley, 2011;Goldenring, 2013). In fact, invasive cells take on a distinct paradigm of polarity with directed membrane delivery to the leading edge (Goldenring, 2013). One example is seen with Rab8, which controls an endosomal-recycling pathway that delivers membrane tubules to the growing leading edge, and disruption of Rab8 function blocks the formation of membrane protrusions (Hattula et al., 2006). However, whether specific Rab GTPases link new membrane insertion to actin remodelling at the leading edge during carcinoma cell invasion and metastasis is unclear.

Rabs are activated by guanine-nucleotide exchange factors (GEFs) that catalyze the exchange of GDP for GTP. The DENN (differentially expressed in normal and neoplastic cells) domain is an evolutionarily ancient and structurally conserved protein module (Levivier et al., 2001;Harsay and Schekman, 2007;Marat et al., 2011;Wu et al., 2011b;Nookala et al., 2012) that functions as a GEF for multiple Rabs (Allaire et al., 2010;Marat and McPherson, 2010;Yoshimura et al., 2010). Currently, there are 26 identified DENN domain proteins (Marat et al., 2011;Zhang et al., 2012;Levine et al., 2013), the majority of which are poorly characterized. One such protein, DENND2B, is a member of the DENND2A-D sub-family that contain a C-terminal DENN domain but few other distinguishing features (Marat et al., 2011). DENND2B was originally identified by screening a cDNA expression library for gene products that suppress the tumorigenicity of HeLa

cells in nude mice, and was named ST5 (suppression of tumorigenicity 5) (Oshimura et al., 1990;Lichy et al., 1992;Lichy et al., 1996). More recently, DENND2B was shown to function as a GEF for Rab9 (Yoshimura et al., 2010). However, the mechanism by which DENND2B regulates tumorigenicity and the potential role of its GEF activity in the control of membrane trafficking in this process remain unknown.

In exploring the role of DENND2B in membrane trafficking we have now discovered, through the use of multiple complementary approaches, that Rab13 is a specific substrate for DENND2B. Rab13 functions in exocytic membrane trafficking from the trans-Golgi network (TGN) to the cell surface via recycling endosomes in polarized epithelial cells (Nokes et al., 2008). Interestingly, Rab13 has also been indirectly implicated in cancer. For example, Rab13 levels are altered in both glioblastoma and carcinoma (Mo et al., 2013;Li et al., 2014b) and Rab13 mRNA is found in membrane protrusions of breast cancer cells (Jakobsen et al., 2013).

Here we demonstrate that DENND2B localizes to the cell surface in association with the actin regulatory protein MICAL-L2 (molecule interacting with CasL-like 2), a Rab13 effector that induces membrane ruffles when bound to active Rab13 (Baldassarre et al., 2009;Sakane et al., 2013). We develop and optimize a novel, FRET-based Rab13 biosensor that reveals selective activation of Rab13 on membrane ruffles at the dynamic leading edge of migrating cells, and we demonstrate that Rab13 activation by DENND2B at the cell surface is required for cell migration and invasion. Finally, we find that disruption of the Rab13/DENND2B trafficking pathway dramatically reduces the migration of highly aggressive breast cancer cells *in vivo*. These findings provide evidence for a DENND2B centered module that appears critical for the metastasis of cancer cells.

2.3 Results

2.3.1 DENND2B is a GEF for Rab13

To examine a potential role for DENND2B in membrane trafficking via Rab activation, we used the DENND2B DENN domain in an affinity-selection screen with a panel of GST-Rabs, including many of the proposed Rab substrates for DENN domain proteins. Flag-DENND2B DENN domain binds to Rab13 with minimal binding to other Rabs, including Rab9 (Fig. 2.1 A and S2.1 A). Notably, DENND2B does not bind to Rab8, which is highly conserved with Rab13 (Fig. S2.1 A). Consistent with previous reports (Allaire et al., 2010;Marat and McPherson, 2010), the DENN domain of connecdenn 1 binds strongly to Rab35 in similar assays (Fig. 2.1 B). In co-immunoprecipitation studies, full-length Flag-DENND2B interacts with Rab13 but not Rab9 (Fig. 2.1 C and S2.1 B). Thus, DENND2B interacts preferentially with Rab13.

To examine if Rab13 has a nucleotide preference in its interaction with DENND2B, we performed binding studies with GST-Rab13 T22N, a constitutively inactive GDP-bound mutant and GST-Rab13 Q67L, a constitutively active GTP-bound mutant. Flag-DENND2B prefers Rab13 T22N (Fig. 2.1 D), a hallmark of GEFs. To verify the GEF activity of DENND2B towards Rab13 we developed a Rab13 activation assay using the Rab13-binding domain (RBD) of MICAL-L1 (Abou-Zeid et al., 2011). We confirmed that GST-RBD binds to GFP-Rab13 Q67L but not GFP-Rab13 T22N (Fig. 2.1 E). Overexpression of full-length, Flag-DENND2B or its DENN domain results in an approximate two-fold increase in binding of endogenous Rab13 to GST-RBD (Fig. 2.1, F and G). Thus, DENND2B is a GEF for Rab13. Previous studies reported that connecdenn 3 possesses weak GEF activity towards Rab13 *in vitro* (Yoshimura et al., 2010). However, overexpression of Flag-

connecdenn 3, full-length or DENN domain does not increase the amount of active Rab13 in cells (Fig. 2.1, H and I).

2.3.2 DENND2B is required for invasive behaviour of epithelial cells

Scattering of epithelial cells induced by the tumor promoter 12-O-tetradecanoylphorbol-13-acetate (TPA) is a model for cell migration and invasion (Imamura et al., 1998), and knockdown of Rab13 decreases TPA-induced epithelial cell scattering (Kanda et al., 2008). We thus sought to examine the role of Rab13 and DENND2B in cell migration and invasion using MCF10A cells, a breast epithelial cell line expressing DENND2B (Fig. S2.2 A). When grown in a monolayer, MCF10A cells form adherent islands, with an epithelial-like morphology (Debnath et al., 2003). However, single cells are dynamic and will actively migrate towards each other to form such islands, or will invade through a thin-layer Matrigel barrier towards high serum when plated in serum-free media (Hu et al., 2014;Pignatelli et al., 2012). Interestingly, when we overexpressed RFP-Rab13 Q67L in MCF10A cells (Fig. S2.2, B and C) we noticed that a percentage of the cells acquired a spindle-like morphology with disruption of the adherent island arrangement, and this was not observed with overexpression of RFP or RFP-Rab13 T22N (Fig. 2.2 A and S2.2 C). An obvious feature of the morphological change is the elongation of the cells and the appearance of plasma membrane protrusions (Fig. 2.2 A). Using protrusion length as a measure of morphological change, we find that expression of GFP-DENND2B or mCherry-(mCh)-Rab13 alone are insufficient to induce a change in morphology but their co-expression induces protrusions similar to mCh-Rab13 Q67L (Fig. 2.2, A and B). Co-expression of mCh-Rab13 with GFP-connecdenn 3 fails to induce membrane protrusions (Fig. 2.2 B). Moreover, expression of active mCh-Rab9 Q66L, or co-expression of wild-type mCh-Rab9 and GFP-DENND2B also fail to induce membrane protrusions (Fig. 2.2 C). Therefore, activation of Rab13 by DENND2B mediates a morphological alteration of MCF10A cells.

As the physiological relevance of the morphological change induced by Rab13/DENND2B overexpression is unclear, we next examined whether Rab13 influences the invasiveness of MCF10A cells. We first grew MCF10A cells expressing RFP or RFP-Rab13 Q67L on a Geltrex matrix to form multi-cell colonies, after which we overlaid them with collagen and performed time-lapse imaging for 3 days. Expression of active Rab13 causes increased cell invasion into the collagen (Fig. 2.2, D-F and Video 2.1). We next examined the invasive behaviour of MCF10A cells in a loss-of-function paradigm, in which we plated MCF10A cells on a thin-layer of Matrigel on transwell membranes. Cells in serum-free media in the upper chamber migrate towards serum-containing media in the bottom chamber, a standard assay of cell invasiveness (Shaw, 2005). We used lentivirus to deliver two independent shRNAmiRs (Ritter et al., 2013), reducing DENND2B expression compared to a non-targeting shRNAmiR control (Fig. 2.2, G and H). Interestingly, knockdown of DENND2B significantly reduces the invasive capacity of MCF10A cells (Fig. 2.2, I and J) with no influence on total cell number or viability during the 14 h time course of the assay (Fig. S2.2, D and E). Together, these data indicate that DENND2B, through its activation of Rab13 is required for epithelial cell invasiveness. Whether or not this enhanced invasiveness correlates to a transformation of the cells is currently unknown.

2.3.3 DENND2B activates Rab13 selectively at the leading edge of migrating cells

To gain insight into the mechanism of Rab13-mediated changes in cell morphology and invasion, we sought to identify the cellular site of Rab13 activation. GFP-DENND2B localizes predominantly to the cell periphery where it co-localizes with actin (Fig. 2.3 A). Rab13 also localizes to the cell periphery with additional pools in the perinuclear region and on cytoplasmic vesicles (Fig. 2.3, A-G).

Interestingly, Rab13 and DENND2B co-localize predominantly at the actin-rich leading edge (Fig. 2.3, A and B).

Consistent with previous studies (Nokes et al., 2008), the perinuclear pool of Rab13 partially co-localizes with TGN46, which at steady-state is found prominently at the TGN, as well as with recycling endosomes labelled with internalized transferrin (Fig. 2.3, C, D and G). There is little or no co-localization with TIP47 and LAMP-1, markers of late endosomes and late endosomes/lysosomes, respectively (Fig. 2.3, E, F and G). Live-cell imaging reveals that wild-type mCh-Rab13 travels on vesicles from the perinuclear region to the cell periphery, where a subset of vesicles appear to associate closely with the plasma membrane, leading to a pool of Rab13 on the cell surface (Fig. 2.4 A, Video 2.2 and Video 2.3). Vesicles are also seen to move away from the surface and it is not currently known if there is a net anterograde flow. mCh-Rab13 Q67L shows a similar trafficking behaviour and also accumulates on the plasma membrane (Fig. 2.4 B and Video 2.4). Surprisingly, mCh-Rab13 T22N also travels on vesicles, however, it does not accumulate on the plasma membrane (Fig. 2.4 C and Video 2.5). We thus speculate that Rab13 travels on vesicles to the cell periphery where it encounters its GEF, DENND2B. This allows for localized activation and association with the plasma membrane.

To directly test our model of localized Rab activation at the plasma membrane, we designed a genetically encoded, single-chain biosensor that uses Förster resonance energy transfer (FRET) for temporal and spatial detection of Rab13 activation. The design of the biosensor is based on that previously reported for a RhoA biosensor (Pertz et al., 2006). From N- to C-terminus, the biosensor encodes the RBD of MICAL-L2, which binds specifically to active Rab13, monomeric Cerulean3 (mCer3) fluorescent protein, an unstructured linker, monomeric circularly permutated Venus (mVen)

fluorescent protein and full-length Rab13 (Fig. 2.5, A and S2.3 A). This design maintains the correct C-terminal structure of the GTPase to preserve prenylation (Pertz et al., 2006). In principle, when Rab13 is activated it will bind the RBD, altering the mCer3 and mVen dipole-coupling state to modulate FRET (Fig. 2.5 A). We first tested and optimized the biosensor construction, measuring the emission spectra in live HEK-293 cells in suspension as described (Pertz et al., 2006). Inserting 3 repeats of an 18 amino acid linker (Whitlow et al., 1993) gives optimal differences in the FRET to mCer3 ratio of the Rab13 Q67L biosensor versus the Rab13 T22N form (Fig. S2.3 B), as does the circular permutation cp229 of mVen (Nagai et al., 2004) (Fig. S2.3 C). The optimized Rab13 Q67L biosensor shows approximately 53% higher FRET/mCer ratio intensity at 524 nm than does the Rab13 T22N biosensor (Fig. 2.5 B and S2.3 D), while the average FRET efficiencies are approximately 17% and 2.5%, respectively (Fig. S2.3 E and F). The enhanced efficiency of the Rab13 Q67L biosensor can also be visualized by ratio imaging in adherent mouse embryonic fibroblasts (MEFs) (Fig. 2.5 C).

As binding of the biosensor to endogenous proteins (effectors or other Rabs) could conceivably influence the FRET signal, we tested whether the biosensor prefers intra- or intermolecular interactions. We created a Rab13-Q67L biosensor in which we replaced the RBD with the Cdc42/Rac1 interactive binding (CRIB) domain from p21-activated kinase (PAK) (Moshfegh et al., 2014). The Rab13-Q67L-PAK-CRIB biosensor shows a lower FRET/mCer ratio compared to Rab13-Q67L-RBD, confirming that the PAK-CRIB domain does not interact with active Rab13 (Fig. S2.3 G). Next, using pull-down assays we find that GST-RBD binds to the Rab13-Q67L-PAK-CRIB biosensor, which lacks intramolecular interactions, but not the Rab13-Q67L-RBD biosensor that has intramolecular interactions (Fig. S2.3 H). This demonstrates that the biosensor prefers intramolecular interactions and that other effectors or Rabs are unlikely to outcompete for binding to the biosensor.

Next, we confirmed that the wild-type biosensor shows the same distribution in MCF10A cells as wild-type Rab13 (Fig. S2.3 I). Finally, we co-expressed wild-type Rab13 biosensor with Flag-DENND2B, full-length or DENN domain, and the DENN domain of connecdenn 1, and observed that DENND2B expression enhances the FRET signal while connecdenn 1 does not (Fig. 2.5 D).

With this characterization in hand, we expressed the biosensor in MCF10A cells and observed robust activation of wild-type Rab13, predominantly at the cell periphery (Fig. 2.5 E). Remarkably, we also observe Rab13 activation at the leading edge of randomly migrating cells (Fig. 2.5 F and Video 2.6), with waves of Rab13 activation at sites of plasma membrane protrusions (Video 2.6). As the ratiometric imaging measurements were made using widefield microscopy, we tested the extent to which cell volume could influence these measurements using a previously developed model (Spiering et al., 2013). We determined that the distribution of the biosensor activity is significantly different from what would be obtained purely based on the volumetric variation (Fig. S2.3 J). Thus, the measured activation patterns are not influenced by the variability in cell thickness. These results confirm that Rab13 activation occurs at the cell periphery, where DENND2B and Rab13 co-localize, and further support a model where local activation of Rab13 by DENND2B contributes to the dynamics of the plasma membrane and the development of a leading edge during cell migration and invasion.

2.3.4 DENND2B functions in a complex with the Rab13 effector MICAL-L2

We next sought to identify determinants in DENND2B required for its localized activation of Rab13. We thus generated a series of DENND2B constructs (Fig. 2.6 A) that we tested for their ability to localize to actin (Fig. 2.6 B) and alter cell morphology when co-expressed with mCh-Rab13 (Fig. 2.6

C). In order to clearly distinguish DENND2B localized to actin, we examined the co-localization of DENND2B with actin stress fibres in HeLa cells (Fig. 2.6 B). As previously demonstrated (Fig. 2.2 B and 2.3 A), full-length DENND2B co-localizes with actin and induces membrane protrusions (Fig. 2.6, B and C). In contrast, the isolated DENN domain is predominantly soluble (Fig. 2.6 B) and does not induce membrane protrusions in the presence of Rab13 (Fig. 2.6 C), despite the fact it activates Rab13 in cells (Fig. 2.1, F-G and 2.5 D). It is likely that the isolated DENN domain fails to alter cell morphology because Rab13 activation occurs away from the cell periphery. A DENND2B N-terminal construct [DENND2B (N-term)] also fails to induce morphological changes despite the fact it has a similar localization as the full-length protein (Fig. 2.6, B and C). This was expected as it lacks the DENN domain. Intriguingly, a DENND2B construct with deletion of the last 17 amino acids [DENND2B (ΔC)], which are C-terminal of the DENN domain, also fails to induce morphological alterations despite the fact it contains the DENN domain and has a similar localization as full-length protein (Fig. 2.6, B and C). Thus, in addition to localized activation of Rab13 on actin, DENND2B must contain the evolutionarily conserved C-terminal 17 amino acid region (Fig. 2.6 D) in order to induce morphological changes required for invasive behaviour.

We hypothesized that the C-terminal region of DENND2B interacts with a protein required for DENND2B/Rab13-mediated alterations in cell morphology. MICAL-L2 is a Rab13 effector (Fig. 2.7 A; (Nishimura and Sasaki, 2008a), which upon binding Rab13 undergoes a conformational change that induces its association with the actin-binding filamin proteins, and both filamins and MICAL-L2 are required to induce actin changes causing membrane ruffling associated with cell migration (Baldassarre et al., 2009;Sakane et al., 2013). Moreover, like Rab13, MICAL-L2 is required for TPA-induced scattering of epithelial cells (Kanda et al., 2008). Remarkably, MICAL-L2, but not the related Rab13 effector MICAL 1, binds to the 17 amino acid C-terminal region of DENND2B (Fig.

2.7, A and B) (Fukuda et al., 2008). Moreover, full-length DENND2B, but not DENND2B lacking the C-terminal region, co-immunoprecipitates with MICAL-L2 (Fig. 2.7 C). Finally, DENND2B and MICAL-L2 co-localize at the cell periphery (Fig. 2.7 D) and expression of MICAL-L2 in the presence of Rab13 induces similar morphological changes as those seen with expression of DENND2B (Fig. 2.7 E). Thus, DENND2B interacts with the Rab13 effector MICAL-L2 and this interaction is required for the morphological alterations observed in MCF10A cells.

We propose a model in which Rab13 is delivered on vesicles to the cell surface where it encounters DENND2B in a complex with MICAL-L2 (Fig. 2.7 F). This serves to ensure that MICAL-L2 is present at sites of Rab13 activation. Once activated, Rab13 stimulates MICAL-L2 to induce the formation of membrane ruffles while active Rab13 vesicles fuse with the plasma membrane to supply new membrane or deliver cargo, such as integrins (Nishikimi et al., 2014), required for migratory/invasive behaviour. In this manner, DENND2B coordinates actin dynamics with vesicle delivery contributing to the formation of a dynamic leading edge for cell migration and invasion.

2.3.5 Rab13 knockdown reduces cancer cell migration and invasion *in vitro*

We next sought to examine the role of the Rab13 pathway in migration/invasion in a disease model and thus turned to MDA-MB-231-1833TR and BT549 breast cancer cells. We used lentivirus to deliver up to three independent shRNA sequences targeting Rab13, leading to efficient, stable Rab13 knockdown in both cell types (Fig. 2.8 A-D). Rab13 knockdown significantly reduces the migratory rate of both cell lines (Fig. 2.8, E and F). We then focused on the 1833TR cells as they have been selected for their robust metastatic capacity (Kang et al., 2003;Kang et al., 2003). Rab13 knockdown strongly decreases the ability of 1833TR cells to invade through Matrigel-coated membranes (Fig. 2.9, A and B) with no influence on cell number or viability over the time course of the experiment

(Fig. 2.9, C and D). However, when measured over several days, Rab13 knockdown does significantly decreased cell proliferation (Figure 2.9, E and F). Thus, in highly metastatic breast cancer cells, Rab13 is required for cell migration, invasion and proliferation, three key aspects of carcinoma progression.

2.3.6 Rab13 knockdown reduces spread of cancer cells *in vivo*

We next tested the involvement of Rab13 in invasive tumor growth *in vivo.* 1833TR cells with stable expression of control vector or Rab13-specific shRNA sequences (Fig. 2.8, A and B) were injected into the tail veins of nude mice as previously described (Knight et al., 2013). The cells also stably express a luciferase cassette allowing for analysis of tumor growth using *in vivo* bioluminescent imaging (Mourskaia et al., 2012). Mice were imaged shortly after injection (Day 0) to confirm seeding of control and Rab13 shRNA cells in the lung microenvironment (Fig. 2.10 A and S2.4). Monitoring of tumor growth by luciferase activity 9 weeks post-injection reveals higher rates of tumor take (80%) in mice injected with control cells compared to those injected with Rab13 shRNA cells (56%) (Fig. 2.10, A and B). Among mice positive for tumors, injection with control cells generates significantly higher luciferase activity 63 days post-injection than Rab13 shRNA cells, which reflects a greater tumor burden (Fig. 2.10, A, C and S2.4). Consistently, histological analysis of lung sections show that mice injected with control cells have larger tumors and a significantly higher number of lung lesions per mouse relative to Rab13 shRNA cells (Fig. 2.10, D and E). While lung lesions from both control and Rab13 shRNA cells demonstrate extravasation and proliferation external to blood vessels indicative of invasive growth, control cells also appeared in other tissues including mammary fat pad, lymph nodes, and bone, reflecting the high metastatic capacity of the cell line (Fig. 2.10 F and S2.4). Remarkably, of those mice positive for lung tumor growth, 62% of mice injected with control cells exhibited cancer cells spread outside of the lungs compared to only

11% of mice injected with Rab13 knockdown cells (Fig. 2.10 G and S2.4). This demonstrates that Rab13 knockdown robustly diminishes the ability of aggressive tumor cells to migrate to new locations despite proliferation in the lung microenvironment. Coupled with the observation that *RAB13* is amplified in multiple tumor types (Fig. 1.1;(Cerami et al., 2012;Gao et al., 2013), our data suggest that Rab13 can promote tumor development and demonstrate that Rab13 knockdown diminishes the growth and spread of highly metastatic cancer cells *in vivo*.

2.4 Discussion

2.4.1 DENND2B is a Rab13 GEF

The identification of DENN domain proteins as a diverse family of Rab GEFs (Allaire et al., 2010;Yoshimura et al., 2010), coupled with the recognition that Rab-mediated membrane trafficking controls the key cellular phenotypes that drive cancer cell biology (Goldenring, 2013;Mellman and Yarden, 2013;Caswell and Norman, 2006;Caswell and Norman, 2008), emphasizes the need to understand the cell physiological relationships between DENN domain proteins and their Rab substrates. Here we present multiple lines of evidence that Rab13 is a physiologically relevant substrate for DENND2B. While it is possible that DENND2B could activate Rab13 indirectly, this seems unlikely as Rab13 and DENND2B interact in pull-down and co-immunoprecipitation assays in a nucleotide dependent manner. Moreover, co-expression of DENND2B and Rab13 cause the same morphological change of cells as that seen with an active Rab13 mutant, and knockdown of either protein decreases the invasive capacity of cells. A previous study reported that all members of the DENND2 family activate Rab9 and consistently, knockdown of DENND2A or Rab9 results in enlarged late endosomes positive for LAMP-1 (Yoshimura et al., 2010). However, knockdown of DENND2B has no effect on the morphology of late endosomes, suggesting that it may act on a

different Rab (Yoshimura et al., 2010). Yoshimura and colleagues (2010) note that while Rab9 is expressed in *Drosophila,* the DENND2 family is not and therefore a GEF other than DENND2 family members must be able to activate Rab9. In fact, DENND2B is absent from all invertebrates including *c. elegans,* the mollusc *Lottia*, and the eel-like invertebrate *Branchiostoma*, a close relative of vertebrates. DENND2B is however present in vertebrates including fish and thus appears to have evolved early in the vertebrate lineage. Interestingly, Rab13 is also absent from invertebrates including *Branchiostoma* and appears to have diverged from its close homologue Rab8 (which is present throughout eukaryotes) in the vertebrate lineage (Klopper et al., 2012). Thus, DENND2B may have evolved in response to the evolution of a new vertebrate Rab.

2.4.2 Localized activation of Rab13 at the plasma membrane leading edge

An intriguing finding of this study is the trafficking of inactive Rab13 on vesicles. The majority of Rabs are thought to associate with membranes upon activation (Goody et al., 2005) and to be extracted from membranes by GDP dissociation inhibitors (GDIs) once they switch to the inactive, GDP-bound form (Pfeffer et al., 1995). However, this does not seem to be the case for all Rabs (Allaire et al., 2010) and Rab13 is notable in that it resists membrane extraction by GDI (Marzesco et al., 1998). Only when the Rab13-labeled vesicles reach the plasma membrane is Rab13 activated by DENND2B, allowing for its association with the plasma membrane. Thus, the primary function of Rab13 appears to be in the fusion or association of TGN/endosome derived transport vesicles with the plasma membrane. The use of the Rab13 biosensor has been paramount in elucidating this mechanism of Rab13 activation. While this type of technology has been applied extensively to the study of GTPases such as Ras, RhoA and Cdc42 (Pertz et al., 2006;Nalbant et al., 2004;Mochizuki et al., 2001;Hanna et al., 2014;Moshfegh et al., 2014), to our knowledge only one other Rab biosensor has been reported (Kitano et al., 2008). Given that there are approximately 70 mammalian Rabs

regulating trafficking at nearly all cellular compartments, future development of Rab biosensors, based on the proof-of-principle concept presented here, will be extremely valuable in understanding how they function.

2.4.3 DENND2B functions in a complex with MICAL-L2

In addition to demonstrating that DENND2B is a GEF for Rab13, we discovered that DENND2B binds to the Rab13 effector MICAL-L2 and associates with MICAL-L2 at the cell periphery. This interaction would serve to concentrate MICAL-L2 at sites where Rab13 is being activated and is necessary for morphological alteration of cells. Such a positive GEF-effector feedback loop has been previously described. In yeast, Sec2p acts as a GEF for the small GTPase Sec4 and binds the Sec4 effector molecule Sec15 on the surface of secretory vesicles to facilitate tethering to the plasma membrane (Walch-Solimena et al., 1997;Guo et al., 1999;Medkova et al., 2006). In mammalian cells, Rab5 is activated by its GEF, Rabex-5, and recruits its effector Rabaptin-5. Rabaptin-5 not only binds to Rabex-5 but enhances its GEF activity for Rab5 (Lippe et al., 2001). Similarly, Cdc42 is activated by its GEF, intersectin, and intersectin binds the Cdc42 effector N-WASP, which further enhances intersectin's GEF activity (Hussain et al., 2001). It will thus be interesting to determine if MICAL-L2 binding enhances the GEF activity of DENND2B.

2.4.4 DENND2B and Rab13 promote cancer phenotypes

A key finding of this study is that the DENND2B/Rab13 pathway promotes migration of cancer cells *in vivo*. During metastasis, epithelial cells exhibit loss of cell-cell contact. Previous studies have shown that knockdown of Rab13 or MICAL-L2 reduces levels of the tight junction proteins claudin-1 and occludin at the plasma membrane (Yamamura et al., 2008). Given the role of Rab13 in vesicle fusion, this could involve alterations in the delivery of these proteins to the cell surface. Rab13 could

also modulate tight junctions indirectly through its effects on actin (Sakane et al., 2012). In fact, tight junction formation relies heavily on F-actin organization. For instance, the actin nucleator Arp2/3 is essential for the assembly of tight junctions and Arp2/3 knockdown causes severe defects in tight junctions of developing embryonic epidermis (Zhou et al., 2013). This is not surprising considering that claudin-1 and occludin are linked to actin by zona occludin-1 (Fanning et al., 1998). Thus, the reported effects of Rab13 on tight junction formation could be explained by its regulation of cortical actin through MICAL-L2.

Metastasis also requires migration of cancer cells away from the primary tumor. Here we demonstrate that Rab13 controls the migration of tumor cells from the lungs to secondary sites. Moreover, we show that Rab13 is activated at the leading edge of migrating cells where actin is being dynamically remodelled. This is consistent with the reported role of Rab13 and MICAL-L2 in cell scattering as inactive Rab13 or MICAL-L2 knockdown inhibit TPA-induced epithelial cell scattering (Kanda et al., 2008). Under normal conditions, MICAL-L2 is auto-inhibited (Sakane et al., 2010). However, local activation of Rab13 by DENND2B at the leading edge relieves this inhibition allowing for actin remodelling through interaction with the actin-binding protein filamin (Sakane et al., 2013). Expression of constitutively active mutants of MICAL-L2 induces the formation of membrane ruffles (Sakane et al., 2013), a process that also depends on filamins (Baldassarre et al., 2009). Thus, the association of DENND2B with MICAL-L2 would allow actin rearrangements to be coupled to new membrane fusion required for cell migration. Through this mechanism, amplification of RAB13 as seen in several cancer types would cause enhanced invasive capacity of cancerous cells.

The ability of DENND2B to promote phenotypes consistent with metastasis and tumorigenicity appears at odds with previous reports that it is a suppressor of tumorigenicity (Lichy et al., 1992). In fact DENND2B was initially discovered as a suppressor of tumorigenicity by screening a cDNA expression library for genes that reduce tumorigenicity of HeLa cells when injected into nude mice (Lichy et al., 1992). However, in addition to the full-length form of DENND2B studied here, a shorter, 70 kDa isoform (p70) exists that contains a truncated N-terminal region. Interestingly, p70 is produced from a distinct promoter and only p70 levels, not full length DENND2B, have been correlated to tumor suppression in cancer cell lines (Lichy et al., 1996). In fact, p70 was found to inhibit DENND2B signalling to restore contact dependent growth (Majidi et al., 2000;Hubbs et al., 1999). We now demonstrate that DENND2B activates Rab13 at the cell surface to promote cell invasiveness and phenotypes consistent with tumorigenicity. Given that the N-terminus is required for proper localization of DENND2B and that this site is absent from p70, perhaps p70 suppresses tumorigenicity by activating Rab13 away from the plasma membrane. This would be consistent with our finding that co-expression of Rab13 with the isolated DENN domain does not induce morphological changes of epithelial cells. It is possible that during cancer, when p70 is down regulated, there would be an increase in localized Rab13 activation on cortical actin resulting in increased metastatic capacity. It will be interesting in future studies to tease apart the functions of DENND2B isoforms in cancer in light of its role as a GEF for Rab13.

Rab GTPases are beginning to be recognized for their role in multiple types of cancer. It is now clear that Rab13 plays an important role in promoting tumorigenicity, but targeted therapies towards Rab13 may be difficult to achieve given the high degree of sequence homology across the Rab GTPase family. Characterization of Rab regulators, such as DENND2B, will provide a better

mechanistic understanding of how Rabs contribute to disease and increase the potential for therapeutic targets.

2.5 Figures

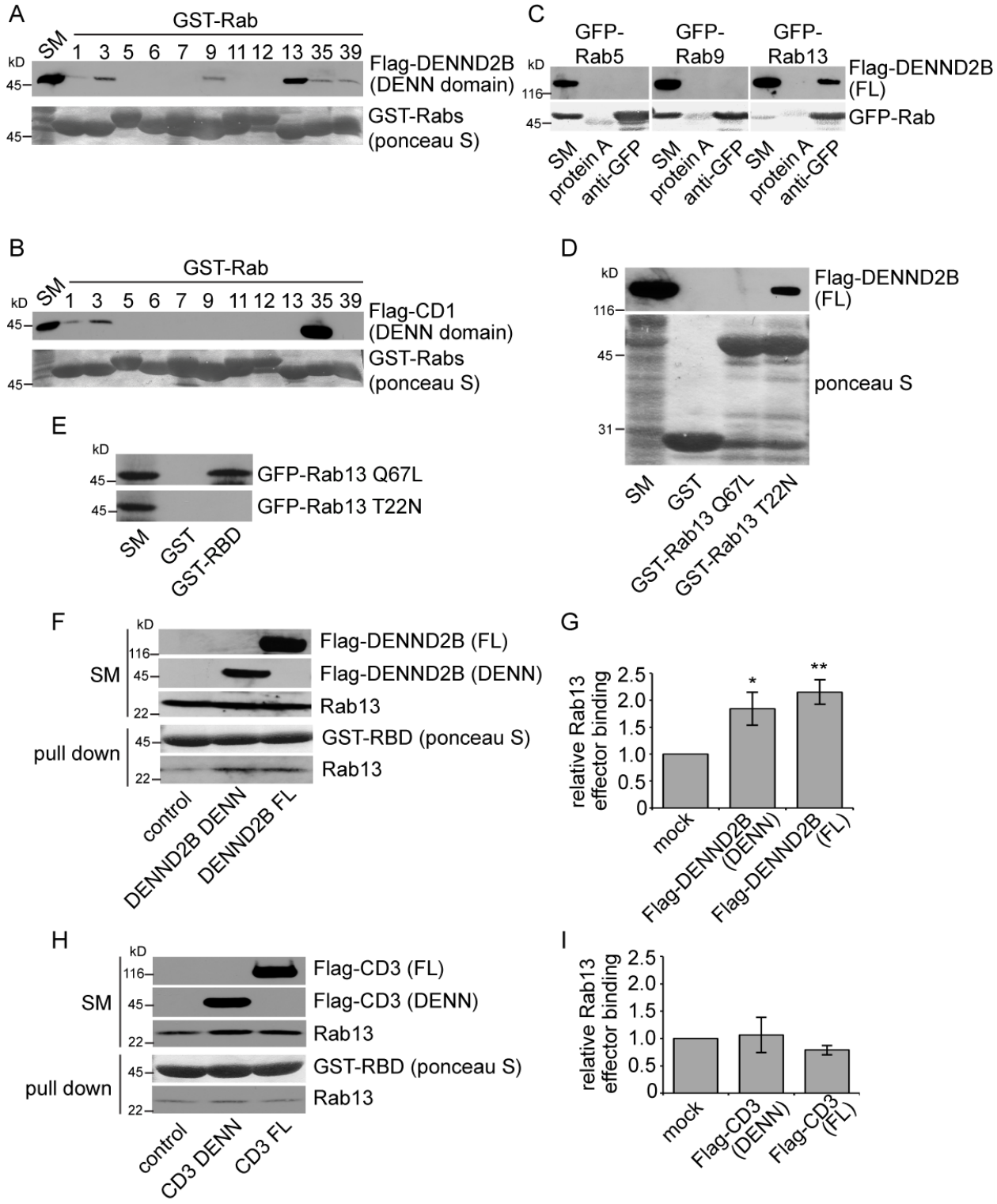

Figure 2.1

Figure 2.1.

DENND2B is a GEF for Rab13. (A-B) GST-Rabs, bound to glutathione beads, were incubated with HEK-293T cell lysates expressing (A) Flag-DENND2B DENN domain or (B) Flag-connecdenn 1 (CD1) DENN domain in the presence of 5 mM EDTA. Ponceau S staining reveals the level of GST-Rabs while specifically bound DENN domains were detected by blot. Starting material (SM) equals 10% of the lysate used per condition. (C) Lysates from HEK-293T cells co-expressing Flag-DENND2B full-length (FL) and GFP-Rabs were immunoprecipitated with anti-GFP antibody in the presence of 5 mM EDTA and the indicated proteins were detected by blot. (D) GST-Rab13 Q67L, T22N, or GST alone, bound to glutathione beads, were incubated with HEK-293T cell lysates expressing Flag-DENND2B full-length (FL) and analyzed as in A. (E) GST-RBD or GST alone, bound to glutathione beads, were incubated with HEK-293T cell lysates expressing GFP-Rab13 Q67L or T22N and analyzed as in A. (F-I) GST-RBD, bound to glutathione beads, was incubated with HEK-293T cell lysates expressing (F) full-length (FL) Flag-DENND2B, or DENN domain or (H) full-length (FL) Flag-connecdenn 3 (CD3), or DENN domain and analyzed as in A. (G) Quantification of F (mean ± SEM where n=7 for mock and DENN domain, n=6 for FL pooled from 4 independent experiments). (I) quantification of H (mean ± SEM where n=6 for mock and DENN domain, n=5 for FL pooled from 3 independent experiments; One-way ANOVA with Dunnett's post-test $p<0.05$, $**p<0.01$).

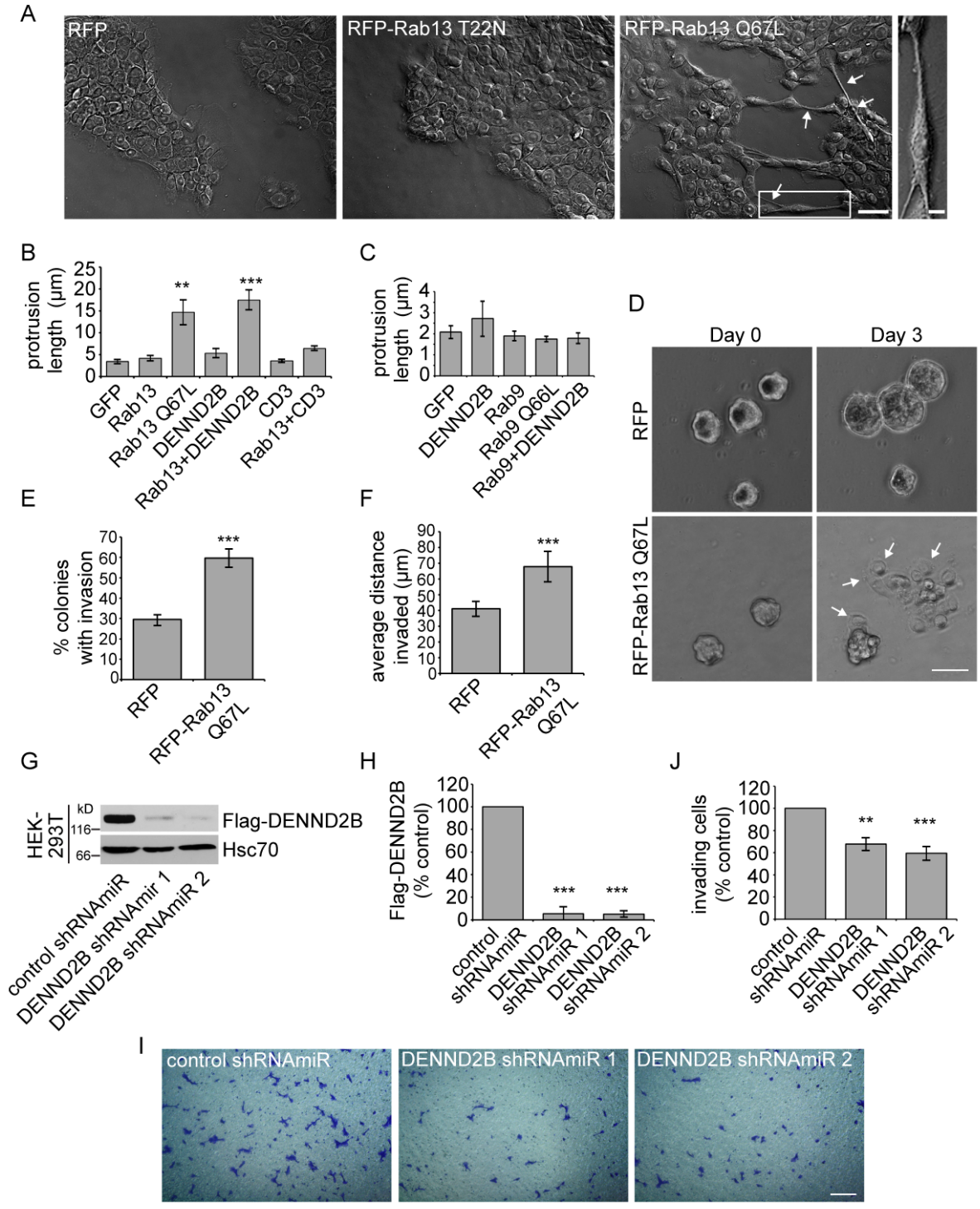
A
RFP
RFP-Rab13 T22N
RFP-Rab13 Q67L
B
protrusion length (μm)
GFP
Rab13
Rab13 Q67L
DENND2B
Rab13+DENND2B
CD3
Rab13+CD3
C
protrusion length (μm)
GFP
DENND2B
Rab9
Rab9 Q66L
Rab9+DENND2B
D
Day 0
Day 3
RFP
RFP-Rab13 Q67L
E
% colonies with invasion
RFP
RFP-Rab13 Q67L
F
average distance invaded (μm)
RFP
RFP-Rab13 Q67L
G
HEK-293T
kD
116
66
Flag-DENND2B
Hsc70
control shRNAmiR
DENND2B shRNAmir 1
DENND2B shRNAmiR 2
H
Flag-DENND2B (% control)
control shRNAmiR
DENND2B shRNAmiR 1
DENND2B shRNAmiR 2
J
invading cells (% control)
control shRNAmiR
DENND2B shRNAmiR 1
DENND2B shRNAmiR 2
I
control shRNAmiR
DENND2B shRNAmiR 1
DENND2B shRNAmiR 2

Figure 2.2

Figure 2.2.

Rab13 and DENND2B promote epithelial cell invasion. (A) MCF10A cells were transduced with lentivirus driving expression of RFP, RFP-Rab13 T22N or Q67L. Cells were fixed and imaged using differential interference contrast microscopy. Arrows indicate the presence of plasma membrane protrusions. Scale bars represent 50 μm, low power view and 10 μm, for the magnified view. (B) Protrusion length of transfected MCF10A cells was quantified (mean ± SEM from a minimum of 3 independent experiments measuring a minimum of 40 cells per condition per experiment; one-way ANOVA with Dunnett's post-test, **p<0.01, ***p<0.001). (C) Transfected MCF10A cells were quantified as in B (Mean ± SEM from 3 independent experiments measuring a minimum of 45 cells per condition per experiment). (D) Invasion of MCF10A spheroids transduced with RFP or RFP-Rab13 Q67L into collagen matrix. Scale bar represents 50 μm. Arrows indicate invading cells. The images correspond to Video 2.1. (E-F) Quantification of the invasion from D (mean ± SD from 3 independent experiments measuring a minimum of 10 spheroids per condition per experiment, Student's t-test, ***p<0.001). (G) Flag-DENND2B expressing HEK-293T cells were transduced with control shRNAmiR or two different shRNAmiRs targeting DENND2B and the indicated proteins were detected by blot. (H) Quantification of Flag-DENND2B levels from G normalized to Hsc70 and expressed relative to the control shRNAmiR cells (mean ± SD from 3 independent experiments; statistical analysis employed as in B). (I) MCF10A cells transduced with the indicated shRNAmiRs were plated on Matrigel-coated membranes for 14 h, and cells that invaded through the membranes were fixed and stained with Crystal violet. Scale bar represents 300 μm. (J) Quantification of MCF10A cell invasion from I normalized to control shRNAmiR cells (mean ± SEM from 4 independent experiments measuring 24 fields of view per condition per experiment, statistical analysis employed as in B).

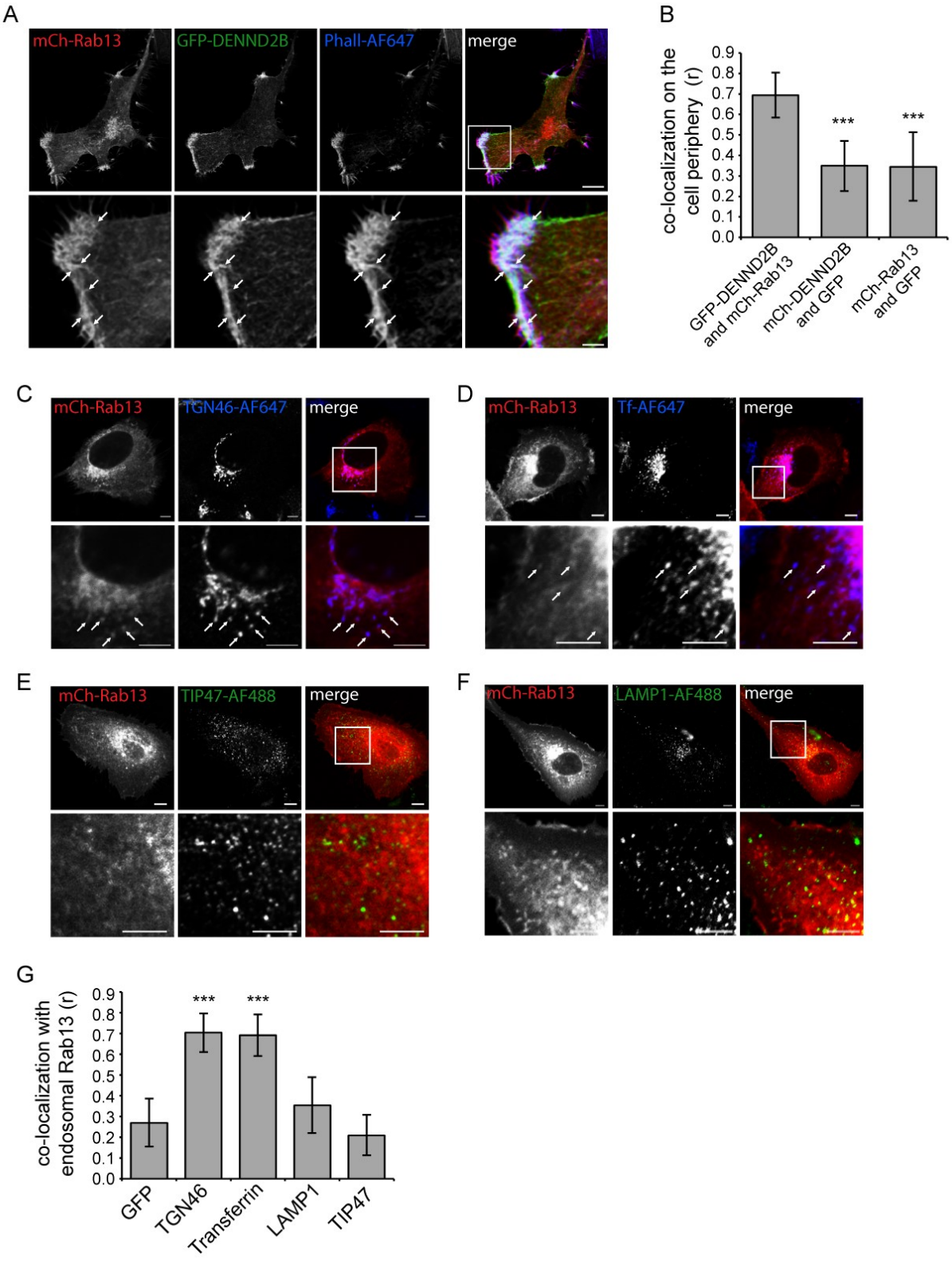
A
mCh-Rab13
GFP-DENND2B
Phall-AF647
merge
B
co-localization on the cell periphery (r)
0.9
0.8
0.7
0.6
0.5
0.4
0.3
0.2
0.1
0.0
***
***
GFP-DENND2B and mCh-Rab13
mCh-DENND2B and GFP
mCh-Rab13 and GFP
C
mCh-Rab13
TGN46-AF647
merge
D
mCh-Rab13
Tf-AF647
merge
E
mCh-Rab13
TIP47-AF488
merge
F
mCh-Rab13
LAMP1-AF488
merge
G
co-localization with endosomal Rab13 (r)
0.9
0.8
0.7
0.6
0.5
0.4
0.3
0.2
0.1
0.0
***
***
GFP
TGN46
Transferrin
LAMP1
TIP47

Figure 2.3

Figure 2.3.

Rab13 co-localizes with DENND2B at the cell's leading edge (A) MCF10A cells were co-transfected with GFP-DENND2B and mCh-Rab13, fixed, and stained with Phalloidin-AF647. Scale bar represents 10 and 2.5 μm for low and high magnification images, respectively. (B) Quantification of co-localization at the cell periphery using Pearson correlation coefficient (mean ± SD measuring 10 cells per condition pooled from 2 independent experiments, one-way ANOVA with Dunnett's post-test, ***$p<0.001$). (C-F) MCF10A expressing mCh-Rab13 were fixed and labeled with TGN46-AF647 (C) internalized transferrin-AF647 (D) TIP47-AF488 (E) or LAMP-1-AF488 (F). Arrows point to co-localizing structures. Scale bars represent 5 μm. (G) Quantification of co-localization from C-F as described in B.

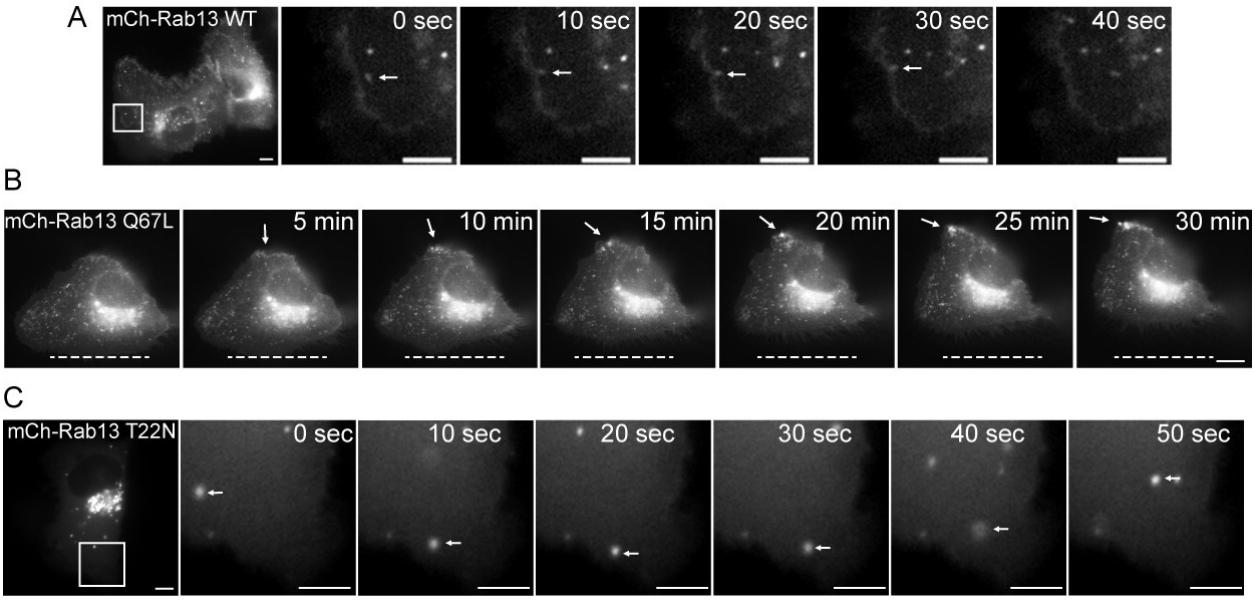

Figure 2.4

Figure 2.4.

Active Rab13 accumulates at the cell's leading edge (A) MCF10A cells expressing wild-type (WT) mCh-Rab13 were imaged live. The arrow follows a vesicle that appears to fuse with the plasma membrane. The images correspond to Videos 2.2 and 2.3 (B) MCF10A cells expressing mCh-Rab13 Q67L were imaged live. The arrow indicates a site of vesicle accumulation. The dashed line indicates the starting position of the lagging edge. The images correspond to Video 2.4 (C) MCF10A cells expressing mCh-Rab13 T22N were imaged live. The arrow follows a vesicle that fails to associate with the plasma membrane. The images correspond to Video 2.5 Scale bar represents 10 μm for (A-C).

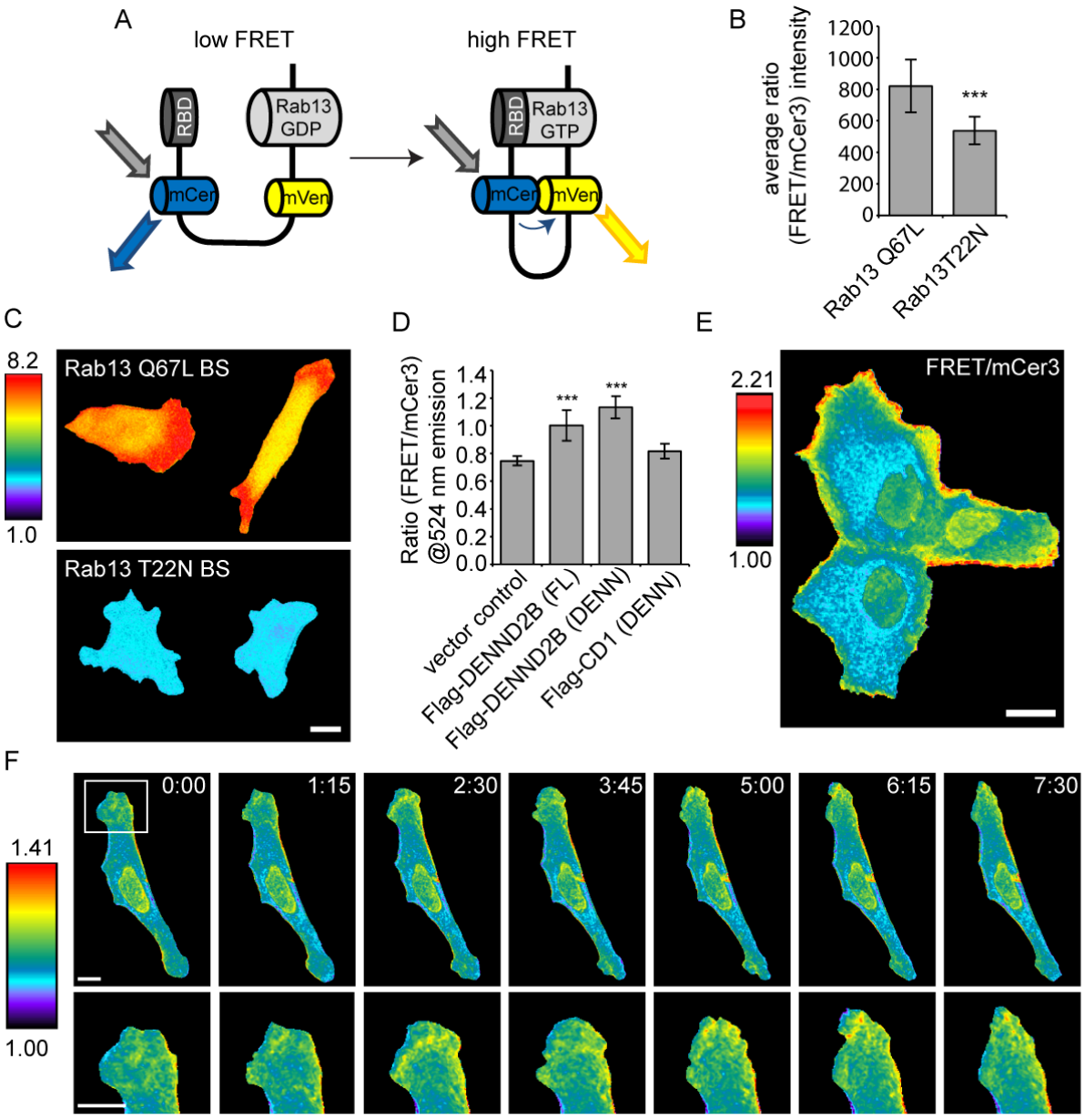
A
low FRET
high FRET
RBD
Rab13 GDP
mCer
mVen
RBD
Rab13 GTP
mCer
mVen
B
average ratio (FRET/mCer3) intensity
1200
1000
800
600
400
200
0
***
Rab13 Q67L
Rab13T22N
C
8.2
1.0
Rab13 Q67L BS
Rab13 T22N BS
D
Ratio (FRET/mCer3) @524 nm emission
1.4
1.2
1.0
0.8
0.6
0.4
0.2
0.0
***
***
vector control
Flag-DENND2B (FL)
Flag-DENND2B (DENN)
Flag-CD1 (DENN)
E
2.21
1.00
FRET/mCer3
F
1.41
1.00
0:00
1:15
2:30
3:45
5:00
6:15
7:30

Figure 2.5

Figure 2.5.

Rab13 activation occurs at the leading edge of migrating cells. (A) Schematic of a Rab13 biosensor. (B) Average emission ratio FRET/mCer3 of the optimized Q67L and T22N Rab13 biosensors in adherent MEFs using whole cell imaging (mean ± SD measuring 14 samples per condition pooled from 2 independent experiments, Student's t-test, **p<0.01). (C) Ratiometric image (FRET/mCer3) of the optimized Q67L and T22N Rab13 biosensors in MEFs using whole cell imaging. (D) Fluorometric analysis of HEK-293T cells in suspension co-expressing Rab13 biosensor and RabGDI with empty vector, Flag-DENND2B FL or DENN domain and Flag-connecdenn 1 (CD1) DENN domain (mean ± SD measuring 6 samples per conditions pooled from 2 independent experiments, one-way ANOVA with Dunnett's post-test,***p<0.001). (E) Ratiometric image (FRET/mCer3) of Rab13 WT biosensor in MCF10A cells. (F) Ratiometric image (FRET/mCer3) of Rab13 biosensor WT in a randomly migrating MEF. The images correspond to Video 2.6. Time in min:sec is indicated. Scale bars represent 10 μm for (C, E and F).

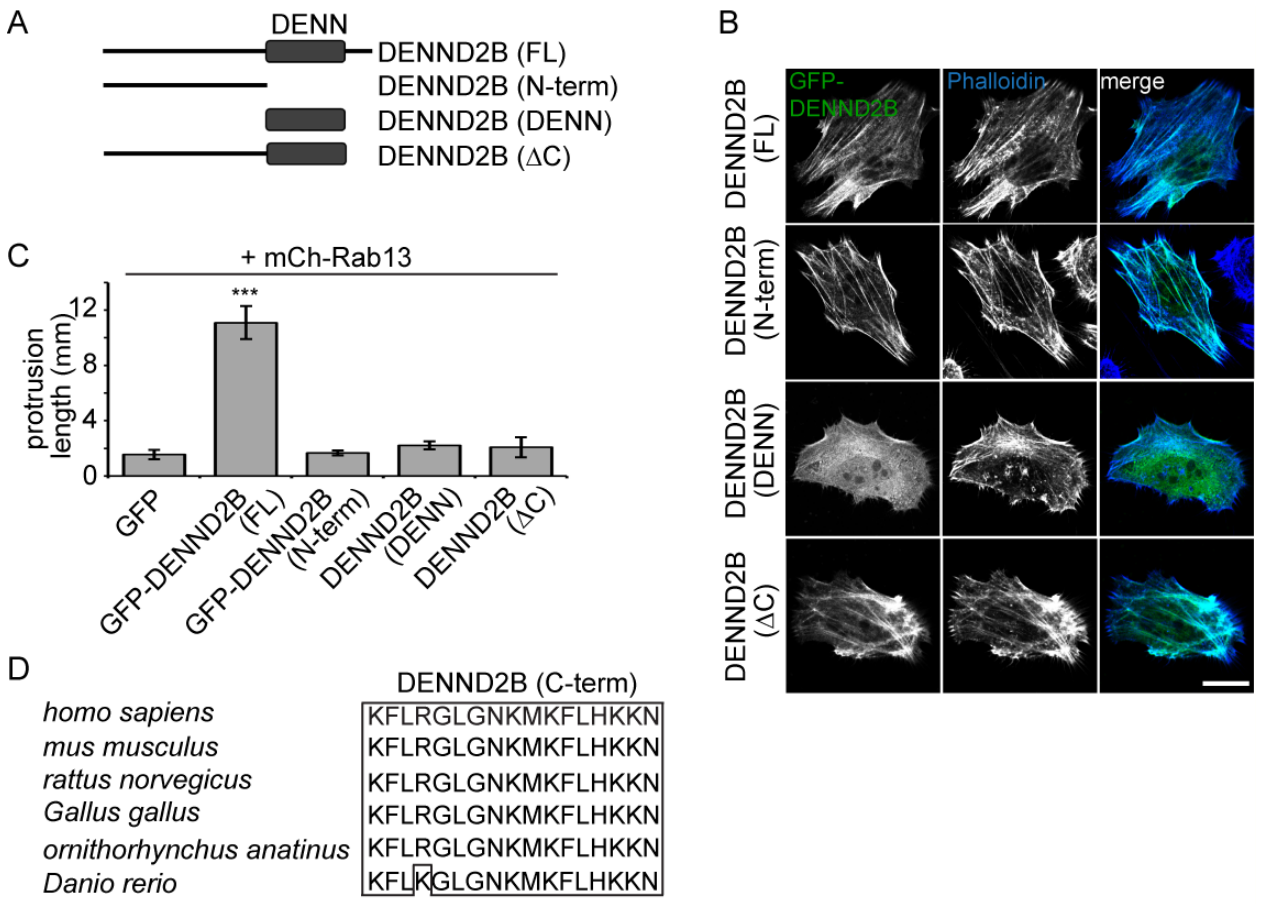

Figure 2.6

Figure 2.6.

DENND2B C-terminal region is required for the morphological transformation of MCF10A cells. (A) Schematic of DENND2B constructs used in these experiments. (B) HeLa cells were transfected with the indicated GFP-DENND2B constructs, fixed and processed for fluorescence for GFP and Phalloidin-AF647. Scale bar represents 10 µm. (C) Protrusion length of MCF10A cells co-transfected with mCh-Rab13 and the indicated constructs was quantified (mean ± SEM from a minimum of 3 independent experiments measuring a minimum of 25 cells per condition per experiment, one-way ANOVA with Dunnett's post-test, ***$p<0.001$). (D) Sequence of the 17 C-terminal residues of human DENND2B aligned to the indicated species. Identical residues are boxed.

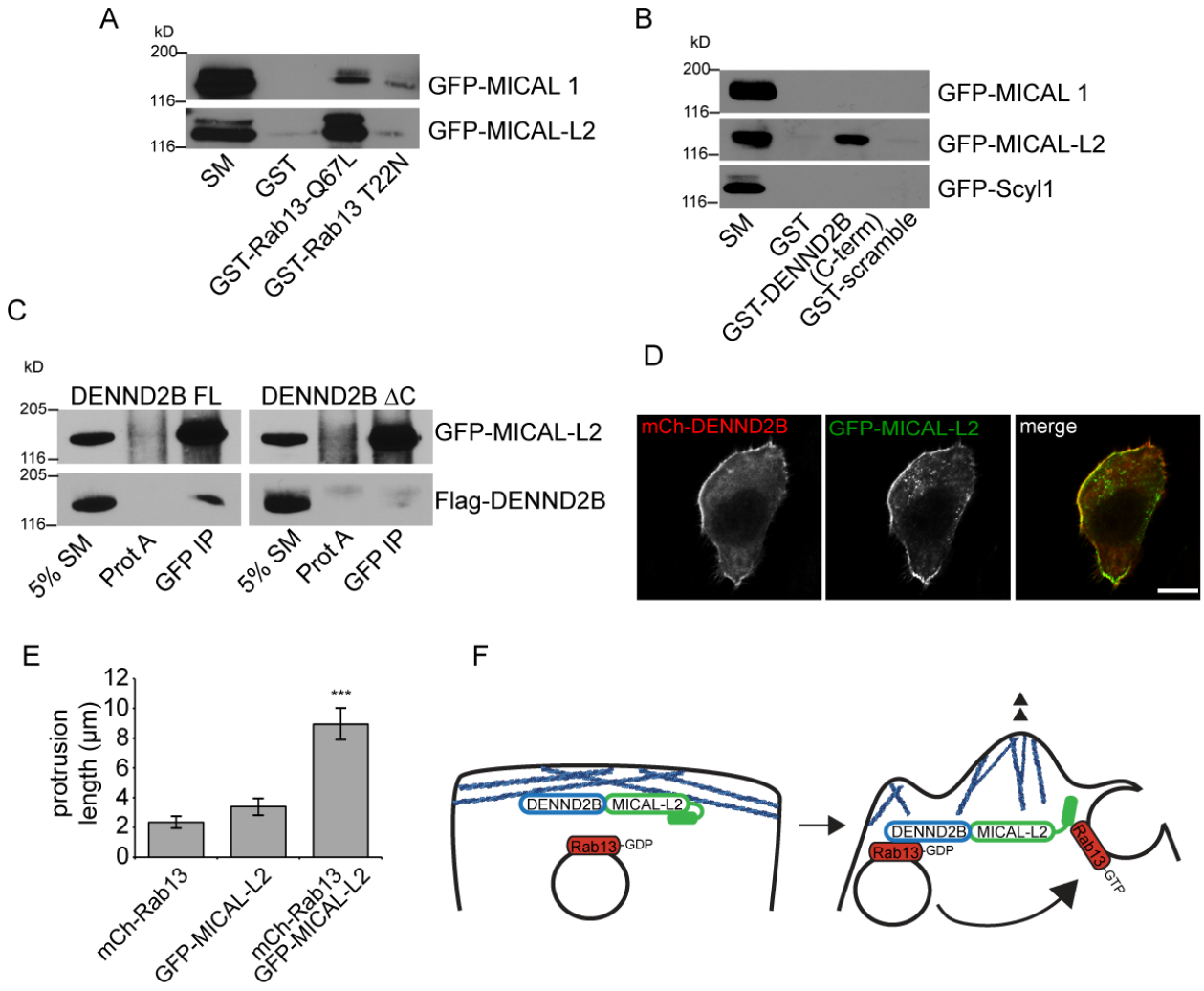
A
kD
200
116
116
GFP-MICAL 1
GFP-MICAL-L2
SM
GST
GST-Rab13-Q67L
GST-Rab13 T22N
B
kD
200
116
116
116
GFP-MICAL 1
GFP-MICAL-L2
GFP-Scyl1
SM
GST
GST-DENND2B (C-term)
GST-scramble
C
kD
DENND2B FL
DENND2B ΔC
205
116
205
116
GFP-MICAL-L2
Flag-DENND2B
5% SM
Prot A
GFP IP
5% SM
Prot A
GFP IP
D
mCh-DENND2B
GFP-MICAL-L2
merge
E
protrusion length (μm)
12
10
8
6
4
2
0
***
mCh-Rab13
GFP-MICAL-L2
mCh-Rab13 GFP-MICAL-L2
F
DENND2B
MICAL-L2
Rab13-GDP
DENND2B
MICAL-L2
Rab13-GDP
Rab13-GTP

Figure 2.7

Figure 2.7.

DENND2B C-term interacts with MICAL-L2 (A) GST-Rab13 Q67L or T22N, bound to glutathione beads were incubated with HEK-293T cell lysates expressing GFP-MICAL 1 or GFP-MICAL-L2 and the indicated proteins were detected by blot. Starting material (SM) equals 5% of the lysate used per condition. (B) GST-DENND2B C-terminal region or GST coupled to a scrambled version of that sequence, bound to glutathione beads, were incubated with HEK-293T cell lysates expressing GFP-MICAL 1, GFP-MICAL-L2 or GFP-Scyl1 and the indicated proteins were detected by blot. Starting material (SM) equals 2.5% of the lysate used per condition. (C) Lysates from HEK-293T cells co-expressing Flag-DENND2B full-length (FL) or FLAG-DENND2BΔC with GFP-MICAL-L2 were immunoprecipitated with anti-GFP antibody and the indicated proteins were detected by blot. (D) MCF10A cells were transfected with mCh-DENND2B and GFP-MICAL-L2, fixed and processed for fluorescence for GFP and mCh. Scale bar represents 10 μm. (E) Protrusion length of transfected MCF10A cells was quantified (mean ± SEM of 3 independent experiments measuring a minimum of 40 cells per conditions per experiment, one-way ANOVA with Dunnett's post-test,***$p<0.001$). (F) Proposed model whereby vesicles carrying GDP-bound Rab13 encounter DENND2B in a complex with MICAL-L2 on cortical actin (blue lines). DENND2B activates Rab13 and the Rab13-GTP-positive vesicles fuse with the plasma membrane. Rab13-GTP also binds to and opens MICAL-L2, which then stimulates actin assembly for the formation of membrane ruffles.

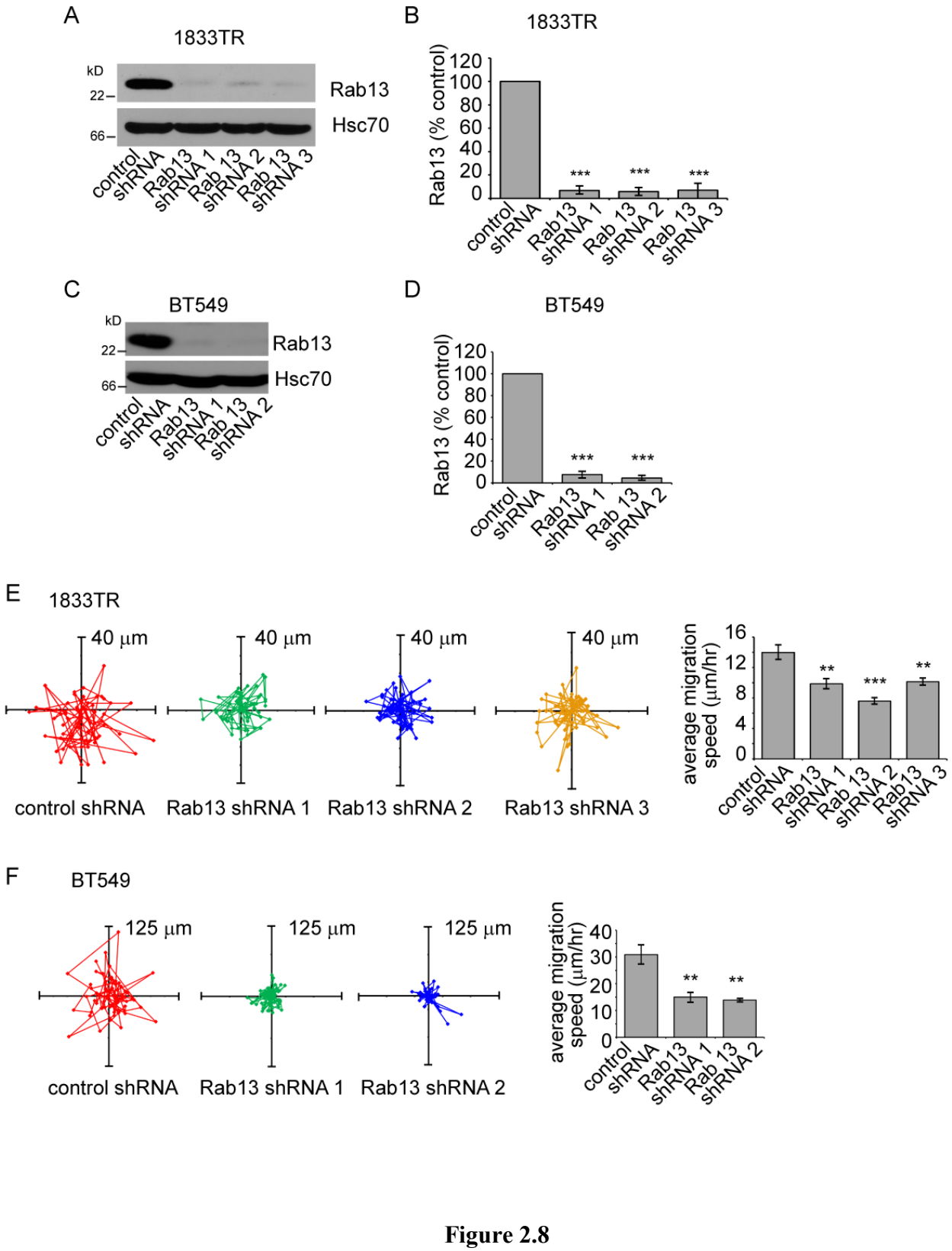
A
1833TR
kD
22
66
Rab13
Hsc70
control shRNA
Rab13 shRNA 1
Rab13 shRNA 2
Rab13 shRNA 3
B
1833TR
Rab13 (% control)
120
100
80
60
40
20
0
***
***
***
control shRNA
Rab13 shRNA 1
Rab 13 shRNA 2
Rab 13 shRNA 3
C
BT549
kD
22
66
Rab13
Hsc70
control shRNA
Rab13 shRNA 1
Rab 13 shRNA 2
D
BT549
Rab13 (% control)
120
100
80
60
40
20
0
***
***
control shRNA
Rab13 shRNA 1
Rab 13 shRNA 2
E
1833TR
40 μm
40 μm
40 μm
40 μm
control shRNA
Rab13 shRNA 1
Rab13 shRNA 2
Rab13 shRNA 3
average migration speed (μm/hr)
16
12
8
4
0
**
***
**
control shRNA
Rab13 shRNA 1
Rab 13 shRNA 2
Rab13 shRNA 3
F
BT549
125 μm
125 μm
125 μm
control shRNA
Rab13 shRNA 1
Rab13 shRNA 2
average migration speed (μm/hr)
40
30
20
10
0
**
**
control shRNA
Rab13 shRNA 1
Rab 13 shRNA 2

Figure 2.8

Figure 2.8.

Rab13 knockdown reduces migration of breast cancer cells. (A) MDA-231-1833TR cells were stably transduced with lentivirus driving expression of control shRNA or three different shRNAs targeting Rab13, and the indicated proteins were detected by blot. (B) The levels of Rab13 from experiments as in A were normalized to Hsc70 and expressed relative to control cells (mean ± SD from 4 independent experiments, one-way ANOVA with Dunnett's post-test, ***$p<0.001$). (C) As in A, but using BT549 cells. (D) As in B, but quantifying knockdown in C. (E) The migration pattern of single 1833TR cells expressing control or Rab13 targeting shRNAs. The average migration speed of all cells measured is shown in the bar graph (mean ± SEM from 3 independent experiments measuring a minimum of 10 cells per condition per experiment, one-way ANOVA with Dunnett's post-test (**$p<0.01$). (F) As in E but with BT549 cells.

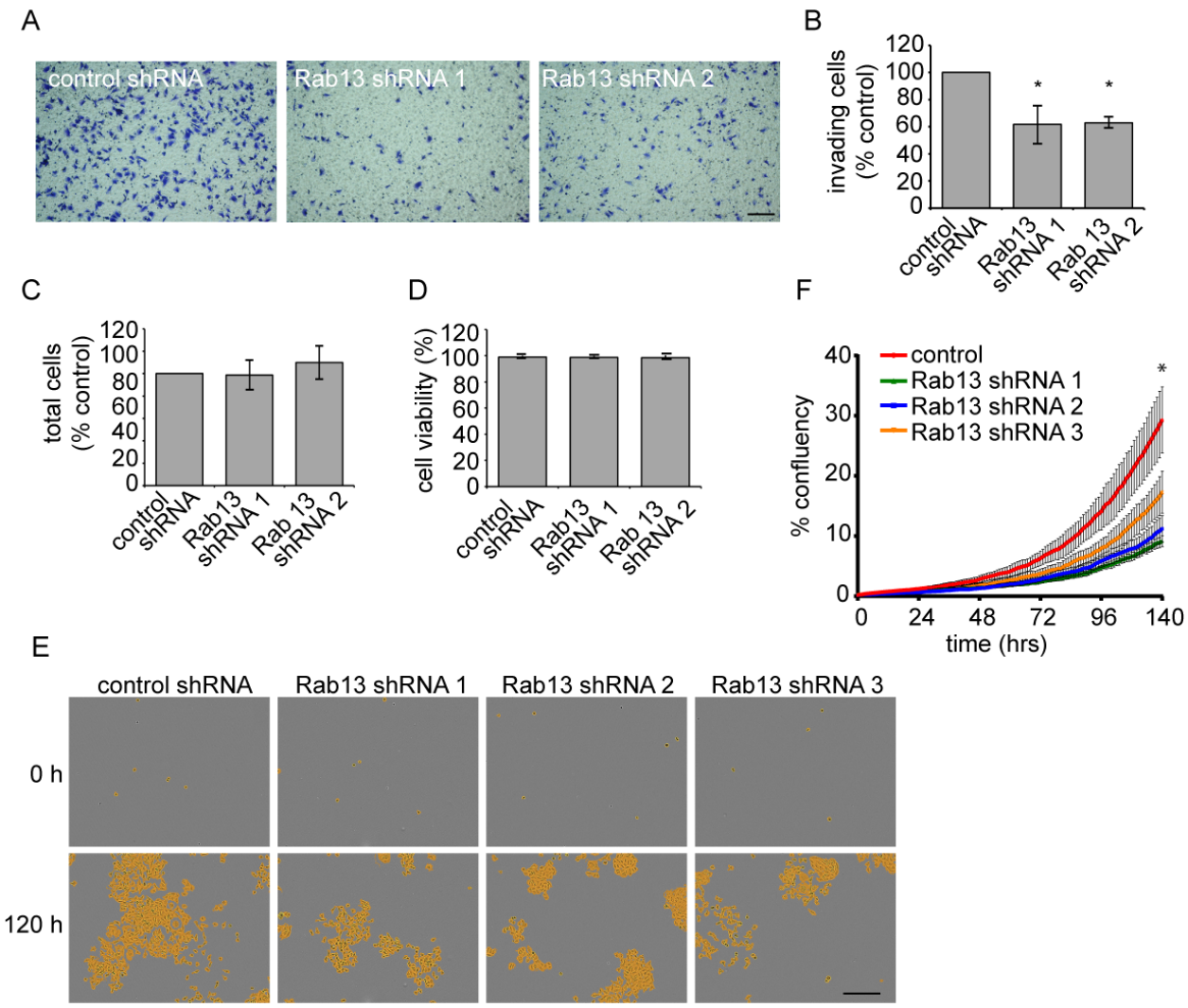
A
control shRNA
Rab13 shRNA 1
Rab13 shRNA 2
B
invading cells (% control)
120
100
80
60
40
20
0
*
*
control shRNA
Rab13 shRNA 1
Rab13 shRNA 2
C
total cells (% control)
120
100
80
60
40
20
0
control shRNA
Rab13 shRNA 1
Rab13 shRNA 2
D
cell viability (%)
120
100
80
60
40
20
0
control shRNA
Rab13 shRNA 1
Rab13 shRNA 2
F
% confluency
40
30
20
10
0
control
Rab13 shRNA 1
Rab13 shRNA 2
Rab13 shRNA 3
*
0
24
48
72
96
140
time (hrs)
E
control shRNA
Rab13 shRNA 1
Rab13 shRNA 2
Rab13 shRNA 3
0 h
120 h

Figure 2.9

Figure 2.9.

Rab13 knockdown reduces invasiveness and growth of breast cancer cells. (A) 1833TR cells with stable expression of control or Rab13 targeting shRNAs were plated on Matrigel-coated membranes for 14 h and invading cells were fixed and stained with Crystal violet. Scale bar represents 300 μm (B) Quantification of invading cells in A. normalized to control shRNA (mean ± SEM from 4 independent experiments measuring 24 fields of view per condition per experiment, one-way ANOVA with Dunnett's post-test, *$p<0.05$). (C) 1833TR cells were plated on Matrigel-coated coverslips for 14 h, stained with Hoescht and the number of cells was quantified (mean ± SEM from 4 independent experiments measuring 24 fields of view per condition per experiment, one-way ANOVA) (D) 1833TR cells were trypsinized, stained with Trypan blue, and the number of viable cells was quantified (mean ± SEM from 5 independent experiments measuring 3 wells per condition per experiment, statistical analysis employed as in B. (E) 1833TR cells, plated at low density were imaged every h for 120 h. Cells detected by imaging software are highlighted in yellow. Scale bars represents 300 μm. (F) Quantification of cell confluency over time as in E. Graph shows a representative experiment (mean ± SD from 3 independent experiments measuring 3 wells per condition per experiment; two-way ANOVA, *$p<0.05$).

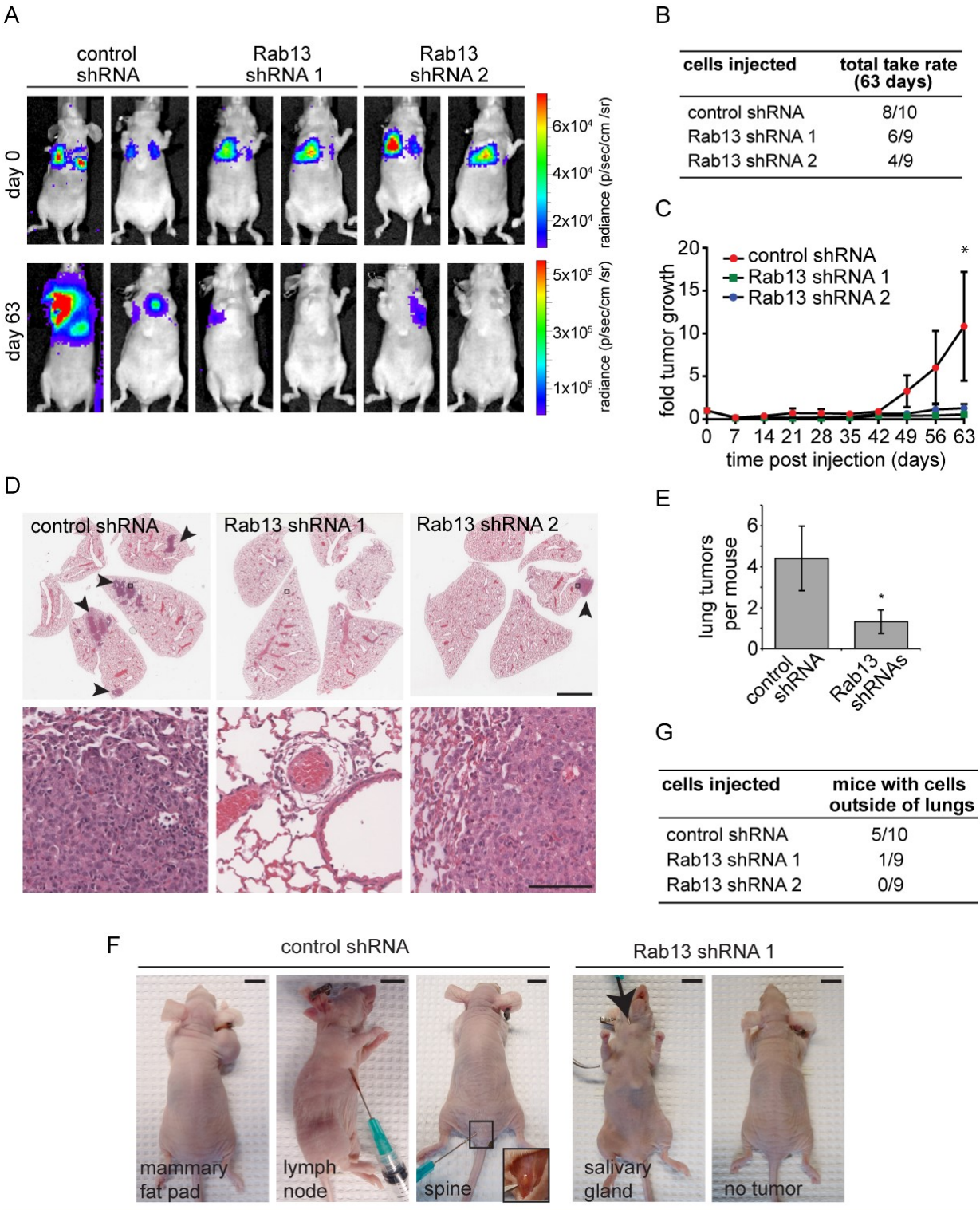
A
control shRNA
Rab13 shRNA 1
Rab13 shRNA 2
day 0
day 63
6x10^4
4x10^4
2x10^4
5x10^5
3x10^5
1x10^5
radiance (p/sec/cm /sr)
B
cells injected
total take rate (63 days)
control shRNA 8/10
Rab13 shRNA 1 6/9
Rab13 shRNA 2 4/9
C
control shRNA
Rab13 shRNA 1
Rab13 shRNA 2
fold tumor growth
time post injection (days)
0 7 14 21 28 35 42 49 56 63
D
control shRNA
Rab13 shRNA 1
Rab13 shRNA 2
E
lung tumors per mouse
control shRNA
Rab13 shRNAs
G
cells injected
mice with cells outside of lungs
control shRNA 5/10
Rab13 shRNA 1 1/9
Rab13 shRNA 2 0/9
F
control shRNA
Rab13 shRNA 1
mammary fat pad
lymph node
spine
salivary gland
no tumor

Figure 2.10

Figure 2.10.

Rab13 knockdown reduces tumor growth and migration *in vivo.* (A) 1833TR cells stably expressing luciferase and either a control vector or shRNAs targeting Rab13 were injected into the tail veins of mice. The panel shows representative bioluminescence images of mice immediately after injection (day 0) and 63 days after injection. See Fig. S3 for all mice used in the study. (B) Tumor take rates of injected mice at day 63. (C) Total bioluminescence of luciferase positive mice was quantified and normalized to day 0 (mean ± SEM from one independent experiment where n=9 for control mice and shRNA 2, n=8 for shRNA 1, two-way ANOVA with tukey post-test *$p<0.05$). (D) Representative H&E staining of lung tissue collected from mice injected with control cells and Rab13 knockdown cells. Arrowheads indicate tumors. The bottom row corresponds to the areas indicated by the black boxes in the top row. Scale bars are 3 mm for the top row and 100 μm for the bottom row. (E) Quantification of tumor numbers in D (mean ± SEM from one independent experiment where n=10 and n=18 for control and Rab13 shRNA, respectively, Student's t-test *$p<0.05$). (F) Injected mice with visible tumors illustrate cell migration outside the lungs. A mouse with no detectable mass is shown for comparison. (G) The number of mice with a luciferase signal anywhere outside of the lung at day 63 was quantified. Scale bars are 1 cm.

2.6 Supplemental Figures

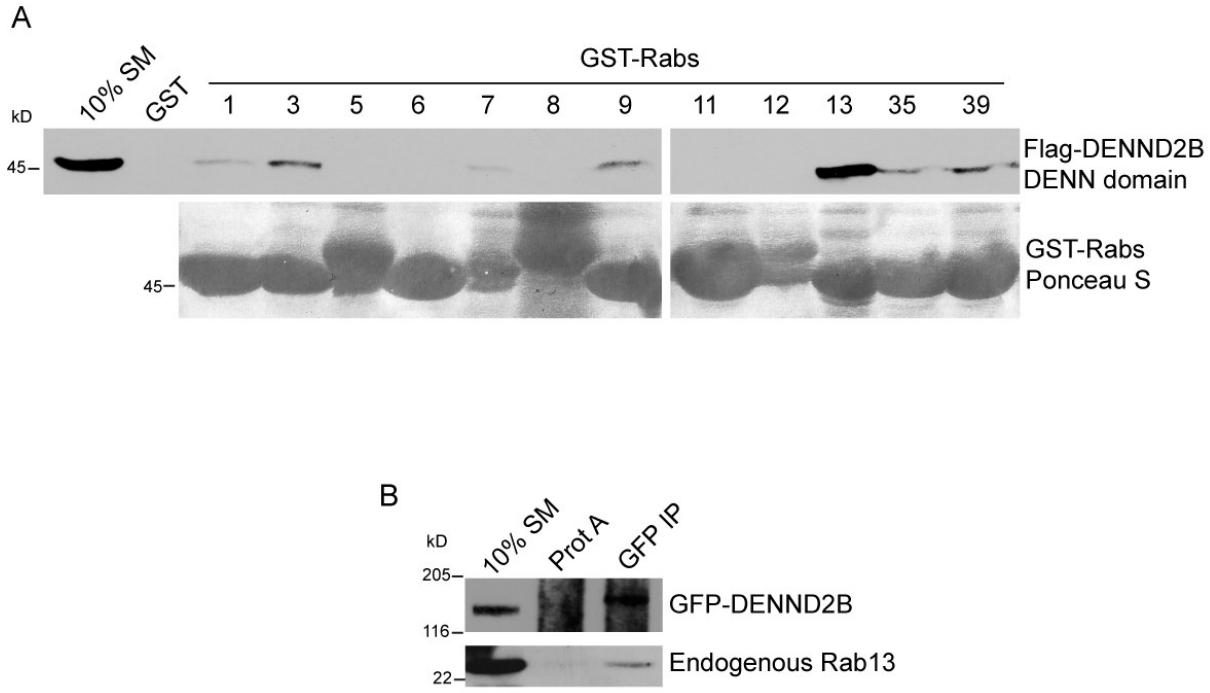

Supplemental Figure 2.1

Supplemental Figure 2.1

DENND2B binds Rab13. (A) GST-Rabs, bound to glutathione beads, were incubated with HEK-293T cell lysates expressing Flag-DENND2B DENN domain, in the presence of 5 mM EDTA. Ponceau S staining reveals the level of GST-Rabs while specifically bound Flag-DENN domain was detected by blot. Starting material (SM) equals 10% of the lysate used per condition. (B) Lysates from HEK-293T cells expressing GFP-DENND2B full-length were immunoprecipitated with anti-GFP antibody in the presence of 5 mM EDTA and the indicated proteins were detected by blot.

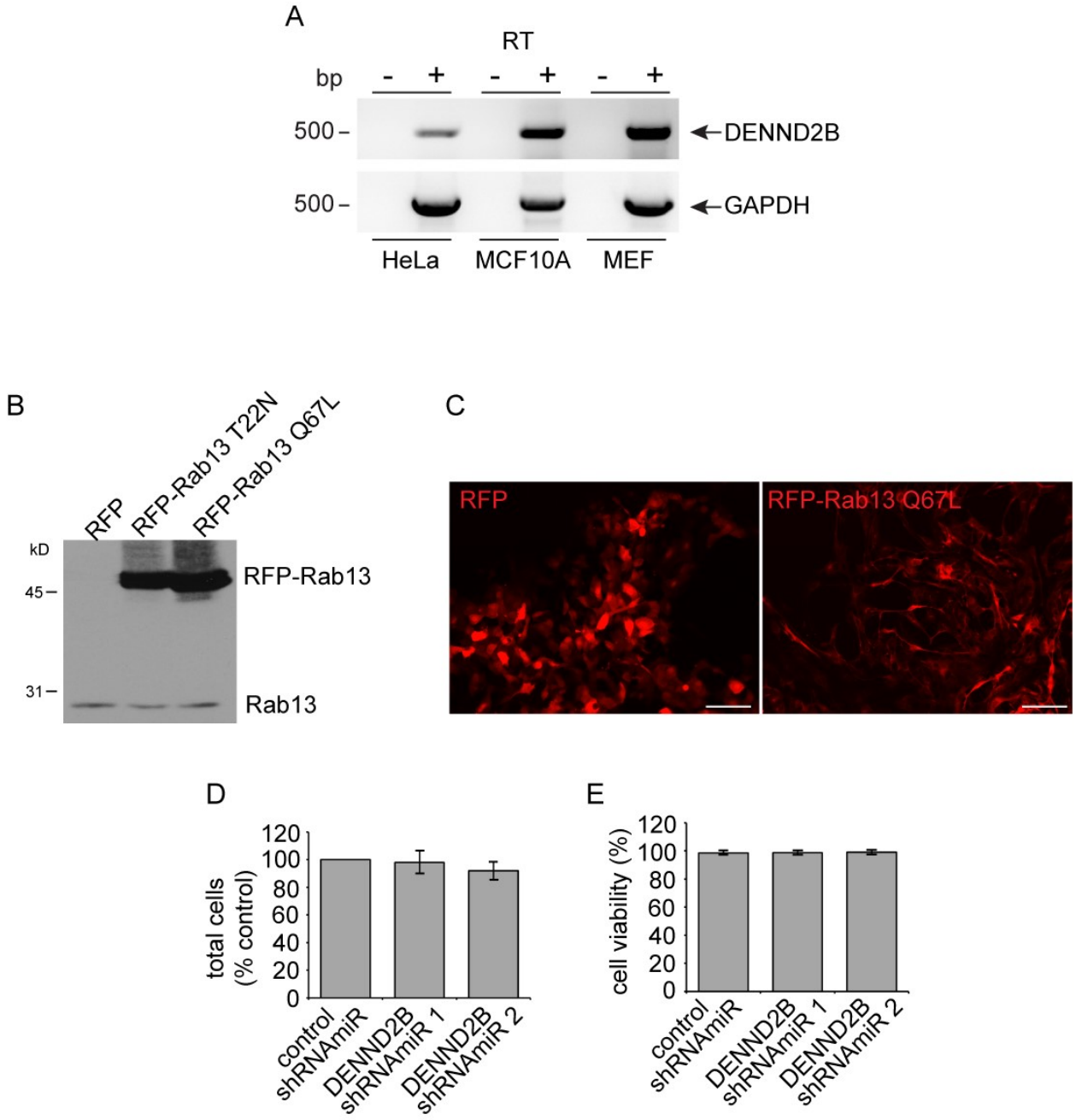

Supplemental Figure 2.2

Supplemental Figure 2.2

Rab13 and DENND2B promote epithelial cell invasion. (A) Oligonucleotides specific for GAPDH or DENND2B were used in PCR reactions with cDNA generated from the indicated cell lines. To control for possible genomic contamination, the reactions to generate cDNA were run without (-) or with (+) reverse transcriptase and the products were used for the PCR reactions shown in the figure. (B) MCF10A cells were transduced with lentivirus driving expression of RFP, RFP-Rab13 T22N or Q67L, lysed and blotted with an antibody recognizing Rab13. (C) Transduced MCF10A cells from B were fixed and imaged. Scale bars represent 100 μm. (D) Transduced MCF10A cells growing on Matrigel-coated coverslips for 14 h were, fixed, stained with Hoescht and the number of cells was quantified and normalized to control shRNAmiR cells (mean ± SEM from 4 independent experiments measuring 8 fields of view for 3 wells per condition per experiment, one-way ANOVA). (E) Transduced MCF10A cells were stained with Trypan blue, and the number of viable cells was quantified normalized to control shRNAmiR cells (mean ± SEM from 3 independent experiments measuring 3 wells per condition per experiment, one-way ANOVA).

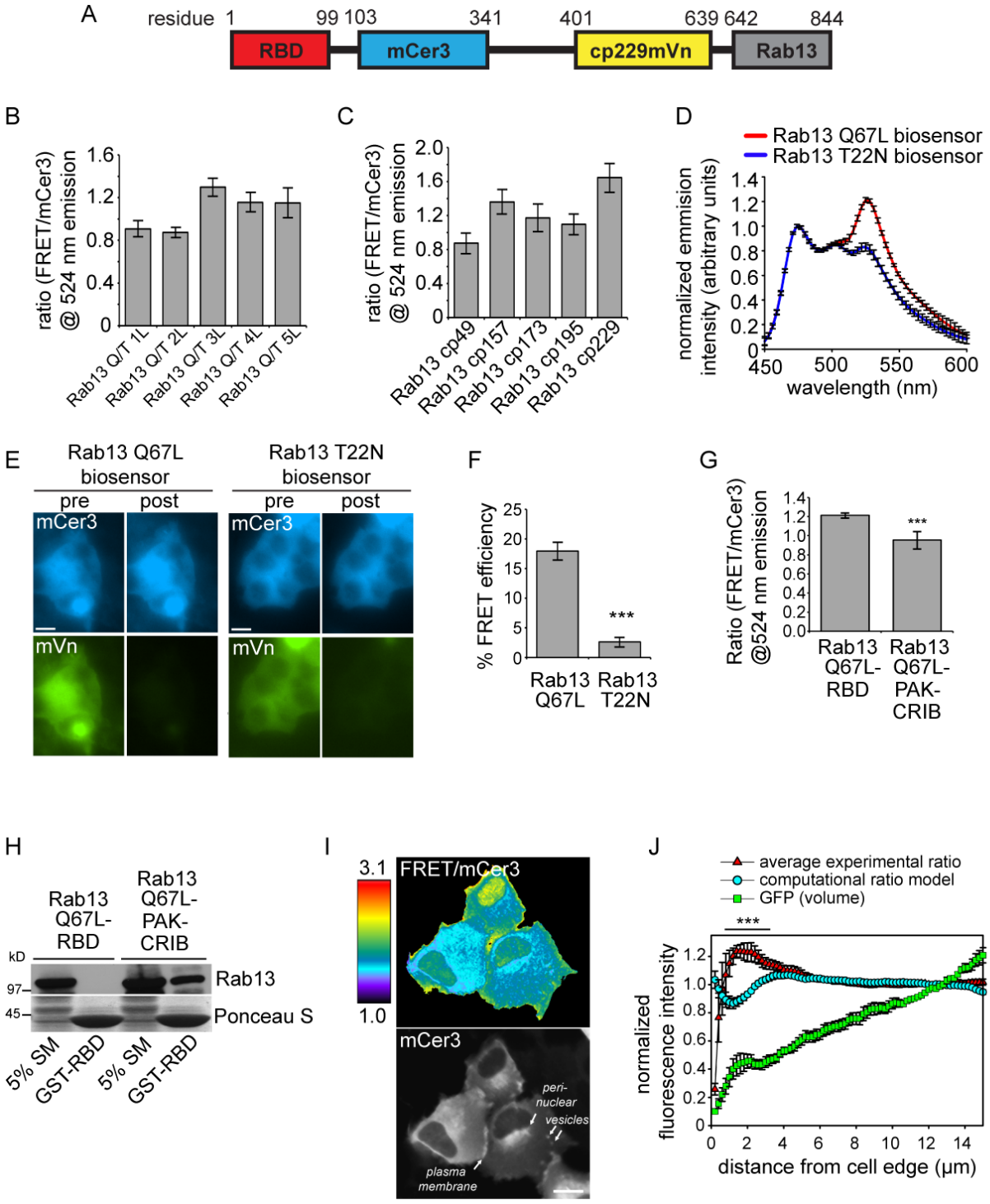

Supplemental Figure 2.3

Supplemental Figure 2.3

Optimization and validation of a Rab13 biosensor. (A) Schematic of the Rab13 biosensor containing Rab13-binding domain (RBD) of MICAL-L2, monomeric Cerulean fluorescent protein (mCer3), monomeric Venus fluorescent protein (mVen) and Rab13. The numbers above indicate the residues of the construct. (B) Rab13 biosensors with 1-5 repeats of the 18 amino acid linker domain (1L-5L) were made with either active Rab13 Q67L (Q) or inactive Rab13 T22N (T). The constructs were transfected in HEK-293T cells and fluorometric analysis of the emission ratio of FRET/mCer3 at 524 nm was used comparing the active to the inactive form (mean ± SD measuring 3 samples per condition per experiment pooled from 2 experiments) (C) Rab13 biosensors with different circular permutations of the mVen were transfected in HEK-293T cells and fluorometric analysis of the ratio of FRET/mCer3 at 524 nm was determined (mean ± SD from 3 independent experiments measuring 3 samples per conditions per experiment). (D) Fluorometric analysis of the optimized (3L/cp229) Q67L and T22N Rab13 biosensor in HEK-293T cell suspensions measured over a spectrum of wavelengths (mean ± SD from 3 independent experiments measuring 3 samples per condition per experiment) (E) Acceptor-photobleaching of the Rab13 Q67L and T22N biosensors in HEK293T cells. mVen was photobleached and the mCer3 emission intensities were measured pre- versus the post-photobleaching. (F) Quantitation of the FRET efficiencies in E. (mean ± SD from 3 independent experiments measuring 3 field of view per condition per experiment, Student's t-test, ***$p<0.001$). (G) Fluorometric analysis of HEK-293T cells in suspension co-expressing Rab13 Q67L biosensor made with RBD or the Cdc42/Rac1 interacting domain of p21 activate protein kinase (PAK-CRIB) (mean ± SD measuring 4 samples per condition pooled from 2 independent experiments, Student's t-test, **$p<0.01$). (H) GST-RBD, bound to glutathione beads, was incubated with HEK-293T cell lysates expressing Rab13 Q67L biosensor made with RBD or PAK-CRIB. Ponceau S staining reveals the level of GST-RBD while specifically bound proteins were immunoblotted with the

indicated antibody. (I) Ratiometric image (FRET/mCer3) and mCer3 image of MCF10A cells expressing the wild-type Rab13 biosensor showing proper localization. Scale bars represent 10 μm. (J) Comparison of Rab13 biosensor ratio intensity (red triangle) to computational ratio intensity (blue circle) predicted solely on cell volume as determined by GFP staining (green square). (mean ± SD measuring 6 cells pooled from 2 independent experiments, Student's t-test, ***$p<0.001$).

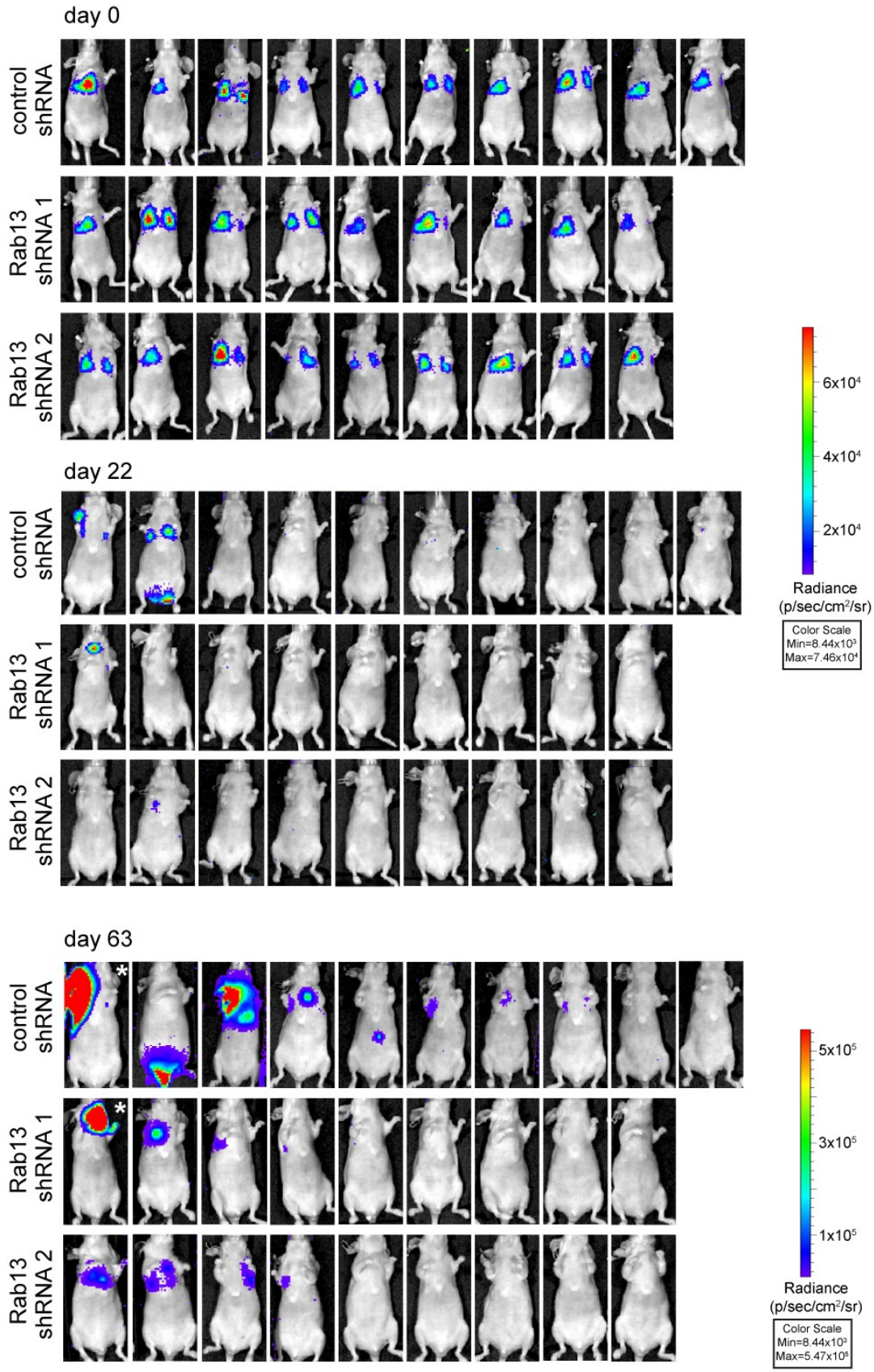

Supplemental Figure 2.4

Supplemental Figure 2.4

Rab13 knockdown limits growth and metastasis of tumors *in vivo* Bioluminescent analysis of mice injected with 1833TR breast cancer cells expressing luciferase and either control shRNA (vector control) or two shRNAs targeting Rab13. Mice were imaged for bioluminescence immediately following injection (day 0) to confirm cell inoculum and at day 22 and day 63 to visualize tumor growth. The luciferase signal in the mice indicated by asterisks is saturated.

2.7 Supplemental Videos

All supplemental videos can be viewed at http://jcb.rupress.org/content/208/5/629/suppl/DC1

Video 2.1.

Active Rab13 drives MCF10A cell invasion into collagen matrix. MCF10A cells transduced with RFP or RFP-Rab13 Q67L were grown on Geltrex to form multi-cell colonies, covered in collagen and analyzed by time-lapse phase contrast microscopy using a widefield microscope (Axiovert200M; Carl Zeiss Inc.). Frames were taken every 30 min for 72 h. Scale bar represents 100 µm. The video is related to Fig. 2 D.

Video 2.2.

Wild-type Rab13 traffics on vesicles to the cell periphery and accumulates on the plasma membrane. MCF10A cells transfected with mCh-Rab13 wild-type (white) were analyzed by time-lapse epifluorescence microscopy using a widefield microscope (Axio Observer; Carl Zeiss Inc.). Frames were taken every 5 sec for 25 min. Scale bar represents 10 µm.

Video 2.3.

Vesicles carrying wild-type Rab13 fuse with the plasma membrane. MCF10A cells transfected with mCh-Rab13 wild-type (white) were analyzed by time-lapse epifluorescence microscopy using a widefield microscope (Axio Obersver; Carl Zeiss Inc.). Frames were taken every 5 sec for 12 min. Arrows indicate fusion events of Rab13 vesicles with the plasma membrane. Scale bar represents 10 µm.

Video 2.4.

Active Rab13 traffics on vesicles to the cell periphery and accumulates on the plasma membrane at the leading edge of a migrating cell. MCF10A cells transfected with mCh-Rab13 Q67L (white) were analyzed by time-lapse epifluorescence microscopy using a widefield microscope (Axio Obersver; Carl Zeiss Inc.). Frames were taken every 5 sec for 30 min. Scale bar represents 10 μm.

Video 2.5.

Inactive Rab13 traffics on vesicles to the cell periphery but does not appear on the plasma membrane. MCF10A cells transfected with mCh-Rab13 T22N (white) were analyzed by time-lapse epifluorescence microscopy using a widefield microscope (Axio Obersver; Carl Zeiss Inc.). Frames were taken every 2 sec for 16.5 min. Scale bar represents 10 μm.

Video 2.6.

Rab13 is activated at the leading edge during cell migration. MEF cells transfected with the Rab13 biosensor were analyzed by time-lapse epifluorescence microscopy on a widefield miscropscope (Olympus IX81ZDC) equipped with a beam splitter to allow simultaneous acquisition of both FRET and mCer3 channels. FRET/mCer3 emission ratio of Rab13 biosensor is shown. Frames were taken every 10 sec for 15 min. Scale bar represent 10 μm.

2.8 Materials and methods

Antibodies

Mouse monoclonal Flag (M2) antibody was from Sigma (St. Louis, MO). Rabbit polyclonal GFP (A6455), Alexa Fluor®647-conjugated Phalloidin, transferrin and anti-sheep, and Alexa Fluor®488-conjugated anti-mouse and anti-rabbit were from Invitrogen (Carlsbad, CA). Chicken polyclonal Rab13 and rabbit monoclonal LAMP-1 antibodies were from Abcam (Cambridge, MA). Rat monoclonal Hsc70 (1B5) antibody was from Enzo LifeSciences (Farmingdale, NY). Rabbit polyclonal TIP47 antibody was from Novus Biologicals (Oakville, ON). Sheep polyclonal TGN46 antibody was from Serotec (Raleigh, NC). HRP-conjugated anti-mouse and anti-rabbit were obtained from Jackson ImmunoResearch (West Grove, PA).

DNA constructs

GST-Rab1a, GST-Rab3a, GST-Rab5, GFP-Rab5, GST-Rab11a, GST-Rab13, GST-Rab35 in pGEX-6P1; Flag-connecdenn 1 full-length, Flag-connecdenn 3 full-length, Flag-connecdenn 3 DENN domain in pCMVtag2B; and GFP-Scyl1 in pEGFP-C2 were previously described (Burman et al., 2008;Allaire et al., 2010;Marat et al., 2012). GFP-Rab7 and GFP-Rab9 (canine) in pEGFP-C1 were a generous gift from Dr. Fred Meunier (University of Queensland). GFP-MICAL 1, MICAL-L1 and MICAL-L2 in pEGFP-C3 were generous gifts from Dr. Steve Caplan (University of Nebraska). His-RabGDI in pETH6 was a generous gift from Dr. William Balch (Scripps Research Institute). Rab6b (BC036864), Rab12 (BC098407), Rab39 (BC028064), and DENND2B (BC036655) were obtained from OpenBiosystems (Hunstville, AL) and cloned into pGEX-6P1 containing a GST tag. DENND2B C-terminal (amino acid 1121-1137) and scrambled control were generated by oligo annealing and subcloned into pGEX-4T1. Rab13 T22N, Rab13 Q67L and Rab9 Q66L were produced using the mega primer approach. These constructs along with MICAL-L1 RBD (691-858),

DENND2B DENN domain (687-1121), DENND2B N-term (1-686) and DENND2B ΔC (1-1121) were cloned into pGEX-6P1 [under the tac promoter and induced with 500 μM isopropyl β-D-1-thiogalactopyranoside (Wisent, Montreal, QC)], pEGFP-C2, mCherry-C2 and/or pCMV-tag2B. Primers used to generate constructs can be found in Table 2.1. All constructs are of human sequences unless otherwise indicated. All constructs were verified by sequence analysis.

RNA extraction and RT PCR

To obtain cellular RNA, 3 x 10^6 cells grown in standard cell culture conditions at roughly 80% confluence were washed with PBS and then processed with QIAGEN RNeasy kit. To generate cDNA, 500ng of RNA was added to a QIAGEN omniscript cDNA reaction according to the manufactures instructions utilizing random nonamer oligonucleotides (Sigma). Final PCR amplicons were generated using a standard PCR reaction with Taq DNA polymerase in a 20 μl final reaction volume, using 2 μl of the cDNA reaction as template. Primers used for PCR reactions can be found in Table 2.1.

Lentivirus production

Target sequences for DENND2B were designed using the Block-iT RNAi Designer (Invitrogen), subcloned first into the pcDNA6.2/GW-EmGFP-miR cassette and subsequently into the pRRLsinPPT viral expression vector (Invitrogen) (Ritter et al., 2013). Viral particles were produced in HEK-293T cells and concentrated as previously described (Thomas et al., 2009;Ritter et al., 2013). Non-targeting control shRNAmiR virus was previously described (Thomas et al., 2009). For Rab13 overexpression virus, Rab13 was subcloned first into pcDNA6.2/GW-EmRFP-miR cassette and subsequently into pRRLsinPPT. Rab13 shRNA 1 (TRCN0000381528), Rab13 shRNA 2 (TRCN0000382005) and Rab13 shRNA 3 (TRCN0000343510) in pLKO-TRC005 were obtained

from the Mission@TRC genome-wide shRNA collection (Sigma). Empty pLKO-TRC005 vector was used as a control. Viral particles were produced by co-expressing Rab13 shRNA or control with packaging plasmids pMD.G, RSV-Rev and pCMVDR8.2 in HEK-293T cells using FuGene (Promega, Madison, WI). The media containing viral particles was collected and filtered with a 0.45 μm filter to remove cell debris. Sequences used to generate shRNA can be found in Table 2.1.

Protein knockdown/overexpression with lentivirus

For knockdown of DENND2B, MCF10A cells were plated the day of the transduction, virus was added at a multiplicity of infection (MOI) of 10 and the media was replaced with fresh culture media the following day. All experiments were performed 4-14 days post-transduction. For over expression of Rab13, virus was added to MCF10A cells at an MOI of 5 and the media was replaced with fresh culture media the following day. All experiments were performed within 5 days of transduction. For knockdown of Rab13, filtered culture media containing viral particles was added to MDA-231-1833TR and BT549 cells in media supplemented with 8 μg/mL polybrene. One day after transduction, the media was replaced with fresh culture media. Starting 2 days after transduction the cells were selected and maintained in media containing 1.5 μg/mL puromycin dihydrochloride (Sigma).

Biochemical Assays

For Rab13 effector binding assays, HEK-293T cells, grown to 40% confluency in 15 cm dishes, were transfected with FLAG-DENN domain constructs. At 18 h post transfection, cells were lysed in 20 mM HEPES pH 7.4, 100 mM NaCl, 10 mM $MgCl_2$, 5% glycerol, 1% Triton-X 100, 0.5% deoxycholate, and 0.1% SDS, supplemented with protease inhibitors (0.83 mM benzamidine, 0.25 mM phenylmethylsulphonyl fluoride, 0.5 μg/ml aprotinin and 0.5 μg/ml leupeptin). Cell lysates were

incubated with 40 µg GST-MICAL-L1 Rab-binding domain (RBD) pre-coupled to glutathione-Sepharose beads for 2 h at 4°C and washed 3 times with the same buffer. Samples were eluted in SDS-PAGE sample buffer, resolved by SDS-PAGE and processed for Western blotting. Various GST-Rab proteins were expressed in *Escherichia coli* BL21 and purified using standard procedures in Tris Buffer (20 mM Tris pH 7.4, 100 mM NaCl, 1 mM dithiothreitol) supplemented with protease inhibitors. Biosensor binding assays were performed in Tris buffer containing 5 mM $MgCl_2$ and protease inhibitors. HEK-293T cells, grown to 40% confluency in 15 cm dishes, were transfected with FLAG-tagged or GFP-tagged constructs. At 18 h post transfection, cells were washed with phosphate-buffered saline, scraped into Tris Buffer supplemented with protease inhibitors, sonicated and Triton X-100 was added to 1% final concentration. After 15 min of incubation at 4°C the lysates were centrifuged at 305 000 x g for 15 min at 4°C. For GST pull down experiments, supernatants were incubated with 40 µg of GST fusion proteins pre-coupled to glutathione-Sepharose beads for 2 h at 4°C. For co-immunoprecipitation experiments, supernatants were incubated with Protein A-Sepharose beads (GE healthcare) and anti-GFP antibody for 2 h at 4°C. Samples were washed 3 times with the same buffer, eluted in SDS-PAGE sample buffer, resolved by SDS-PAGE and processed for Western blotting.

Invasion and cell viability assays

Invasion assays were performed in Boyden Chambers using Transwell® Permeable Inserts with 8.0 µm pores in 24-well plates (Corning, Tewksbury, MA). Matrigel (BD, Mississauga, ON) was diluted to 0.25 µg/µL in serum-free media and 50 µL was added to the top reservoir of the chamber using chilled pipette tips and allowed to solidify at 37°C for 1 h. MCF10A or MDA-231-1833TR cells were grown to 100% confluence the day of the assay, trypsinized, re-suspended in serum-free media containing 0.1% BSA, and 2 $x10^4$ cells in 100 µL were added to the top reservoir while 650 µL

serum-containing media was added to the bottom chamber. The chambers were then placed at 37°C for 14 h. Cells from the top reservoir that did not invade were removed using a cotton swab. Invading cells were fixed in 4% paraformaldehyde (PFA) at room temperature for 15 min and stained in 0.2% crystal violet at room temperature for 15 min. Excess stain was removed by rinsing in water and dried cells were imaged using an AxioObserver Z1 microscope (Zeiss) equipped with a Fluar 10x air objective (NA=0.5) with transmitted light and a Canon® EOS Rebel XS f/18-55mm-IS digital camera. Acquisition and analyses were performed using Cannon Eos Utility software version 2.8. The number of invaded cells per field of view was quantified. To measure viability, MCF10A or MDA-231-1833TR cells were grown to 100% confluence for the day of the assay, trypsinized, and re-suspended in serum-free media containing 0.1% BSA. Cells were stained with Trypan blue and the number of viable cells was quantified on a haemocytometer. For Geltrex invasion assays, 20ul of Geltrex reduced growth factor basement membrane (Life technologies) was spread into each well of an eight well Lab-Tek II chambered coverglass (Thermo Scientific) that had been pretreated for 10min with 100% ethanol. After 30min at 37ºC, $1.5x10^3$ cells/well were plated in complete media containing 2% Geltrex and cultured for 4 days to form colonies. Media was removed and colonies were covered with 100ul of 2.5 mg/ml rat tail collagen I (Invitrogen) in DMEM, 0.7%$NaHCO_3$, 0.1M HEPES and incubated 1h at 37ºC. 300ul of complete media/well was added and invasion proceeded for 72h (37ºC, 5% CO_2). Images were collected using an Axiovert200M (Zeiss) equipped with a LD A-PLAN 20X Ph1 objective (NA=0.3) with transmitted light and an Axiocam HRm camera (Zeiss). Quantification was performed using MetaMorph software version 7.6.4 (Molecular Devices, Sunnyvale CA).

Proliferation and cell migration assays

For short time proliferation assays, Matrigel was diluted to 0.25 µg/µL in serum-free media and 300 µL was used to coat glass coverslips. Aliquots of MCF10A or MDA-231-1833TR cells ($2.4x10^5$ cells in 600 µL serum-free media) were added and incubated for 14 h at 37°C. Cells were fixed with 4% PFA and stained with Hoescht. The total number of cells per field of view was quantified. For longer term proliferation assays, 500 MDA-231-1833TR cells per well were plated in a 96-well plate and imaged every h for 5 days using the IncuCyte™ Kinetic Live Cell Imaging System (Essen Biosciences, Ann Arbor, MI). The cell confluency was determined using the IncuCyte software. Cell migration distances were tracked using MetaMorph software version 7.6.4.

Cellular imaging and protrusion assays

For live-cell imaging, MCF10A cells were plated at 60% confluence on poly-L-lysine-coated 35 mm No. 1.5 glass bottom dishes (MatTek Corporation) in complete MCF10A media. Cells were transfected with DNA constructs using JetPrime Reagent and incubated for 12-14 h. Live-cell imaging was performed using an AxioObserver Z1 (Zeiss) microscope equipped with a plan-aprochromat 40x oil objective (NA=1.4), Definite Focus system and an AxioCam MR3 camera (Zeiss). Cells were kept at 37°C in 5% CO_2 using Incubation System S (Pecon, Germany). GFP and mCherry were imaged using 470 nm and 591 nm laser lines respectively, from a Colibri.2 illumination source (Zeiss). Acquisition and analyses were performed using ZEN 11.0 software (Zeiss), while movies were made using ImageJ 1.43m. MCF10A or HeLa cells were plated on poly-L-lysine coated glass coverslips and transfected with DNA constructs using jetPRIME® transfection Reagent (Polyplus) according to the manufacturer's instructions. For internalization of transferrin, transfected cells were serum starved for 1 h and incubated in serum-free media containing 25 µg/mL labelled transferrin for 30 min. Cells were washed in PBS and fixed for 15 min in 3% PFA.

Following fixation, cells were permeabilized with 0.2% Triton-X-100 in PBS and processed for immunofluorescence with the appropriate antibodies in PBS. Imaging was performed using a 710 Laser Scanning Confocal Microscope equipped with a plan-aprochromat 63x oil objective (NA=1.4) (Zeiss). Acquisition was performed using ZEN 11.0 software (Zeiss), and analysis was done using ImageJ 1.43m. For differential interference contrast (DIC) microscopy, MCF10A cells were prepared on 35 mm No. 1.5 glass bottom dishes (MatTek Corporation; Ashland, MA). Imaging was performed using AxioObserver Z1 microscope equipped with a plan-aprochromat 20x oil objective (NA=0.8), DIC II 0.35/0.4 condenser module and an AxioCam MR3 camera (Zeiss). Acquisition and analyses were performed using ZEN 11.0 software (Zeiss). For protrusion assays, healthy transfected cells were selected blind in the DAPI channel and imaged for GFP or mCherry. The length of the longest protrusion was measured using ImageJ 1.43m. Pearson correlation coefficients were determined using the colocalization analysis plugin from McMaster Biophotonics Facility ImageJ for Microscopy bundle (Collins, 2007).

Rab13 biosensor, construction and optimization

In order to make the Rab13 construct compatible with the vector system used to construct the biosensor (Pertz et al., 2006), the internal restriction sites NcoI and XhoI were silenced using site-directed mutagenesis. Primers used to generate Rab13 biosensors can be found in Table 2.1. The Rab-binding domain of MICAL-L2 (a.a. 808 – 904) and Rab13 (wild-type, Q67L and T22N) were PCR amplified, digested and ligated into the biosensor backbone system as shown in Fig S3 A. Constitutively active Rab13 biosensor (Q67L mutant version) was modified to abrogate the binding of the integral RBD to Rab13 GTPase by exchanging the RBD with the CRIB domain of p21 activated kinase 1, containing mutations to eliminate any GTPase binding effects (H83/86D and W103D mutations) (Moshfegh et al., 2014). Point mutagenesis was performed using the Quikchange

PCR mutagenesis kit (Stratagene). The intramolecular linker length between the mCerulean3 and mVenus fluorescent proteins (Fig S3 A) was optimized for the best FRET ratio difference between the constitutively active (Q67L) versus the dominant negative (T22N) versions of the biosensor, by using cassettes of 18 amino acid flexible, structure-less, and protease-resistant linker encoding the sequence TSGSGKPGSGEGSTKGGS (Whitlow et al., 1993) in increments between 1-5 linker units. To further optimize the FRET dipole-coupling angles, circularly permutated Venus fluorescent proteins were tested on the 3-linker version of the biosensor. The circularly permutated monomeric Venus (cp49, 157, 173, 195, 229) (Nagai et al., 2004) fluorescent proteins were PCR amplified, digested with NotI and EcoRI and ligated into position. For fluorometric measurements, the Rab13 biosensors were expressed in HEK-293T cells using Lipofectamine2000 following the manufacturer's protocols (Invitrogen). In situations where RabGDI or DENND2B constructs were not used, an empty pCDNA3.1 vector was used as a DNA control. The DNA constructs were transfected with the cDNA concentration ratio of 1:4:4 for the biosensor:GDI:GEF. The procedure for the fluorometry followed the previously published protocols (Pertz et al., 2006). Briefly, at 48 h post transfection, cells were briefly trypsinized and detached into cold PBS. The cell suspensions were transferred to a cuvette and the fluorometric measurements were performed. Emission spectra between 450-600 nm were obtained upon 433 nm excitation of the cell suspensions in a Fluorolog-MF2 spectrofluorometer (Horiba Jovin-Yvon). The mock-transfected cell suspension was used to obtain the background fluorescence response, which was subtracted from the raw data. The emission maximum value at 475 nm was used to normalize the entire spectrum and the changes in the FRET emission at 525 nm were quantified.

Acceptor photobleaching analysis

Constitutively active (Q67L) and dominant negative (S22N) Rab13 biosensors were transiently transfected into HEK293T cells using the JetPrime reagent (Polyplus) following the manufacturer's protocols. Cells were plated onto coverslips and imaged with an Olympus IX81ZDC inverted microscope equipped with an 40x oil immersion DIC objective lens (NA=1.3) and a Coolsnap ESII CCD camera (Roper Photometrics, Tuscon, AZ), using the fluorescence excitation and emission optical configuration as used for imaging of the FRET biosensor MCF10A and MEF cell lines. The mCer3 fluorescence emission intensities were recorded from 10 random field of views (FOV), followed by additional 10 random FOVs but after irradiated through FF01-525/50-25 (Semrock) filter for 2min to photobleach the mcp229Venus, using the 100W Hg Arc lamp as the light source. The flat-field corrected and background subtracted mCer3 images pre- and post- photobleaching were analyzed for the average per pixel gray levels and the FRET efficiency limits were calculated using the following equation:

$$F_E = 1 - \frac{mCer3_{pre}}{mCer3_{post}}$$

Live cell imaging of the Rab13 biosensor

MCF10A cells and MEFs were plated on poly-L-lysine coated coverslips and fibronectin-coated coverslips, respectively, and transfected with the Rab13 biosensor using JetPrime. MCF10A were imaged after 14 h transfection and MEFs after 8 h transfection. Imaging was performed in Ham's F-12K without phenol red (Biosource, Camarillo, CA) containing 2% fetal bovine serum and 5% horse serum for MEFs and MCF10A, respectively, in a closed chamber heated to 37°C. Activation of Rab13 was determined by monitoring the ratio of FRET between mCer3 to mVen and the donor mCer3 intensities for the Rab13 sensor (Bravo-Cordero et al., 2011;Pertz et al., 2006).Time-lapse sequences were acquired using an Olympus IX81ZDC inverted microscope equipped with two

internal beam splitters [T555LPXR (Chroma Technology, Rockingham, VT) for the internal prism replacement and T505LPXR (Chroma Technology) for the FRET/CFP split in the external beam splitter attached to the left side camera port] to allow simultaneous acquisition of both FRET and mCerulean3 channels using two Coolsnap ESII CCD cameras operating at 2x2 binning mode (Spiering et al., 2013). Images were acquired using an Olympus 60x PlanApoN 1.45 NA objective and MetaMorph ver.7.1.5 software. The filter sets used were ET436/20X (excitation) and ET480/40M (emission) for mCerulean3 and ET436/20X (excitation) and ET535/30M (emission) for FRET (Chroma Technology, Rockingham, VT). Cells were illuminated with a 100W Mercury lamp through 5-10% transmittance neutral density filters. mCer3 and FRET images were recorded simultaneously for 700-1000 ms exposure times. Imaging and post-acquisition processing were performed using Metamorph ver. 7.8.8 software, and Matlab R2012b as previously described (Hodgson et al., 2006;Hodgson et al., 2008;Hodgson et al., 2010). Briefly, camera noise image was subtracted from the raw mCer3 and FRET image stacks, followed by a flatfield-correction using a set of shading images acquired from cell-free fields of view under identical imaging conditions as the actual raw image data stacks. The flatfield-correction corrects for the uneven illumination in the field of view, stemming primarily from the defocusing of the arc lamp source used. This is performed by dividing the camera noise-subtracted raw data images by the corresponding shading images of each channel. The camera noise-subtracted and flatfield-corrected images are then convolved against a 3x3 median filter kernel (Matlab: medfilt2.m) to eliminate the hot pixels. The program to perform the steps up to this point is available as “scImage.m” (Spiering et al., 2013). The camera-noise subtracted, flatfield-corrected, and median-filtered image stacks were then processed for the background subtraction. Because of the flatfield-correction, the cell-free regions within the field of view should have near uniform intensity values, thus the cell-free background intensity values within a small region of interest is averaged and subtracted from the entire field of view, and repeated for

every timepoint of the timelapse data stacks in both mCer3 and FRET sets. This process is performed using Metamorph software using the "statistical correction" tool. The background-subtracted images are corrected for pixel-by-pixel matching in order to eliminate alignment-related artifacts stemming from small differences in the mounting angles of the two cameras (also including imperfections in the mounting angles of the dichromatic mirrors and emission filters in the light path) used during the simultaneous imaging. To do this, the misalignments in the mCer3 and FRET channels are characterized using a calibration slide containing multispectral beads (Tetraspeck micropheres; Invitrogen). The calibration images are used to determine the non-linear coordinate transformation parameters, using Matlab programs "tkMorph.m" (Spiering et al., 2013) and the "spot-detector" (Thomann et al., 2002) which fits the Gaussian point-spread function to the fluorescent bead spots to determine the centroid location with subpixel accuracy. The coordinate transformation parameters obtained from this calibration steps are used to align the processed mCer3 and FRET image stacks, using an *affine* transformation ("morph.m" program in Matlab) (Spiering et al., 2013). The coordinate-transformed mCer3 and FRET image stacks were intensity thresholded using the thresholding tool in the Metamoph software to generate binary masks. The binary masks are then multiplied into the corresponding image stacks, which sets the regions outside of the cell to zero thus eliminating the outside-of-cell noise during the final ratiometric processing. Prior to the ratiometric calculation, the binary-masked image stacks of mCer3 and FRET channels are globally optimized against each other at subpixel accuracy by an x-y translational image alignment tool based on the normalized cross-correlation method using the Matlab program "regFC2.m" (Shen et al., 2006;Spiering et al., 2013). This second level of image alignment following the non-linear coordinate transformation procedure is necessary because the image cropping step following processing of the coordinate transformation may produce a slight x-y misalignment depending on the severity of the non-linear correction applied. The ratio stack of images was obtained by dividing the

aligned and masked FRET image by the masked mCerulean3 image. The time-lapse ratio image set was corrected for photobleaching by modeling the intensity decay in the ratio as a second order exponential function, accounting for the two photobleaching components as previously described (Hodgson et al., 2006). This assumption is based on the idea that the majority of GTPases in cytosol exists in complex with the GDI and thus is a passive component in the modulation of the ratio signals, and that only a very small fraction of the total Rab goes through activation cycles at any given time (del Pozo et al., 2002). The whole-cell average ratio values are calculated and the double exponential fit is performed using a Matlab program "bleachcorrectWhole.m" (Shen et al., 2006;Spiering et al., 2013). The inverse of the resulting double exponential function is then multiplied at each time point of the ratio image stack to obtain the corrected ratio data. To test for the influence of cell volume on ratio measurements, line scans were made perpendicular to the cell edge in 6 cells from 3 independent experiments, and the following parameters were measured, averaged and normalized arbitrarily to a position 12 microns away from the edge: 1) EGFP was non-specifically expressed in the cytoplasm of parental MCF10A cells without biosensor to determine the average cell volume distribution at the edge; mCer3 intensities were measured in the biosensor expressing MCF10A cells to reflect the distribution of the Rab13 biosensor; and 3) Ratio intensities of the biosensor measurements were taken in MCF10A cells expressing the wild-type Rab13 biosensor. The predicted FRET/mCer3 was calculated using the previously described calculation (Spiering et al., 2013):

$$\frac{FRET}{mCer3} = \frac{\propto mCer3 + \rho_{FRET} Ah}{mCer3 + \rho_{mCer3} Ah}$$

The optical bleedthrough from the mCer3 to the FRET channel on our imaging system was assumed to be a constant and at 0.6 : 1.0 (FRET : mCer3). We calculated the theoretical distribution of the ratio values if it was based on the volume and the biosensor distribution alone. Where mCer3

intensity is experimentally determined, ρFRET and ρmCer3 describes the optical bleedthrough of 0.6 and 1.0 respectively from our optical configuration, Ah is the volume as measured by the GFP distribution and averaged over 10 cells, and α-factor is parameter to match the maximum Ratio between the model predictions and the actual ratio.

Analysis of tumor growth and migration *in vivo*

Female nude mice (six to eight weeks old, Taconic Farms, Inc.) were injected via the tail vein with $7.5x10^4$ MDA-MB-231 1833TR cells (Vector Control n = 10 mice, Rab13 shRNA 1 n = 9 mice, Rab13 shRNA 2 n = 9 mice). Luciferase activity in the lungs was confirmed and measured immediately post-injection using bioluminescence imaging and mice were imaged once per week thereafter to monitor the development of metastases. For imaging, mice were anaesthetized with isoflurane and injected intraperitoneally with 50µl of the luciferase substrate D-luciferin (PerkinElmer) (30mg/ml in PBS) and bioluminescence was detected at 1 minute intervals for 10 minutes using Xenogen IVIS 100 (Caliper Life Sciences, Inc) in batches of 5 mice. All images to be compared were opened as a group using Living Image Version 4.2 software to allow visualization on a uniform scale and analysis using the Measurement ROI tool to quantify all detectable regions of luciferase activity in the body of each mouse. The resulting sum total luminescence signal per mouse was normalized to the signal generated by the initial cell inoculum for that mouse as measured on the day of injection. Tumor outgrowth was then expressed as a fold change in luminescence signal. Mice negative for luciferase activity at day 63 were excluded from tumor outgrowth quantification. Similarly, 2 mice without reliable quantification due to oversaturation (1 shRNA control and 1 Rab13 shRNA 1) were excluded from quantitative analysis. Tumor “take” was considered positive if luciferase activity was detectable anywhere in the animal at 63 days post-injection. Mice were sacrificed 10 weeks post-injection. Metastases were confirmed and counted at necropsy and by

histological analysis. Tissue samples for histology were fixed for 24h in 10% formalin, embedded in paraffin, and sectioned at 5μm. Sections were stained with H&E and imaged using an Aperio-XT slide scanner (Aperio Technologies). The number of lesions in the lungs was quantified blind. All animal experiments were carried out in accordance with the guidelines of the McGill University Animal Ethics Committee and the Canadian Council on Animal Care as a protocol approved by the Facility Animal Care Committee (Protocols #5562).

Supplemental Table 2.1

Oligonucleotides used in Chapter 2

A. Primers for fusion proteins	
Primer	Sequence (5'→ 3')
DENND2B aa 1 EcoRI F	GCGGAATTCATGACCATGACTGCCAACAAGAACTCCAGCATCACCCACGGAGC
DENND2B aa 1137 SalI R	GCGGTCGACTTAATTCTTCTTGTGGAGAAACTTC
DENND2B aa 686 R-SalI R	GCGGTCGACTTACAGCTCCAGCGTGCGATAGC
DENND2B aa 687 F-BglII F	GCGAGATCTGAGCTGCTGGAGTGGCAGG
DENND2B aa 1121 EcoRI R	GCGGAATTCTCACTTATTCATTCCACTCTGCTCAG
DENND2B aa 687 EcoRI F	GCGGAATTCGAGCTGCTGGAGTGGCAGG
DENND2B aa 1121 BamHI R	GCGGGATCCTTACTTATTCATTCCACTCTGCTCAG
DENND2B aa 1121 BamHI F	GATCCAAGTTTCTCCGAGGTTTGGGCAACAAAATGAAGTTTCTCCACAAGAAGAATTAAC
DENND2B aa 1137 XhoI R	TCGAGTTAATTCTTCTTGTGGAGAAACTTCATTTTGTTGCCCAAACCTCGGAGAAACTTG
C-term scramble BamHI F	GATCCAATAAGAAGCACCTCTTTAAGATGAAAAACGGCTTGGGTCGACTCTTTAAGTAAC
C-term scramble XhoI R	TCGAGTTACTTAAAGAGTCGACCCAAGCCGTTTTTCATCTTAAAGAGGTGCTTCTTATTG
Rab6b aa 1 BamHI F	GCGGGATCCATGTCCACGGGCGGAGACTT
Rab6b aa 208 NotI R	CGCCGCCGGCGTTAGCAGGAACAGCCT
Rab7a aa 1 SalI F (canine)	GCGGTCGACTCATGACCTCTAGGAAGAAAGTGTTG
Rab7a aa 207 NotI R (canine)	GCGGCGGCCGCTCAGCAACTGCAGCTTTCCGC
Rab9 aa 1 XhoI F (canine)	GCGCTCGAGCGATGGCAGGAAAATCTTCACTTTTTAAAG
Rab9 aa 201 BamHI F (canine)	GCGGGATCCTCAACAGCAAGATGAGCTAGGCTTG
Rab8a aa 1 BamHI F (canine)	GCGGGATCCATGGCGAAGACCTACGATTACC
Rab8a aa207 EcoRI R (canine)	GCGGAATTCTCACAGAAGAACACATCGGAAAAAGC
Rab9 aa 1 BamHI F (canine)	GCGGGATCCATGGCAGGAAAATCTTCACTTTTTAAAG
Rab9 aa 201 NotI R (canine)	GCGGCGGCCGCTCAACAGCAAGATGAGCTAGGCTTG
Rab9 Q66L MP F (canine)	GCAGATTTGGGACACAGCCGGTCTAGAGCGATTCAGAAGCCTGAGGACG
Rab12 aa 1 EcoRI F	GCGGAATTCATGGATCCGGGCGCCGCG
Rab12 aa 244 XhoI R	GCGCTCGAGTCAACAGCATCGGACATGTGGTC
Rab13 aa 1 EcoRI F	GCGGAATTCATGGCCAAAGCCTACGAC
Rab13 aa 203 BamHI R	GCGGGATCCTCAGCCCAGGGAGCACTTGTTGG
Rab13 aa 1 BamHI F	GCGGGATCCATGGCCAAAGCCTACGACCAC
Rab13 aa 203 PacI R	GCGTTAATTAAGTCGACTCAGCCCAGGGAGCACTTGTT

Rab13 aa 203 EcoRI R	GCGGAATTCTCAGCCCAGGGAGCACTTGTTGG
Rab13 Q67L megaprimer F	CAAGTCTGGGACACGGCTGGCCTAGAGCGGTTCAAGACAATAACTACTGC
Rab13 T22N megaprimer F	GGGGACTCGGGGGTGGGCAAGAATTGTCTGATCATTCGCTTTGCAGAGG
Rab39 aa 1 BamHI F	GCGGGATCCATGGAGACCATCTGGATCTACC
Rab39 aa 217 NotI F	CGCCGCCGGCGTCAGCAGAAGCATTCTTTCCTGGG
MICAL-L1 aa 690 BamHI F	GCGGGATCCATTGAGCGCCGGCTGGATGC
MICAL-L1 aa 863 EcoRI R	GCGGAATTCTCAGGACTTGCTCTTGGCATCACG
B. Primers for RT PCR	
DENND2B F (mouse)	CAGAACAGAAAATCCTTCGAGT
DENND2B R (mouse)	CTTTGGACAAGCTTGGGAATGC
DENND2B F	AGCAGAAAATCCTTTTGAGTTTG
DENND2B R	CTTTGGACAAGCTTGGGAATGC
GAPDH F (human/mouse)	ATGGGGAAGGTGAAGGTCGG
GAPDH R (human/mouse)	CGCCACAGTTTCCCGGAGGG
C. Sequences for shRNAs	
DENND2B shRNAmiR #1	TGCTGTGAGGTTTCACTATCACTGAGGTTTTGGCCACTGACTGACCTCAGTGAGTGAAACCTCA
DENND2B shRNAmiR #2	TGCTGCTTGGATGAAGCCAGCAAACAGTTTTGGCCACTGACTGACTGTTTGCTCTTCATCCAAG
Rab13 shRNA #1	GTACCGGAGAGCGGTTCAAGACAATAACCTCGAGGTTATTGTCTTGAACCGCTCTTTTTTTG
Rab13 shRNA #2	GTACCGGAGAAGGAGCAGGCCGATAAGTCTCGAGACTTATCGGCCTGCTCCTTCTTTTTTTG
Rab13 shRNA #3	CCGGATGAGAAATCTTTCGAGAATACTCGAGTATTCTCGAAAGATTTCTCATTTTTTG
D. Primers for Rab13 biosensors	
MICAL-L2 aa 808 NcoI F	GCAATTTATATGCATGGAAAGGATCCGGAGAGGAGCAGCAGCTGGACATCGAGGG
MICAL-L2 aa 904 BamHI R	CCTGCCGGCTAAATATAGTCCTAAGCTTCCCTGGGAGGGGCTGCTTTTGCTTTTTG
Rab13 aa 1 EcoRI F	GCAATGATATATTTCGCTTAGAATTCATGGCCAAAGCCTACGACCAC
Rab13 aa 203 XhoI R	CTTTAACCACGCAATAATTCCTCGAGTCAGCCCAGGGAGCACTTGTTG
Rab13 to remove NcoI site F	CTGCCTACTACCGTGGAGCGATGGGCATTATCCTAGTATAC
Rab13 to remove NcoI site R	GTATACTAGGATAATGCCCATCGCTCCACGGTAGTAGGCAG
Rab13 to remove XhoI site F	GAGCAGGCCGATAAGTTGGCACGAGAGCATGGAATCCGATT
Rab13 to remove XhoI site R	AATCGGATTCCATGCTCTCGTGCCAACTTATCGGCCTGCTC
mVenus cp49 NotI F	CATAAGAATGCGGCCGCAATGACCGGCAAGCTGCCCG
mVenus cp49 EcoRI R	GGGGGAATTCCTTGGTGCAGATCAACTTCAGGGTC
mVenus cp157 NotI F	CATAAGAATGCGGCCGCAATGCAGAAGAACGGCATCAAGGC
mVenus cp157 EcoRI R	GGCCGAATTCCTTCTTGTCGGCGGTGATATAGAC

mVenus cp173 NotI F	CATAAGAATGCGGCCGCAATGGACGGCGGCGTGCAGC
mVenus cp173 EcoRI R	CCGGAATTCCTTCTCGATGTTGTGGCGGATCTTG
mVenus cp195 NotI F	CATAAGAATGCGGCCGCAATGCTGCCCGACAACCACTACC
mVenus cp195 EcoRI R	CCGGAATTCCTTCAGCACGGGGCCGTCG
mVenus cp229 NotI F	CATAAGAATGCGGCCGCAATGATCACTCTCGGCATGGACGAG
mVenus cp229 EcoRI R	GGAATTCCTTCCCGGCGGCGGTCACGAACTC
PAK1 aa 57 NcoI F	GGAACATTATAGCATAGCAACCATGGGGATTTTACCTGGAGATAAAACAAA
PAK1 aa 121 BamHI R	GCAACTTAATGCATATGCAAGGATCCTTTCTGGCTGTTGGATGTCTTCTTC
PAK1 H83/86D F	CCTTCAGATTTTGAAGACACAATTGATGTCGGTTTTGATGCTGG
PAK1 H83/86D R	CCAGCATCAAAACCGACATCAATTGTGTCTTCAAAATCTGAAGG
PAK1 W103D F	GAATGCCAGAGCAGGACGCCCGCTTGCTTCAGACATC
PAK1 W103D R	GATGTCTGAAGCAAGCGGGCGTCCTGCTCTGGCATTC

C-term, C-terminal; F, forward; R, reverse; MP, megaprimer.

2.9 Acknowledgments

We thank Dr. Pietro De Camilli and Dr. Andrea L. Marat for comments on the manuscript, Dr. Jonathan M. Lee for helpful discussion and Jacynthe Philie for excellent technical assistance. We thank Dr. William Balch for the RabGDI construct, Dr. Steve Caplan for the MICAL constructs, Dr. Fred Meunier for GFP-Rab7 and GFP-Rab9 and Dr. Peter Siegel for the MDA-231-1833TR cell line. This work was supported by grant MOP-62684 from the Canadian Institutes of Health Research (CIHR) to PSM, National Institutes of Health GM093121 to LH. MSI was supported by a Frederick Banting and Charles Best Canada Graduate Scholarship from CIHR. PSM is a James McGill Professor.

PREFACE TO CHAPTER 3

Rab GTPases cycle between an active GTP-bound form and an inactive GDP-bound form. GTP-bound Rabs are anchored to membranes via a C-terminal hydrophobic prenyl group. Following inactivation, GDP-bound Rabs are thought to be extracted from membrane by GDI and held soluble in the cytosol until reactivation occurs. While this mechanism holds true for several GTPases, several examples in the literature exist whereby inactive Rabs remain on membrane bound structures. For instance GDP-bound Rab35 is present on the plasma membrane and GDP-bound Rab11 is found on cytoplasmic vesicles that are presumably derived from recycling endosomes (Allaire et al., 2010;Savina et al., 2002). In fact, GTP-bound Rab11 that binds FIP3 and dynein to facilitate minus-end microtubule transport while GDP-bound Rab11 interacts with protrudin and KIF5 to facilitate plus-end microtubule transport (Shirane and Nakayama, 2006). This questions the currently held belief that GDP-bound Rabs are simply "off" and suggests that GDP-bound Rabs may play a more active role in membrane trafficking. In Chapter 2, we discovered that GDP-Rab13 can be found on cytoplasmic vesicles; however the mechanism by which GDP-Rab13 can associate with these vesicles and the identity of these vesicles remain elusive. In Chapter 3, we find that in addition to recycling endosomes, Rab13 can be found on vesicles containing markers of the late endocytic compartment. Furthermore we discovered that GDP-Rab13 does not require C-terminal prenylation in order to traffic on vesicles but is recruited to these vesicles via protein-protein interactions.

CHAPTER 3

RAB13 TRAFFICS ON VESICLES INDEPENDENT OF PRENYLATION

Maria S. Ioannou, Martine Girard, & Peter S. McPherson

Department of Neurology and Neurosurgery, Montreal Neurological Institute, McGill University, Montreal, Quebec H3A 2B4, Canada

Originally published in The Journal of Biological Chemistry

doi: 10.1074/jbc.M116.722298

3.1 Abstract

Rab GTPases are critical regulators of membrane trafficking. The canonical view is that Rabs are soluble in their inactive GDP-bound form, and only upon activation and conversion to their GTP-bound state are they anchored to membranes through membrane insertion of a C-terminal prenyl group. Here, we demonstrate that C-terminal prenylation is not required for Rab13 to associate with and traffic on vesicles. Instead, inactive Rab13 appears to associate with vesicles via protein-protein interactions. Only following activation does Rab13 associate with the plasma membrane presumably with insertion of the C-terminal prenyl group into the membrane.

3.2 Introduction

Rab GTPases control all aspects of membrane trafficking ranging from vesicle formation and transport to tethering and fusion with the target membrane (Stenmark, 2009). The understanding of Rab regulation is thus critical for a full understanding of membrane trafficking. Furthermore, disturbances in Rab function are observed in several diseases. Notably, alterations in the levels or activity of Rab5, Rab35, Rab8 and Rab13 have been implicated in phenotypes associated with cancer (Yang et al., 2011;Allaire et al., 2013;Bravo-Cordero et al., 2007;Ioannou et al., 2015).

As for all small GTPases, Rabs cycle between an active GTP-bound form and an inactive GDP-bound form. They are activated by guanine-nucleotide exchange factors (GEFs) that facilitate the exchange of GDP for GTP, and they are inactived by GTPase activating proteins (GAPs), which enhance Rab-mediated hydrolysis of GTP to GDP. Furthermore, Rabs are post-translationally modified by prenylation; that is the covalent attachment of either a C15 (farnesyl) or C20 (geranylgeranyl) isoprenoid to cysteine residues at the carboxyl terminus (Pereira-Leal et al.,

2001). When the Rab is active it associates with membranes with insertion of the prenyl group into the lipid bilayer, while effector molecules bind to the switch region (Stenmark and Olkkonen, 2001). This allows the Rab to coordinate the function of the effector protein to the membrane compartment where it is anchored. When the Rab is inactive, it loses affinity for the effector molecules and is extracted from membrane by GDP dissociation inhibitors (GDIs) (Soldati et al., 1993;Pfeffer et al., 1995). GDIs bind the hydrophobic prenyl group to prevent its re-association with membrane and keep the Rab soluble in the cytosol. Consistently, deletion or mutation of the C-terminal cysteine residues results in complete cytosolic localization of both Rab4 and Rab5 (Gomes et al., 2003).

Rabs are thought to associate with membranes only upon activation (Goody et al., 2005). However, it seems that at least some Rabs can associate with membrane in their inactive GDP-bound form. For example, inactive Rab35 exists on the plasma membrane while inactive Rab11 can be found on cytoplasmic vesicles (Allaire et al., 2010;Savina et al., 2002). Here, we show that inactive Rab13 in the absence of prenylation traffics on vesicles derived from recycling and late endosomal compartments. Instead, Rab13 associates with these vesicles as part of a protein complex.

3.3 Materials and Methods

Antibodies, DNA Constructs, and shRNA

Mouse monoclonal antibodies were from the following sources: Rab8, flotillin (BD Biosciences, Mississauga, ON); Rab9 (Abcam; Cambridge, MA); Na^+/K^+ ATPase (Upstate Biotechnology,

Lake Placid, NY). Rabbit and chicken polyclonal antibodies against Rab5 and Rab13, respectively, were from Abcam. Rat monoclonal Hsc70 (1B5) antibody was obtained from Enzo Life Sciences. Homemade rabbit polyclonal antibodies against Rab35 and RME-8 were previously described (Allaire et al., 2010;Girard et al., 2005b). mCherry (mCh) tagged Rab13 (human amino acids 1-203) wild-type (WT), T22N and Q67L were previously described (Ioannou et al., 2015). Rab13 C-terminal deletion construct (human, amino acids 1-199) and hypervariable domain deletion constructs (human, amino acids 1-175) were PCR amplified, digested with EcoRI and BamHI, and ligated into the mCherry-C2 vector. Cellubrevin and TI-VAMP in pEGFP-C3 were previously described and were a gift form Dr. T. Galli (Martinez-Arca et al., 2000;Galli et al., 1994). Rab7 and Rab9 (canine) in pEGFP-C1 were a gift from F. Meunier (University of Queensland, Brisbane, Australia). Rab5 in pEGFP-C2 was previously described (Allaire et al., 2010). Stable Rab13 knockdown in HEK-293T cells was achieved using lentivirus to drive expression Rab13 shRNA1 (TRCN0000381528), shRNA2 (TRCN0000382005), shRNA3 (TRCN0000343510), or control vector of pLKO-TRC005 obtained from the Mission@TRC genome-wide shRNA collection (Sigma) as previously described (Ioannou et al., 2015). Primers used to generate constructs and shRNAs can be found in Table S1. All constructs were verified by sequence analysis.

Subcellular Fractionation

Various rat tissues or cultured cells were homogenized in HEPES buffer [20 mM HEPES, pH 7.4, containing protease inhibitors (0.83 mM benzamidine, 0.23 mM phenylmethylsulfonyl fluoride, 0.5 μg/ml aprotinin, and 0.5 μg/ml leupeptin)] and centrifuged at 800 × *g* for 10 min at 4°C to remove cell debris. The supernatant was centrifuged at 200,000 × *g* for 30 min yielding

the supernatant (S1) and pellet (P1) fractions. P1 was subsequently resuspended in HEPES buffer with or without NaCl, KCl, EDTA, detergents [1% Triton-X 100, 1% NP-40, 25 µg/mL digitonin or 1% SDS and 0.5% deoxycholate (DOC)] or in 50 mM $NaCO_3$ at pH 11.0. Following incubation for 15 min the samples were centrifuged at 200,000 × *g* for 30 min yielding the S2 and P2 fractions. Equal protein aliquots of the fractions were analyzed by SDS-PAGE and Western blot. Blots were analyzed using ImageJ 1.43m (National Institutes of Health).

Rab GDI Extraction

HEK-293T cells were transfected with His-myc-Rab GDI. At 18 hours post-transfection, cells were lysed in binding buffer (50 mM HEPES pH 8.0, 300 mM NaCl, 20 mM imidazole, 1% Triton X-100 and protease inhibitors), centrifuged at 200,000 x g for 15 min at 4°C and incubated with Ni-NTA agarose beads (Qiagen) rocking for 2 h at 4°C. Beads were washed once in binding buffer, twice in wash buffer (50 mM HEPES pH 6.5, 300 mM NaCl, 20 mM imidazole and protease inhibitors) and eluted from beads in elution buffer (50 mM HEPEs pH 6.5, 300 mM NaCl, 200 mM NaCl and protease inhibitors). Purified His-myc-Rab GDI was concentrated and buffer exchanged into HEPES buffer using Amicon®Ultra 10K centrifugal filter (Millipore). For GDI extraction, HEK-293T cells were treated as described above and P1 was resuspended in HEPES buffer containing increasing concentrations of purified His-myc-Rab GDI, incubated for 30 min at 37°C and centrifuged at 200,000 × *g* for 30 min at 4°C yielding the S2 and P2 fractions. Equal protein aliquots of the fractions were analyzed by SDS-PAGE and Western blot.

Discontinuous Sucrose Gradient

Sucrose gradients were performed as described in (Kumari and Francesconi, 2011). In brief, HEK-293T cells were washed twice in PBS and lysed in HNEX buffer (20 mM HEPES, 150 mM NaCl, 5 mM EDTA, 10% Triton X-100 and protease inhibitors), sonicated, incubated on ice for 10 min and spun at 800 x g for 10 min at 4°C to remove cell debris. Sucrose solutions were prepared in HNE buffer (20 mM HEPES, 150 mM NaCl, 5 mM EDTA). The cell extract was adjusted to 40% sucrose. 3 mL of 5% sucrose solution was underlaid with 6 mL of 30% sucrose solution followed by 4 mL of cell extract. Samples were centrifuged at 230,000 x g for 16 h at 4°C and 1 mL fractions were collected and analyzed by SDS-PAGE and Western blot.

Immunofluorescence and Live Cell Imaging

For live-cell imaging, MCF10A cells were plated on poly-L-lysine-coated 35 mm No. 1.5 glass bottom dishes (MatTek Corporation). Cells were transfected using JetPrime Reagent and incubated for 14 h. PC12 cells were differentiated in reduced serum media containing 50 ng/mL NGF for 36 hours and transfected using JetPrime Reagent and incubated for 14 h. For internalization of transferrin, transfected cells were serum starved for 1 h and incubated in serum-free media containing 25 µg/mL transferrin-Alexafluor647 for 30-60 min as previously shown to allow the internalized transferrin to reach recycling endosomes (Sheff et al., 2002). Cells were washed and imaged in complete media. Live-cell imaging was performed using an AxioObserver Z1 (Zeiss) microscope equipped with a plan-aprochromat 40x oil objective (NA=1.4), a Definite Focus system, and an AxioCam MR3 camera (Zeiss). Cells were kept at 37°C in 5% CO_2 using Incubation System S (Pecon, Germany). GFP and mCherry were imaged using 470 nm and 591 nm LEDs respectively, from a Colibri.2 illumination source (Zeiss).

Acquisition and analyses were performed using ZEN 11.0 software (Zeiss). For co-localization analysis, MCF10A cells were plated on poly-L-lysine-coated coverglass and transfected using JetPrime Reagent and incubated for 14 h. Cells were subsequently washed in PBS at 37°C and fixed for 10 min in 3% PFA at 37°C. Cells were mounted using dako mounting medium (Agilent Technologies) and imaging was performed using a 710 Laser Scanning Confocal Microscope equipped with a plan-aprochromat 63x oil objective (NA=1.4) (Zeiss). Acquisition was performed using ZEN 11.0 software (Zeiss). Percentage of co-localization was determined thresholding images of cells, create a binary image for each channel, and using the co-localization plug-in on ImageJ to calculate the percentage of overlap between the two channels.

Statistical Analysis

Statistics were analyzed using SPSS version 17. Mean and SEM were used to determine significant differences between pairs. Comparisons of groups were performed using Student's t-test or one-way analysis of variance (ANOVA) and Dunnet post-test for multiple comparisons. *$p<0.05$, **$p<0.01$ and ***$p<0.001$.

3.4 Results and Discussion

Inactive Rab13 traffics on vesicles

It is generally assumed that Rabs are soluble when in their inactive GDP-bound form and only upon activation and conversion to the GTP-bound form do they associate with membranes. However, as we have previously described, both constitutively active (Q67L) and constitutively inactive (T22N) mutant forms of Rab13 are present on vesicles in MCF10A epithelial cells (Fig.

3.1 A). In fact, Rab13 T22N traffics on dynamic vesicles into and out of the perinuclear region similar to Rab13 Q67L (Ioannou et al., 2015). The mutant Rabs in these experiments are commonly used to study GTPase function; the active Q67L mutation abolishes GTP hydrolysis, rendering the Rab GTP-locked, while the inactive T22N mutation disrupts Mg^{2+} binding thereby reducing the affinity for GTP by 100-fold without affecting the affinity for GDP, resulting in a GDP-locked Rab (Farnsworth and Feig, 1991;Nuoffer et al., 1994). However, in some cases dominant-negative mutations may not completely inactivate the protein but rather slow its activation. This is the case in *Drosophila*, where Rab7 T22N overexpression can partially rescue Rab7 null mutants showing that Rab7 T22N retains some of its wild-type function (Cherry et al., 2013). Therefore, we sought to examine if the mCh-Rab13 T22N mutant retains wild-type function by performing pull-down assays using the Rab-binding domain of the Rab13 effector MICAL-L1 (Abou-Zeid et al., 2011). While mCh-Rab13 Q67L binds strongly to the effector domain, mCh-Rab13 T22N is unable to bind (Fig. 3.1 B). This is consistent with previous studies showing that expression of Rab13 T22N in functional assays acts in a dominant-negative fashion (Sakane et al., 2010). Thus, Rab13 T22N is indeed in its inactive form as it traffics on vesicles.

Interestingly, while both Rab13 mutants are found on cytoplasmic vesicles, only mCh-Rab13-Q67L is found on the plasma membrane (Fig. 3.1 A and C). Previously, we determined that Rab13 is activated specifically at the plasma membrane where its GEFs DENND1C and DENND2B are localized (Ioannou et al., 2015;Marat et al., 2012). This suggests that activation by its GEF is required for association of Rab13 with the plasma membrane. This is consistent with the notion that GEFs play an important role in targeting Rabs to specific membranes (Blumer et al., 2013). For example, knockdown of the GEF for Rab32, BLOC-3 prevents the targeting of Rab32 to ring-like membrane structures in melanosomes (Gerondopoulos et al.,

2012). Interestingly, Rab32 could still be found on small puncta following BLOC-3 knockdown. Thus, BLOC-3 functions to target Rab32 to specific membrane compartments. The same appears to hold true for Rab13 as only the active form is found on the plasma membrane.

Rab13 has been predominantly studied in epithelial cells as Rab13 activity regulates tight junction assembly and stimulates cell invasion and migration (Marzesco et al., 2002;Kohler et al., 2004;Wu et al., 2011a;Ioannou et al., 2015). However, Rab13 is also required for NGF-induced neurite outgrowth in PC12 cells and dorsal root ganglion neurons (Di et al., 2005;Sakane et al., 2010). We thus sought to determine whether trafficking of inactive Rab13 on vesicles is a characteristic of cell types other than MCF10A. mCh-Rab13 T22N traffics on vesicles in neurites of differentiated PC12 cells (Fig. 3.1 D). Therefore, the targeting and trafficking of inactive Rab13 on vesicles is likely to be characteristic of multiple cells types.

Inactive Rab13 traffics on vesicles derived from multiple endosomal compartments

Rab13 controls the delivery of cargo that traffic through recycling endosomes to the plasma membrane (Nokes et al., 2008). Consistently, Rab13 is localized to the TGN, recycling endosomes and the plasma membrane (Nokes et al., 2008;Ioannou et al., 2015). To confirm that the vesicles carrying inactive Rab13 are functional we tested for co-trafficking with internalized transferrin, a major recycling cargo that passes through recycling endosomes and has been previously shown to co-localize with wild-type Rab13 (Yamashiro et al., 1984;Nokes et al., 2008). mCh-Rab13 T22N co-localizes with internalized transferrin and traffics on vesicles that contain the internalized ligand (Fig. 3.2 A). Thus, inactive Rab13 is present on functional vesicles, likely derived from recycling endosomes.

As several trafficking routes exist to recycle cargo back to the plasma membrane, we sought to further define the identity of vesicles carrying Rab13. Exocytosis of transferrin-containing vesicles is partially regulated by the tetanus toxin-sensitive v-SNARE cellubrevin (Galli et al., 1994). However, there was limited co-localization of Rab13 (inactive or active) with cellubrevin (Fig. 3.2 B and C). Instead, we discovered that a large fraction of both mutants of Rab13 co-localize with tetanus-insensitive TI-VAMP (VAMP7) (Fig. 3.2 B and C). This result was particularly interesting given that TI-VAMP regulates many of the same physiological functions as Rab13 including plasma membrane delivery of GLUT4, neurite outgrowth, and cell migration (Chaineau et al., 2009). While TI-VAMP can be found at the plasma membrane and TGN, where Rab13 has been localized, TI-VAMP is predominantly found on late endosomal compartments (Chaineau et al., 2009). Intriguingly, wild-type Rab13 also localizes in part to Rab7-positive late endosomes (Abou-Zeid et al., 2011). In fact we found that both active and inactive Rab13 constructs co-localize with late endosomal markers Rab7 and Rab9 with much less co-localization with early endosomal marker Rab5 (Fig. 3.2 B and C). Together our data suggest that both active and inactive Rab13 traffic on two distinct populations of vesicles; those carrying transferrin from recycling endosomes and TI-VAMP/Rab7 positive vesicles derived from late endosomes. However, it remains unknown how inactive Rab13 associates with these vesicles.

Inactive Rab13 resists membrane extraction by Rab GDI

We next sought to characterize the association of inactive Rab13 on endosome-derived vesicles. Classically, following inactivation Rabs are solubilized from the membrane by GDI. GDI binds to prenylated Rabs in their inactive GDP-bound form, extracts them from the membrane and holds them soluble in the cytosol until reactivation (Pfeffer and Aivazian, 2004). However,

Rab13 resists extraction from membranes by GDI (Marzesco et al., 1998). Here we show that in addition to endogenous Rab13, both mCh-Rab13 Q67L and mCh-Rab13 T22N resist extraction from membranes by purified GDI, whereas Rab9 shows a clear dose-dependent extraction (Fig. 3.3 A). Although PDE-delta can partially solubilize Rab13 from the particulate fraction (Marzesco et al., 1998), GDIs bind Rabs with little to no specificity (Ullrich et al., 1993). We therefore reasoned that some mechanism must be in place in order to prevent the solubilisation of Rab13 by GDI. One possibility is that Rab13 traffics on lipid rafts. Lipid rafts are stable microdomains within membranes that are enriched in cholesterol and sphingolipids (Simons and Ikonen, 1997). Elevated levels of cholesterol on these membrane domains reduce the ability of GDI to extract certain Rabs from membranes (Lebrand et al., 2002;Ganley and Pfeffer, 2006). Because lipid raft markers cycle between the TGN and the plasma membrane, where Rab13 also functions, we tested whether Rab13 was present on lipid rafts (Nichols et al., 2001). Using sucrose gradients, we found that Rab13 from HEK-293T cell lysates does not co-fractionate (float) with detergent-resistant membranes revealed by the raft marker flotillin (Fig. 3.3 B). While we cannot exclude that Rab13 associates with lipid rafts in other cell types, it does not in HEK-293T cells and therefore another mechanism must be in place to mediate the resistance to GDI extraction.

C-terminal prenylation is not required for the targeting of inactive Rab13 to vesicles

As GDIs bind to the hydrophobic prenyl group on Rabs, and Rab13 resists extraction by GDI, we tested whether Rab13 requires C-terminal prenylation in order to interact with cytoplasmic vesicles. Rab13 is geranylgeranylated on the cysteine residue of its CaaX motif found at the extreme C-terminus (Joberty et al., 1993). Therefore we deleted the last 4 amino acids of the

protein containing the prenylation site (Rab13ΔC) (Fig. 3.4 A). Interestingly, inactive mCh-Rab13 T22N-ΔC remains associated with vesicles (Fig 3.4 B and C). These vesicles retain the proper perinuclear localization and have no obvious trafficking defects (Fig. 3.4 B and D). Again, we verified that these vesicles were functional as mCh-Rab13 T22N-ΔC co-traffics with internalized transferrin (Fig. 3.4 E). Thus, inactive Rab13 is present on vesicles carrying recycling cargo even in the absence of prenylation. Furthermore, we found that mCh-Rab13 T22N-ΔC traffics on vesicles in neurites of differentiated PC12 cells showing this is a general feature of Rab13 and is not cell specific (Fig. 3.4 F). These data indicate that inactive Rab13 is recruited to vesicles in a prenylation independent manner.

Several studies have indicated that the hypervariable domain (HVD) of Rabs contributes to membrane targeting (Chavrier et al., 1991;Li et al., 2014a). The HVD is an unstructured region directly adjacent to the prenylation motif and is the most divergent region of Rabs. The HVD is required for membrane targeting of several Rabs including Rab7 and Rab35, but is not required for membrane targeting of Rab1 or Rab5 (Ali et al., 2004;Li et al., 2014a). Deletion of both the HVD and C-terminal of inactive Rab13 (Fig. 3.4 A) reduced the number of cells containing Rab13-positive vesicles, but did not lead to a complete redistribution to the cytosol (Fig. 3.4 B and C). Thus, inactive Rab13 can be recruited to vesicles in the absence of its HVD and prenylation.

Endogenous Rab13 associates with membranes through protein-protein interactions

The retention of inactive Rab13 on vesicles despite deletion of the HVD and the C-terminal prenylation site suggests that interactions within the switch regions are important for vesicle

association. Proteins that interact preferentially with the GDP-bound form of Rab13 could mediate this vesicle association. While GEFs and GDIs are thought to be the predominant binding partners for GDP-bound Rabs, other interacting proteins have been described. For instance, the GRAM domain of myotubularin-related protein 6 (MTMR6) interacts preferentially with GDP-bound Rab1b (Mochizuki et al., 2013). Furthermore, protrudin interacts preferentially with GDP-bound Rab11 (Shirane and Nakayama, 2006) In fact, GDP-bound Rab11 binds protrudin and KIF5 to facilitate plus-end microtubule transport while GTP-bound Rab11 that binds FIP3 and dynein to facilitate minus-end microtubule transport suggesting that GTP/GDP cycling of Rabs is not as simple as an on/off switch (Welz et al., 2014;Shirane and Nakayama, 2006).

Thus, we speculate that inactive Rab13 associates with vesicle membranes through interactions with proteins. We therefore used subcellular fractionation and classic membrane extraction protocols to examine the association of endogenous Rab13 with membranes. Ultra-speed centrifugation was employed to separate HEK-293 cell lysates into particulate (P) and cytosolic (S) fractions, the P fraction was resuspended in various buffers and a second high speed centrifugation yielded S2 and P2 fractions. We first used Triton X-100 in the absence of salt, which will solubilize integral membrane proteins such as the Na^+K^+ATPase, as well as proteins anchored to membranes through insertion of prenyl groups, such as Rab5 and Rab9 (Fig. 5*A* and *B*) (Girard et al., 2005b). Consistent with our transfection studies, endogenous Rab13 largely resisted extraction under this condition (Fig. 3.5 A and B). We next utilized carbonate buffer at pH 11.0, which disrupts most protein-protein complexes and solubilizes large scaffolding proteins that are anchored to membranes through protein-protein interactions, such as RME-8,

but leaves membranes intact and will thus not alter the pelleting of prenylated proteins such as Rab9 or integral membrane proteins such as Na^+K^+ATPase (Fig. 3.5 A and C) (Girard et al., 2005b). This condition leads to the extraction of a significant percentage of Rab13, whereas Rab35, Rab5 and Rab9 remain entirely in the P2 fraction (Fig. 3.5 A and C). In the epithelial cell lines MCF10A and MCH46 we also found that the majority of Rab13 extracts in pH 11.0 and not in Triton X-100 demonstrating that the observed results are a general characteristic of Rab13 and are not cell specific (Fig. 3.5 D and E). To confirm that the Rab13 antibody is indeed targeting endogenous Rab13 we performed knockdown of Rab13 using three different shRNAs and observed a large reduction of the immunoreactive band (Fig. 3.5 F). Furthermore, Rab13 resists extraction in multiple non-ionic detergents in the absence of salt but is extracted in a mixture of the anionic/denaturing detergents sodium deoxycholate and sodium dodecyl sulphate, similar to the extrinsic membrane protein RME-8 (Fig. 3.5 G) (Girard et al., 2005b). Rab13 also resists extraction with physiological concentrations of salt, and only partially extracts in 100 mM NaCl containing Triton X-100 (Fig. 3.5 H and I). Thus Rab13 behaves as a peripheral membrane protein in cell lines.

Some Rabs may pellet due to interactions with the cytoskeleton; for example Rab24 distributes to the particulate fraction due to interactions with microtubules (Militello et al., 2013). Since Rab13 interacts with actin binding proteins, we wondered whether the extraction behavior of Rab13 in our biochemical experiments could be attributed to cytoskeletal associations. Resuspension of the particulate fraction in ice cold HEPEs leads to spontaneous disassembly of the cytoskeleton and redistribution of the majority of both actin and tubulin into the supernatant following a second high speed centrifugation (Fig. 3.5 J and K). However, Rab13 remains

entirely in the pellet under these conditions (Fig. 3.5 J and K). Since Rab13 does not solubilize along with the cytoskeleton, this suggests that protein-protein interactions in addition to those with the cytoskeleton are responsible for the extraction behavior of Rab13.

Next, we wondered whether this phenotype was specific to cultured cells or could also be observed with endogenous Rab13 from tissue. In fact Rab13 extracts from the particulate fraction in pH 11.0, and only partially extracts in Triton X-100 in both rat brain (Fig. 3.6 A and C) and liver (Fig. 3.6 B and D). Consistent with our cell line data, Rab5 extracted only with Triton X-100 and not in pH 11.0 (Fig. 3.6 A-D). Thus, our data suggest that a pool Rab13 is likely stabilized on membranes through protein-protein interactions and not through insertion of a hydrophobic prenyl group. We also wondered whether the nucleotide status of Rab13 affects its ability to associate with protein complexes. We repeated our ultra-speed centrifugation of HEK-293 cell lysates and found that Rab13 resists extraction with the addition of EDTA to render the protein nucleotide free (Fig. 3.7 A). Furthermore, we found that mCh-Rab13 WT, mCh-Rab13 Q67L, mCh-Rab13 T22N and mCh-Rab13 T22N-ΔC all resist extraction with Triton-X100 and largely extract in pH 11.0 (Fig. 3.7 A). Therefore, Rab13 associates with membranes likely through protein-protein interactions independent of its nucleotide status or prenylation.

Conclusion

Here we show that Rab13 traffics on vesicles derived from both recycling and late endosomal compartments in both its inactive and active form while only active Rab13 is found on the plasma membrane. We have discovered that inactive Rab13 does not require C-terminal

prenylation to traffic on these vesicles. Instead Rab13 exists on vesicles likely as part of a large protein complex. It will be interesting in the future to investigate whether other Rabs can associate with membranes independent of prenylation. With roughly 70 mammalian Rabs, the largest family of small GTPases, this could represent a conserved mechanism used by a subset of Rabs to regulate membrane trafficking.

3.5 Tables and Figure

Supplemental Table 3.1.

Oligonucleotides used in the study

Primers for fusion proteins	
Rab13 aa 1 EcoRI F	GCGGAATTCATGGCCAAAGCCTACGACCAC
Rab13 aa 199 BamHI R	GCGGGATCCTCACTTGTTGGTGTTCTTCTTGTCAC
Rab13 aa 175 BamHI R	GCGGGATCCTCAGCCTCCTGACTTGAGCAAGATG
Sequences for shRNAs	
Rab13 shRNA #1	GTACCGGAGAGCGGTTCAAGACAATAACCTCGAGGTTATTGTCTTGAACCGCTCTTTTTTTG
Rab13 shRNA #2	GTACCGGAGAAGGAGCAGGCCGATAAGTCTCGAGACTTATCGGCCTGCTCCTTCTTTTTTTG
Rab13 shRNA #3	CCGGATGAGAAATCTTTCGAGAATACTCGAGTATTCTCGAAAGATTTCTCATTTTTTG

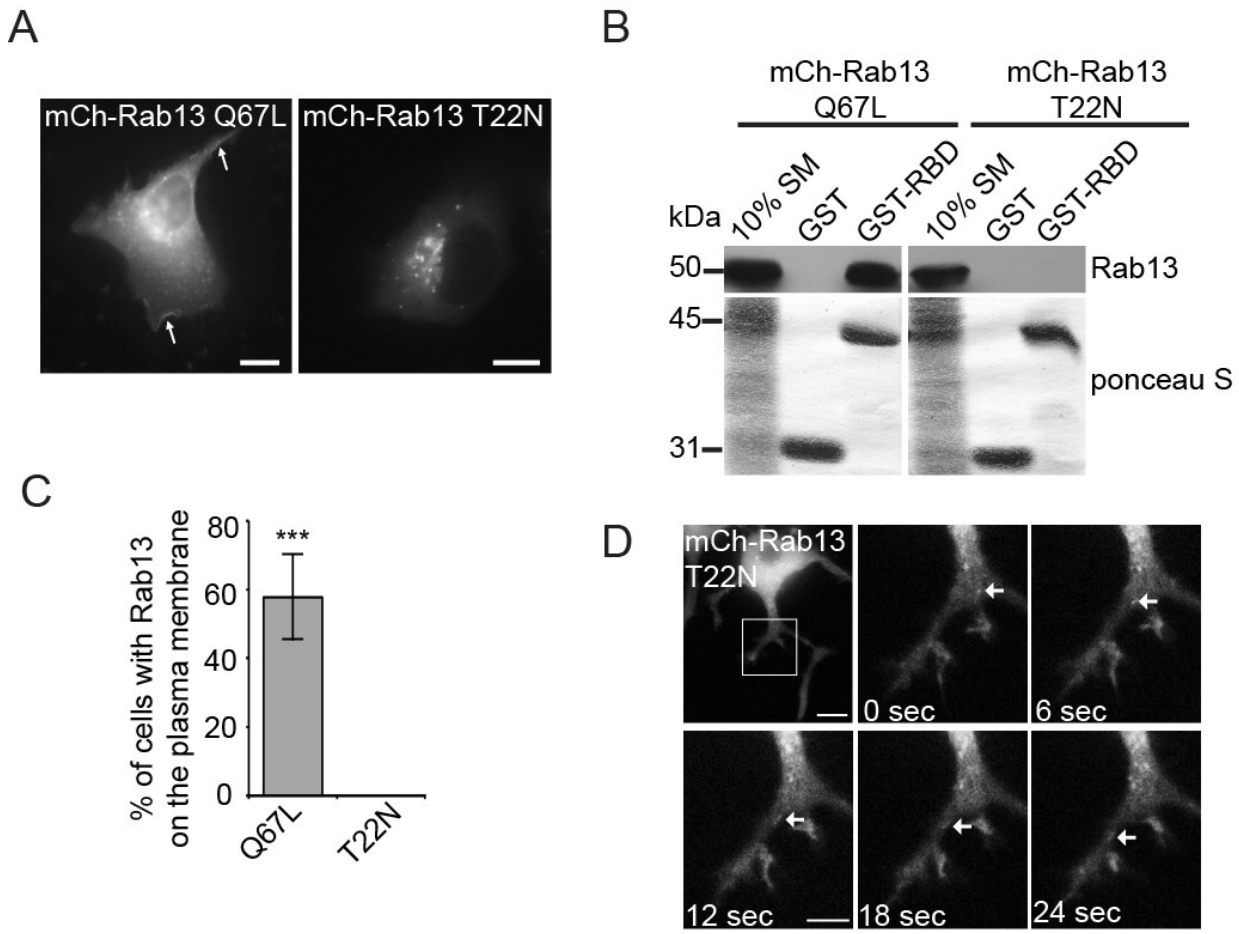
A
mCh-Rab13 Q67L
mCh-Rab13 T22N
B
mCh-Rab13 Q67L
mCh-Rab13 T22N
kDa
10% SM
GST
GST-RBD
10% SM
GST
GST-RBD
50
45
31
Rab13
ponceau S
C
% of cells with Rab13 on the plasma membrane
80
60
40
20
0
***
Q67L
T22N
D
mCh-Rab13 T22N
0 sec
6 sec
12 sec
18 sec
24 sec

Figure 3.1.

Figure 3.1.

Inactive Rab13 traffics on vesicles. (A) MCF10A cells expressing mCh-Rab13 Q67L or mCh-Rab13 T22N were imaged live. *Arrows* illustrate localization on the plasma membrane. *Scale bars*: 10 μm. (B) GST-Rab-binding domain (RBD) or GST alone, bound to glutathione Sepharose were incubated with HEK-293T cell lysates expressing mCh-Rab13 Q67L or T22N. Ponceau S staining reveals the level of GST-Rabs while specifically bound Rab13 was detected by blot. Starting material (SM) equals 10% of the lysate used per condition. (C) Percentage of transfected cells with mCh-Rab13 constructs on the plasma membrane. Mean ± SD, measuring a minimum of 20 cells per experiment from a minimum of 3 independent experiments. Student's t-test; *** $p<0.001$. (D) PC12 cells differentiated for 24 hours by addition of 50 ng/mL NGF and expressing mCh-Rab13 T22N were imaged live. *Boxed region* is magnified. *Arrows* follow a vesicle trafficking along a neurite. *Scale bar*: 10 μm for top panel and 5 μm for magnified panel.

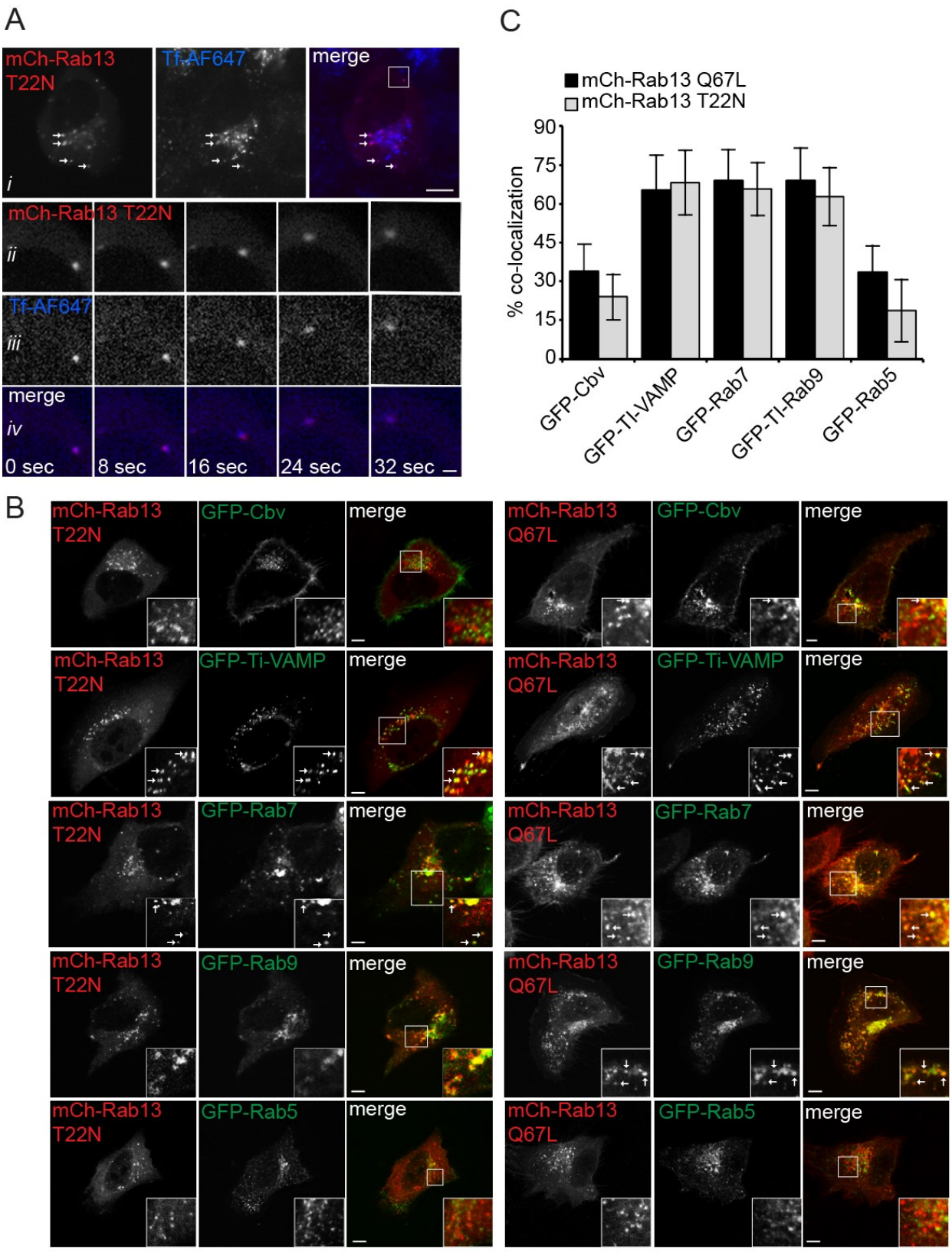
A
mCh-Rab13 T22N
Tf-AF647
merge
i
mCh-Rab13 T22N
ii
Tf-AF647
iii
merge
iv
0 sec
8 sec
16 sec
24 sec
32 sec
C
mCh-Rab13 Q67L
mCh-Rab13 T22N
% co-localization
90
75
60
45
30
15
0
GFP-Cbv
GFP-Ti-VAMP
GFP-Rab7
GFP-Ti-Rab9
GFP-Rab5
B
mCh-Rab13 T22N
GFP-Cbv
merge
mCh-Rab13 Q67L
GFP-Cbv
merge
mCh-Rab13 T22N
GFP-Ti-VAMP
merge
mCh-Rab13 Q67L
GFP-Ti-VAMP
merge
mCh-Rab13 T22N
GFP-Rab7
merge
mCh-Rab13 Q67L
GFP-Rab7
merge
mCh-Rab13 T22N
GFP-Rab9
merge
mCh-Rab13 Q67L
GFP-Rab9
merge
mCh-Rab13 T22N
GFP-Rab5
merge
mCh-Rab13 Q67L
GFP-Rab5
merge

Figure 3.2

Figure 3.2.

Rab13 is found on vesicles with multiple endosomal origins. (A) MCF10A cells expressing mCh-Rab13 T22N and internalized Alexa-fluor(AF) 647-labelled transferrin were imaged live (*i*). *Arrows* illustrate co-localization. The *boxed region* from *i* is magnified below over a time lapse imaging series (ii-iv). *Scale bars*: 10 μm for top panel and 1 μm for magnified panels. (B) MCF10A cells expressing mCh-Rab13 T22N or mCh-Rab13 Q67L co-expressed with GFP-cellubrevin (Cbv), GFP-TI-VAMP, GFP-Rab7, GFP-Rab9 or GFP-Rab5 were fixed and imaged. The b*oxed region* in each image is magnified in the insets. *Arrows* illustrate co-localization. *Scale bars*: 10 μm. (C) Quantification of percent co-localization as determined in experiments such as those in Fig 2*B*. Mean ± SD, measuring a minimum of 8 cells per experiment from a minimum of 2 independent experiments.

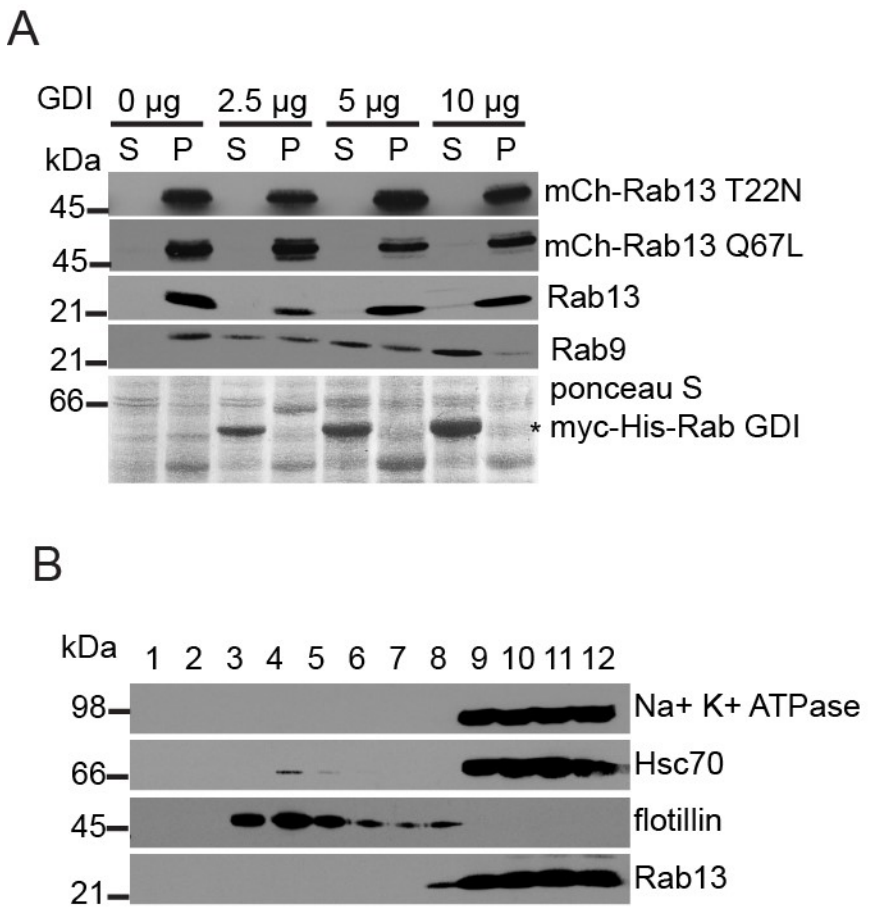
A
GDI
0 µg
2.5 µg
5 µg
10 µg
S P S P S P S P
kDa
45
45
21
21
66
mCh-Rab13 T22N
mCh-Rab13 Q67L
Rab13
Rab9
ponceau S
* myc-His-Rab GDI
B
kDa
1 2 3 4 5 6 7 8 9 10 11 12
98
66
45
21
Na+ K+ ATPase
Hsc70
flotillin
Rab13

Figure 3.3

Figure 3.3.

Rab13 resists membrane extraction by GDI. (A) HEK-293T cell homogenates were spun for 30 min at 200,000 x g and the resulting pellet was resuspended in HEPES buffer and incubated without or with increasing concentrations of purified myc-His-GDI as indicated. After 30 min of incubation at 37°C, samples were spun for 30 min at 200,000 x g and the resulting supernatant (*S*) and pellet (*P*) fractions were analyzed by Western blot using the indicated antibodies. The ponceau S stained transfer reveals the presence of the purified GDI. (B) HEK-293T cells were lysed in buffer containing 1% Triton X-100. Cell lysates were placed at the bottom of a discontinuous sucrose gradient and centrifuged at 230,000 x g for 16 h at 4°C. Twelve fractions of 1 ml each were collected with fraction 1 from the top and fraction 12 from the bottom of the gradient. The fractions were analyzed by Western blot with the indicated antibodies.

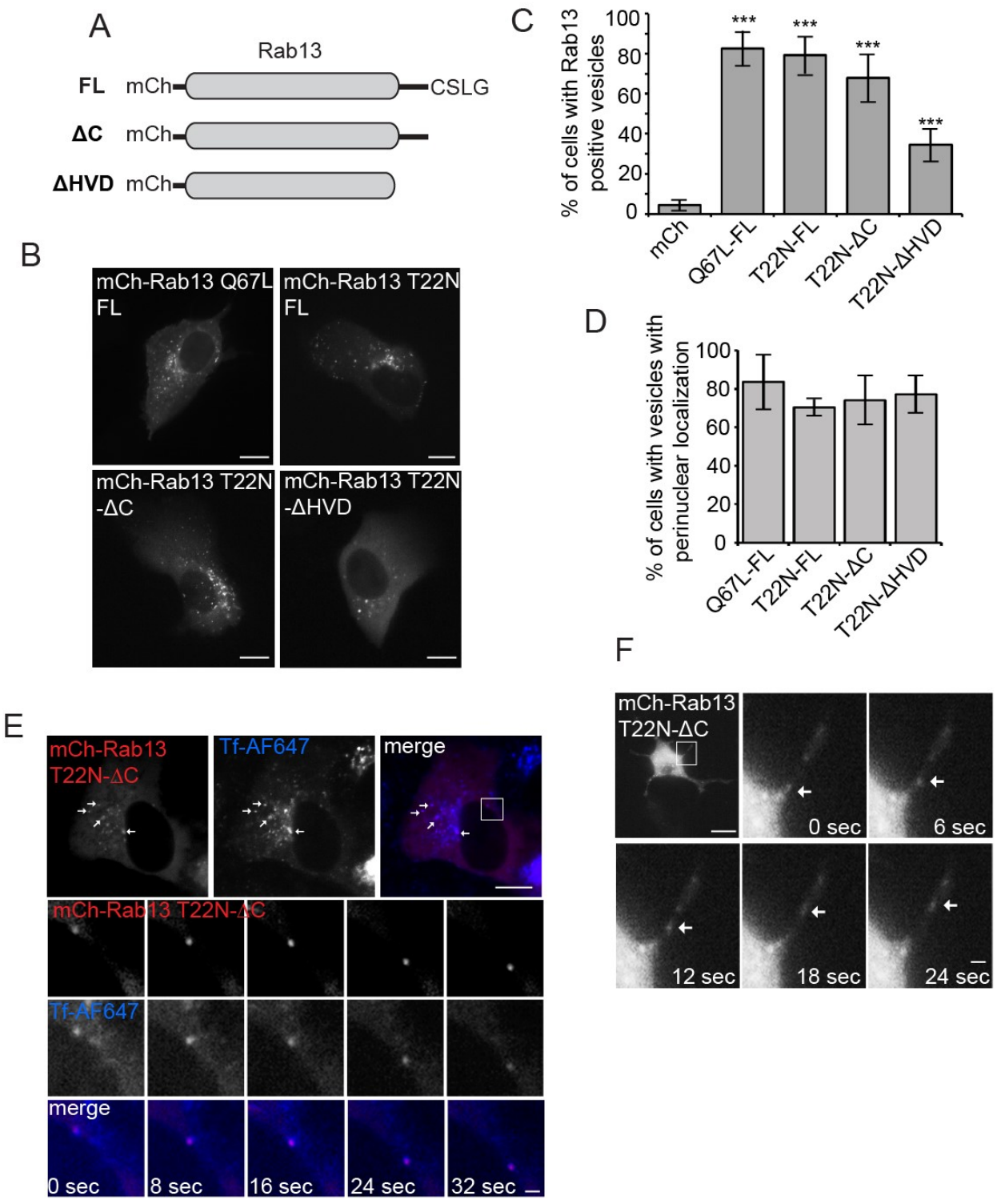
A
Rab13
FL mCh CSLG
ΔC mCh
ΔHVD mCh
B
mCh-Rab13 Q67L FL
mCh-Rab13 T22N FL
mCh-Rab13 T22N -ΔC
mCh-Rab13 T22N -ΔHVD
C
% of cells with Rab13 positive vesicles
100
80
60
40
20
0
***
mCh
Q67L-FL
T22N-FL
T22N-ΔC
T22N-ΔHVD
D
% of cells with vesicles with perinuclear localization
100
80
60
40
20
0
Q67L-FL
T22N-FL
T22N-ΔC
T22N-ΔHVD
E
mCh-Rab13 T22N-ΔC
Tf-AF647
merge
mCh-Rab13 T22N-ΔC
Tf-AF647
merge
0 sec
8 sec
16 sec
24 sec
32 sec
F
mCh-Rab13 T22N-ΔC
0 sec
6 sec
12 sec
18 sec
24 sec

Figure 3.4

Figure 3.4.

Inactive Rab13 traffics on vesicles following deletion of the C-terminal prenylation motif. (A) Schematic of constructs used in the figure. FL, full-length; ΔC, C-terminal deletion (last 4 amino acids); ΔHVD, hypervariable domain deletion. (B) MCF10A cells expressing mCh-Rab13 Q67L FL, T22N FL, or T22N deletion constructs, as indicated, were imaged live. *Scale bars*: 10 µm. (C) Percentage of transfected cells with mCh-Rab13 constructs on vesicles. Mean ± SD, measuring a minimum of 20 cells per experiment from a minimum of 3 independent experiments. (D) Percentage of cells from experiments as in *B* with mCh-Rab13 on vesicles that exhibit perinuclear localization. Mean ± SD, measuring a minimum of 20 cells per experiment from a minimum of 3 independent experiments. (E) MCF10A cells expressing mCh-Rab13 T22N ΔC and internalized Alexa-fluor(AF) 647-labelled transferrin were imaged live. *Arrows* in the top set on panels illustrate co-localization. The *boxed region* from the top set of panels is magnified below over a time lapse imaging series. *Scale bars*: 10 µm for top panel and 1 µm for magnified panels. (F) PC12 cells differentiated for 24 h with 50 ng/mL NGF and expressing mCh-Rab13 T22N-ΔC were imaged live. The *Boxed region* is magnified. *Arrows* follow vesicle trafficking along a neurite. *Scale bar*: 10 µm for top panel and 2.5 µm for magnified panel.

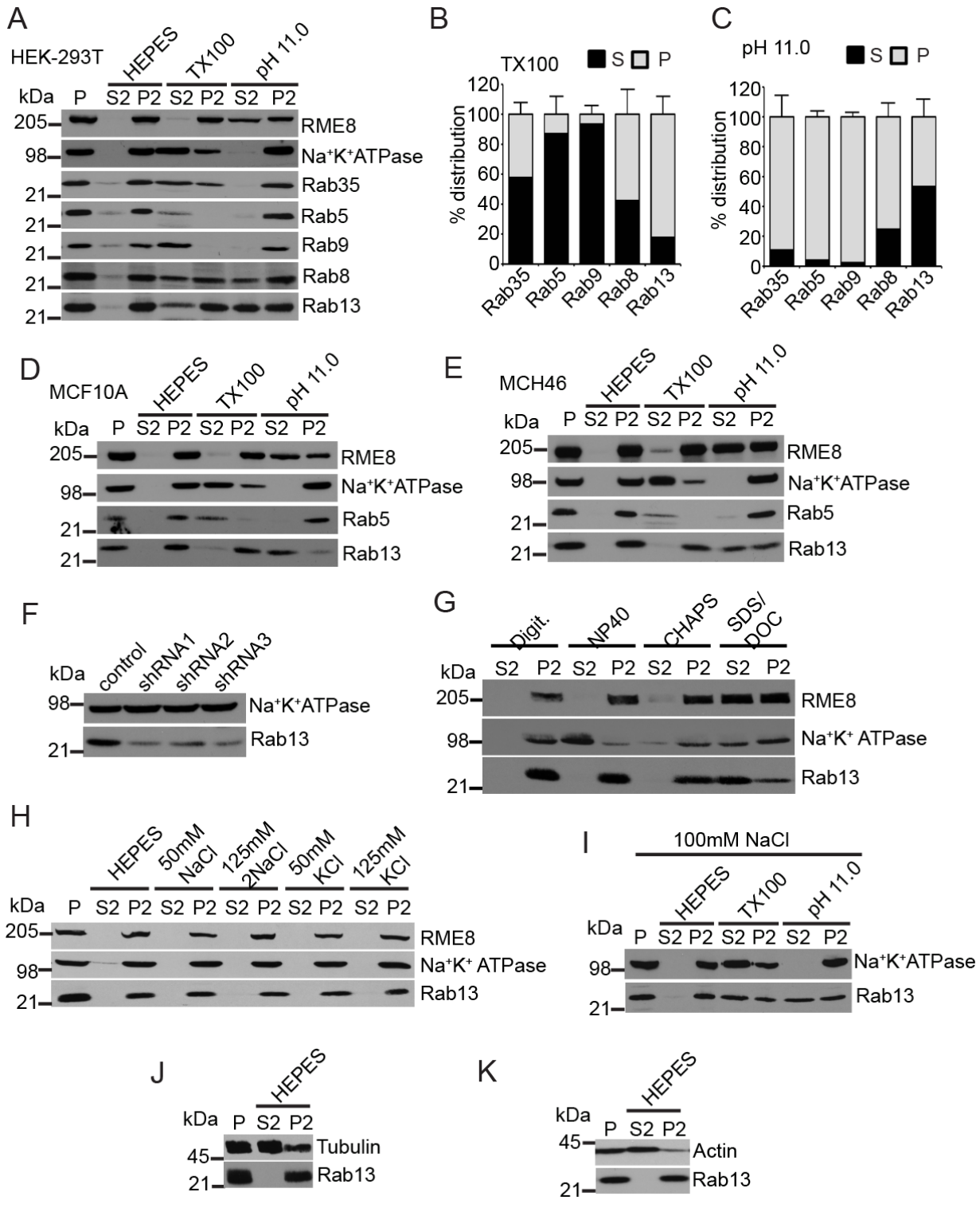
A
HEK-293T
HEPES
TX100
pH 11.0
kDa
P
S2 P2 S2 P2 S2 P2
205
RME8
98
Na+K+ATPase
Rab35
21
Rab5
Rab9
Rab8
Rab13
B
TX100
S
P
% distribution
120
100
80
60
40
20
0
Rab35
Rab5
Rab9
Rab8
Rab13
C
pH 11.0
S
P
% distribution
Rab35
Rab5
Rab9
Rab8
Rab13
D
MCF10A
HEPES
TX100
pH 11.0
kDa
P S2 P2 S2 P2 S2 P2
205
RME8
98
Na+K+ATPase
Rab5
21
Rab13
E
MCH46
HEPES
TX100
pH 11.0
kDa
P S2 P2 S2 P2 S2 P2
205
RME8
98
Na+K+ATPase
Rab5
21
Rab13
F
kDa
control
shRNA1
shRNA2
shRNA3
98
Na+K+ATPase
21
Rab13
G
Digit.
NP40
CHAPS
SDS/
DOC
kDa
S2 P2 S2 P2 S2 P2 S2 P2
205
RME8
98
Na+K+ ATPase
21
Rab13
H
HEPES
50mM
NaCl
125mM
2NaCl
50mM
KCl
125mM
KCl
kDa
P S2 P2 S2 P2 S2 P2 S2 P2 S2 P2
205
RME8
98
Na+K+ ATPase
21
Rab13
I
100mM NaCl
HEPES
TX100
pH 11.0
kDa
P S2 P2 S2 P2 S2 P2
98
Na+K+ATPase
21
Rab13
J
HEPES
kDa
P S2 P2
45
Tubulin
21
Rab13
K
HEPES
kDa
P S2 P2
45
Actin
21
Rab13

Figure 3.5

Figure 3.5.

Rab13 associates with membranes via protein-protein interactions in cells. (A) HEK-293T cell homogenates in HEPES buffer were spun for 30 min at 200,000 x g and equal protein aliquots of the resulting pellet (*P*) were resuspended in HEPES buffer with or without 1% Triton X-100 (TX100) or $NaCO_3$ at pH 11.0. After 15 min of incubation, samples were spun for 30 min at 200,000 x g and the resulting supernatant (*S2*) and pellet (*P2*) fractions were analyzed by Western blot using the indicated antibodies. (B-C) Quantification of the distribution of Rab proteins resuspended in Triton X-100 (B) and pH 11.0 (C). Mean ± SD; n=7 for Rab13, n=5 for and Rab5, n=4 for Rab8 and Rab35 and n=3 for Rab9. (D-E) Lysates of MCF10A cells (*D*) and MCH46 cells (*E*) were processed and analyzed as in *A*. (F) HEK-293T cells were stably transduced with lentivirus driving expression of control shRNA or three different shRNAs targeting Rab13, and the indicated proteins were detected by blot. (G) HEK-293T cell homogenates in HEPES buffer were spun for 30 min at 200,000 x g and equal protein aliquots of the resulting pellet (*P*) were resuspended in HEPES buffer with digitonin (digit.), NP-40, CHAPS or SDS/DOC. After 15 min of incubation, samples were spun for 30 min at 200,000 x g and the resulting supernatant (*S2*) and pellet (*P2*) fractions were analyzed by Western blot using the indicated antibodies. (H) HEK-293T cell homogenates in HEPES buffer were spun for 30 min at 200,000 x g and equal protein aliquots of the resulting pellet (*P*) were resuspended in HEPES buffer with or without NaCl or KCl and the indicated concentrations. After 15 min of incubation, samples were spun for 30 min at 200,000 x g and the resulting supernatant (*S2*) and pellets (*P2*) were analyzed by Western blot using the indicated antibodies. (I) HEK-293T cell

homogenates in HEPES buffer were spun for 30 min at 200,000 x g and equal protein aliquots of the resulting pellet (*P*) were resuspended in HEPES buffer containing 100 mM NaCl with or without 1% Triton X-100 (TX100) or $NaCO_3$ at pH 11.0. After 15 min of incubation, samples were spun for 30 min at 200,000 x g and the resulting supernatant (*S2*) and pellet (*P2*) fractions were analyzed by Western blot using the indicated antibodies. *(*J-K), HEK-293T cell homogenates in HEPES buffer were spun for 30 min at 200,000 x g and equal protein aliquots of the resulting pellet (P) were resuspended in ice cold HEPES buffer. After 15 min of incubation, samples were spun for 30 min at 200,000 x g and the resulting supernatant (S2) and pellets (P2) were analyzed by Western blot using the indicated antibodies.

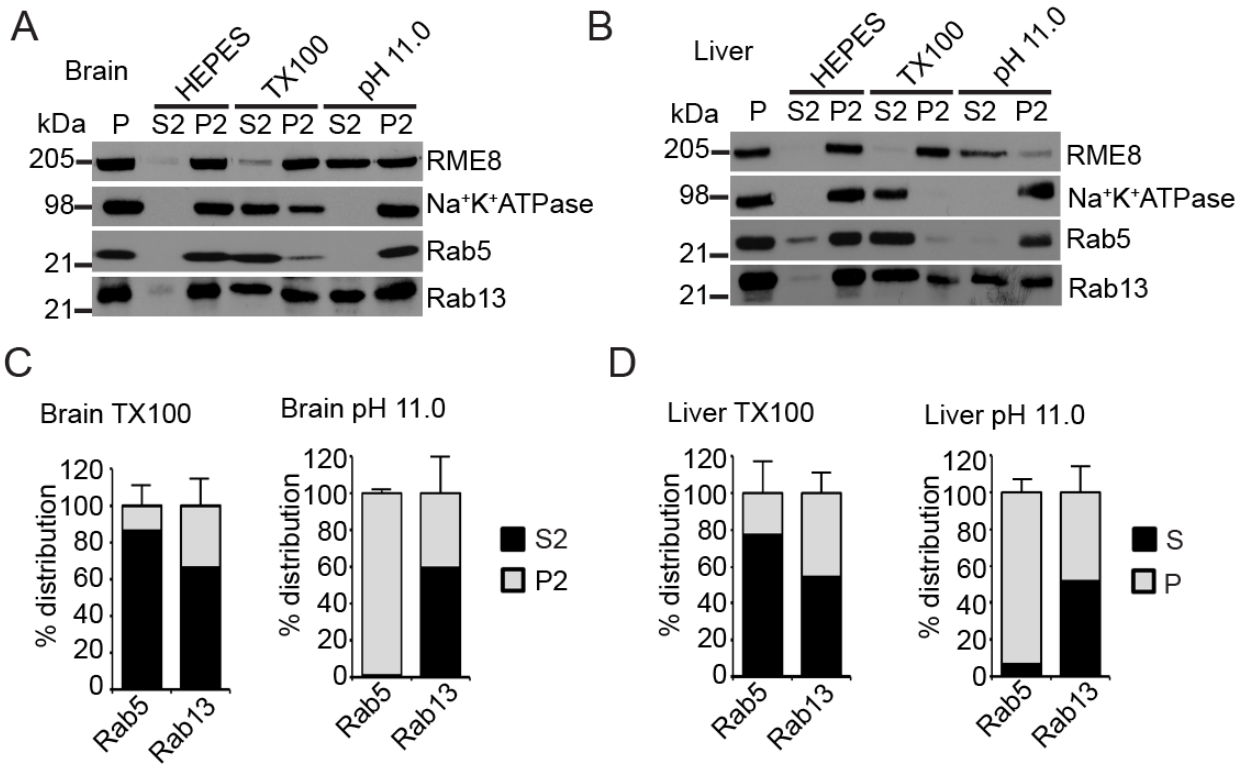
A
Brain
HEPES
TX100
pH 11.0
kDa
P
S2
P2
S2
P2
S2
P2
205
98
21
21
RME8
Na+K+ATPase
Rab5
Rab13
B
Liver
HEPES
TX100
pH 11.0
kDa
P
S2
P2
S2
P2
S2
P2
205
98
21
21
RME8
Na+K+ATPase
Rab5
Rab13
C
Brain TX100
Brain pH 11.0
% distribution
120
100
80
60
40
20
0
Rab5
Rab13
S2
P2
D
Liver TX100
Liver pH 11.0
% distribution
120
100
80
60
40
20
0
Rab5
Rab13
S
P

Figure 3.6.

Figure 3.6.

Rab13 associates with membranes via protein-protein interactions in tissue (A-B) Equal protein aliquots of rat brain (*A*) of rat liver (*B*) homogenate in HEPES buffer were spun for 30 min at 200,000 x g and the resulting pellet fraction (*P*) was resuspended in HEPES buffer with or without 1% Triton X-100 (TX100) or $NaCO_3$ at pH 11.0. After 15 min of incubation, samples were spun for 30 min at 200,000 x g and the resulting supernatant (*S2*) and pellets (*P2*) were analyzed by Western blot using the indicated antibodies. (C) Quantification of the distribution of Rab proteins from extraction experiments as in *A*. Mean ± SD, n=3 for Rab13 and Rab5. (D) Quantification of the distribution of Rab proteins from extraction experiments as in *B*. Mean ± SD, n=5 for Rab5 and n=3 Rab13.

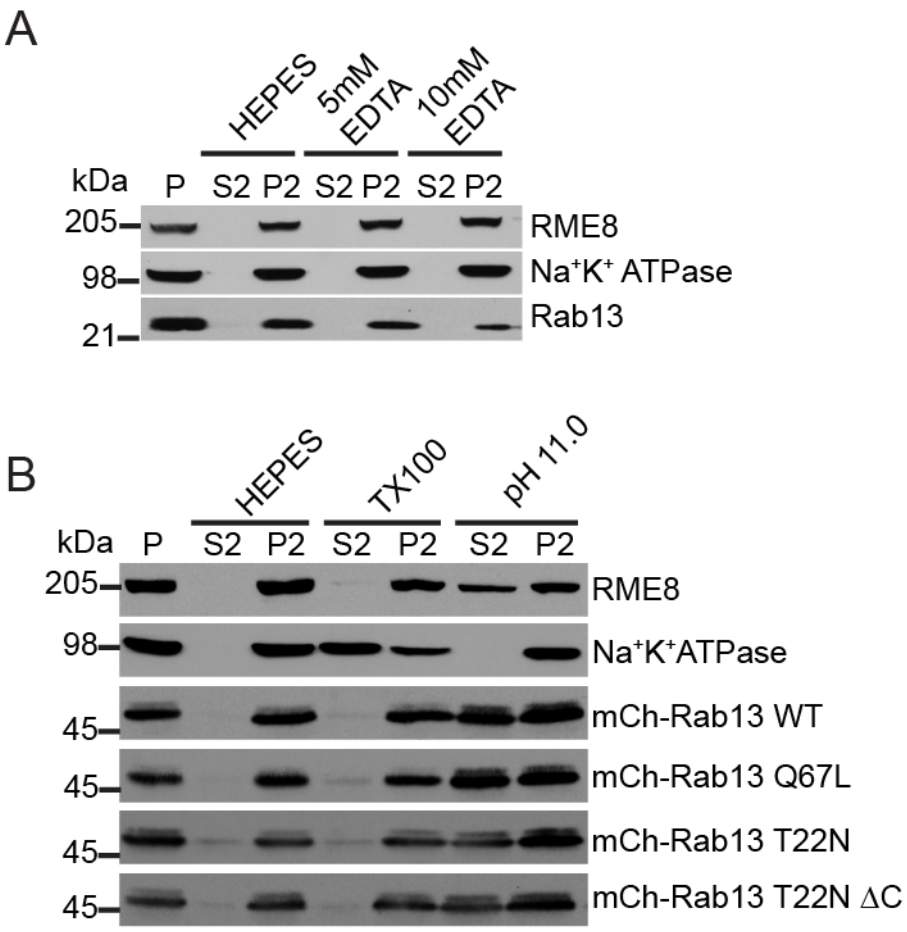
A
HEPES
5mM EDTA
10mM EDTA
kDa
P
S2
P2
S2
P2
S2
P2
205
98
21
RME8
Na+K+ ATPase
Rab13
B
HEPES
TX100
pH 11.0
kDa
P
S2
P2
S2
P2
S2
P2
205
98
45
45
45
45
RME8
Na+K+ATPase
mCh-Rab13 WT
mCh-Rab13 Q67L
mCh-Rab13 T22N
mCh-Rab13 T22N ΔC

Figure 3.7

Figure 3.7.

Rab13 associates in a protein complex independent of nucleotide status. (A) HEK-293T cell homogenates in HEPES buffer were spun for 30 min at 200,000 x g and equal protein aliquots of the resulting pellet (*P*) were resuspended in HEPES buffer with or without EDTA at the indicated concentrations. After 15 min of incubation, samples were spun for 30 min at 200,000 x g and the resulting supernatant (*S2*) and pellets (*P2*) were analyzed by Western blot using the indicated antibodies. (B) HEK-293T cells were left untransfected or were transfected with various mCh-Rab13 constructs as indicated. Cell homogenates in HEPES buffer were spun for 30 min at 200,000 x g and equal protein aliquots of the resulting pellet (*P*) were resuspended in HEPES buffer with or without 1% Triton X-100 (TX100) or $NaCO_3$ at pH 11.0. After 15 min of incubation, samples were spun for 30 min at 200,000 x g and the resulting supernatant (*S2*) and pellets (*P2*) were analyzed by Western blot using the indicated antibodies for the top two panels and an antibody against Rab13 to detect the various Rab13 constructs.

3.6 Acknowledgements

We thank Jacynthe Philie for excellent technical assistance. We thank Dr. Martin Schmeing, Dr. Andrea L. Marat and all members of the McPherson lab for helpful discussions on the project. This work was supported by grant MOP-62684 from the Canadian Institutes of Health Research to PSM. MSI was supported by a Jeanne Timmins Costello fellowship and an Anne and Richard Sievers Award in Neuroscience. PSM is a James McGill Professor and Fellow of the Royal Society of Canada.

CHAPTER 4 DISCUSSION AND GENERAL CONCLUSIONS

4.1 Summary of original contributions to scientific knowledge

In summary, we sought to characterize the role of Rab13 in membrane trafficking as well as define its role in the progression of cancer cell behavior. Thus, in this thesis we present several original contributions to the advancement of science.

1. Crucial for understanding the behavior of any small GTPase is the identification of its GEF(s). While previous studies show that the DENN containing protein connecdenn3 has GEF activity for Rab13, certain Rabs are activated by different GEFs to promote different biological outputs (Marat and McPherson, 2010;Marat et al., 2012). Here we identified DENND2B as specific GEF for Rab13 and show that activation of Rab13 by DENND2B regulates epithelial cell morphology. In fact, we define a novel mechanism whereby DENND2B interacts with the Rab13 effector MICAL-L2 on the cell periphery and this interaction is required for the morphological changes induced by active Rab13 (Figure 4.1).

2. As Rab13 can be localized to several subcellular compartments, a key unknown question is where is Rab13 being activated? Staining for an endogenous Rab does not give information about its activation status and there are limitations to using dominant-negative and constitutively active mutants to determine where activation occurs. Therefore, new tools are required in order to investigate the spatial and temporal activation of Rab13. Here we developed a novel FRET-based biosensor to show that Rab13 is activated specifically at the cell periphery and at the leading edge of migrating cells where it co-localizes with its GEF

DENND2B. Therefore we have not only discovered the localized nature of Rab13 activation but we have created a valuable tool for future studies on Rab13 and generated proof of concept for the development of biosensors targeted to a diverse array of Rabs (Figure 4.1).

3. The finding that Rab13 is active specifically on the plasma membrane was particularly interesting considering Rab13 can also be localized to several intracellular compartments. Consistent with this, we found that inactive Rab13 mutants are recruited to and traffic on cytoplasmic vesicles but never associate with the plasma membrane. This discovery challenges the long held belief that Rab GTPases only associate with membranes upon activation. In fact, we discovered that inactive Rab13 is recruited to these vesicles independent of anchoring of its prenyl group into the vesicular membrane. Instead inactive Rab13 associates with vesicles as part of a protein complex that is intimately linked with the actin cytoskeleton (Figure 4.1).

4. Given that Rab13 traffics on small vesicles to and from the plasma membrane, a great deal of interest lies in defining the identity of these vesicles. Rab13 regulates recycling of cargos to the surface such as integrin or the glucose transporter GLUT4 (Nishikimi et al., 2014;Sun et al., 2010). Furthermore, we as well as others have found Rab13 co-localizes with additional recycling cargos transferrin and TGN46. These data suggest that Rab13 traffics on a slow recycling compartment from the TGN to the plasma membrane. Here we show that Rab13 is largely on late endocytic compartments. Previous studies had identified Rab13 on Rab7 positive endosomes and we extend this finding by showing that Rab13 vesicles also contain the tetanus-insensitive SNARE TI-VAMP known to mediate secretion from late endosomes

thereby suggesting an alternative route that Rab13 may take to arrive at the plasma membrane.

5. Rab13 has been implicated in several phenotypes associated with cancer, from disrupting tight junction assembly to the scattering of epithelial cells in culture (Kohler et al., 2004;Kanda et al., 2008). We extended these studies by showing that activation of Rab13 by DENND2B is required for several cancer related processes such as cell migration and invasion through a basement membrane matrix. Furthermore, no study had investigated Rab13 in a well-defined cancer model. Here, using an *in vivo* model of cancer, we show that Rab13 is required for both the growth and metastasis of tumor cells in mice suggesting that Rab13 and its interacting partners may serve as potential targets for future therapies.

4.2 Discussion

4.2.1 Rab13 in exocytosis

Rab13 has been shown to play an important role in trafficking cargo to the plasma membrane. Our finding that Rab13 is activated specifically at the plasma membrane and that vesicles carrying GDP-Rab13 approach but fail to associate with the plasma membrane suggests that Rab13 may play a role in the fusion of these vesicles. Soluble N-ethylmaleimide-sensitive factor attachment protein receptors (SNAREs) are integral components of the machinery required for membrane fusion. Membrane fusion requires the assembly of a trans-SNARE complex composed of SNARE proteins located on both the donor and recipient membrane (Proux-Gillardeaux et al., 2005b). Over one hundred SNARE proteins exist, many of which are found on specific subcellular compartments, thus like Rabs, SNAREs are thought to mediate selective

functions in membrane trafficking (Jahn and Sudhof, 1999;Scales et al., 2000;Chen and Scheller, 2001). For example, post-Golgi trafficking of biosynthetic cargo involves both tetanus-sensitive and tetanus-insensitive SNARE-dependent pathways (Galli et al., 1994). Interestingly, the binary interaction of certain SNARE complexes is inhibited by PKA, an effector for Rab13, which is consistent with a role for Rab13 in exocytic fusion (Kohler and Zahraoui, 2005). For instance, phosphorylation of syntaxin-4 by PKA abolishes binding to SNAP23 thereby reducing exocytosis in non-neuronal cells (Foster et al., 1998), while analogous PKA-mediated phosphorylation of SNAP25 prevents vesicle release in neuronal cells (Nagy et al., 2004). Thus, by inhibiting PKA activity, active Rab13 would promote vesicle fusion (Kohler et al., 2004). However, no studies had yet identified the appropriate SNAREs trafficking on Rab13-positive vesicles.

Cellubrevin is a non-neuronal, tetanus-sensitive SNARE involved in the recycling of plasma membrane receptors such as the transferrin-receptor (Galli et al., 1994). Furthermore, tetanus-dependent cleavage of cellubrevin inhibits integrin recycling and therefore the migration of epithelial cells (Proux-Gillardeaux et al., 2005a). Given the co-trafficking of Rab13 with transferrin and its role in cell migration and integrin recycling, we initially hypothesized that Rab13 positive-vesicles would contain cellubrevin. However, in chapter 3 we found only slight co-localization of cellubrevin with Rab13 as the majority of Rab13 vesicles did not contain cellubrevin. We observed slightly higher co-localization of cellubrevin with active Rab13 which is consistent with both proteins localizing on the plasma membrane unlike inactive Rab13. Cellubrevin is thought to function predominantly between early endosomes and the plasma membrane to mediate a fast recycling pathways (Proux-Gillardeaux et al., 2005b). We also

overserved little to no co-localization of Rab13 with early endosomal markers and thus it is unlikely that Rab13 mediates a fast recycling pathway from early endosomes.

Several exocytic pathways are partially resistant to tetanus, for instance transferrin receptor recycling and apical transport in epithelial cells. The tetanus insensitive SNARE TI-VAMP regulates lysosomal secretion in epithelial cells which is required for cell migration (Proux-Gillardeaux et al., 2007). We now discovered that the majority of Rab13 co-localizes with TI-VAMP and the late endosomal marker Rab7. The presence of Rab13 on late endosomes is particularly intriguing as the majority of studies have focused on the role of Rab13 in a secretory or slow trafficking pathway from the TGN to the plasma membrane via recycling endosomes (Nokes et al., 2008;Terai et al., 2006;Yamamoto et al., 2003). Curiously, we also found co-localization of Rab13 with the late endosomal marker Rab9 but not with another late-endosomal/lysosomal marked LAMP-1. Similarly, Rab13 fails to co-localize with the Rab9 effector TIP47 that mediates transport from late endosomes to the TGN. As Rab7 and Rab9 define distinct domains on late endosomes, further studies are necessary to determine what role Rab13 plays on Rab9 positive domains (Barbero et al., 2002). However, a separate study confirmed the presence of both Rab13 and its effector MICAL-L1 on Rab7 positive endosomes (Abou-Zeid et al., 2011). These authors found that EGFR accumulated on late endosomes with MICAL-L1 overexpression and observed an increase in EGFR degradation following MICAL-L1 knockdown. Therefore, instead of acting to deliver proteins for lysosomal degradation, their findings are consistent with a role for Rab13 and MICAL-L1 sorting from late endosomes, as EGFR only defaults to degradation by the lysosomes when MICAL-L1 is disrupted (Abou-Zeid et al., 2011). In light of our findings that Rab13 is selectively activated and accumulates at the

leading edge of migrating cells and that Rab13 co-localizes with TI-VAMP which regulates exocytosis from late endosomes we speculate that a large fraction of Rab13 traffics on late endosomes that go on to fuse with the plasma membrane. Thus Rab13 could play an exocytic role, mediating fusion of vesicles derived from both recycling and late endosomal compartments.

Exocytosis is also required for the polarized delivery of proteins and lipids to growing neurites and so the SNARE fusion machinery is critical for neurite outgrowth to occur (Martinez-Arca et al., 2001). Neurite outgrowth is resistant to tetanus and knockout of the tetanus sensitive SNARE synaptobrevin impairs neurotransmitter release in drosophila, but has no effect on neurite outgrowth in either drosophila or PC12 cell lines (Deitcher et al., 1998;Leoni et al., 1999). Thus, a tetanus-insensitive SNARE must be responsible for the fusion at the tips of growing neurites. While VAMP8 mediates tetanus-insensitive exocytosis and can reach the plasma membrane, it is not expressed in neurons and thus cannot regulate neurite outgrowth (Steegmaier et al., 2000;Antonin et al., 2000). Instead, the tetanus insensitive TI-VAMP is crucial for neurite outgrowth (Martinez-Arca et al., 2000). Thus the presence of Rab13 on TI-VAMP containing vesicles is consistent with the role of Rab13 in inducing neurite outgrowth (Sakane et al., 2010;Di et al., 2005).

However, one caveat of these findings is that co-localization was studied using overexpressed protein which may cause Rab13 to mislocalize to some endosomal compartments. Therefore, it will be important to validate these findings by performing co-localization analysis with endogenous Rab13 perhaps through the use of genome editing to tag the endogenous protein.

4.2.2. Rab13 trafficking cascades

The progression or maturation of endosomal trafficking from one compartment to another is mediated by the coordination of different Rabs in the form of a Rab cascade. Such as cascade might exist between Rab13 and Rab8A on recycling endosomes originating at the TGN. Rab8A and Rab13 act at consecutive steps of insulin-induced GLUT4 recycling. While Rab13 localizes to both the TGN and plasma membrane, Rab8A is restricted to the perinuclear area (Sun et al., 2010). Both Rab8A and Rab13 expression rescue defects in GLUT4 recycling caused by knock down of their common GAP AS160 (Sun et al., 2010). Interestingly, Rab8A activation precedes that of Rab13 in response to insulin and inhibition of GLUT4 translocation by Rab13 knock down could not be rescued by Rab8A (Sun et al., 2010). This shows that the two Rabs are not redundant and instead act sequentially to translocate GLUT4 from the perinuclear pool to the plasma membrane. This work supports our findings that Rab13 is activated and functions at the cell periphery. Perhaps activation of Rab8A in the perinuclear region is necessary to initiate transport of inactive Rab13 to the plasma membrane. Consistent with this Rab cascade model, like Rab13, Rab8A also promotes tumor cell invasion (Bravo-Cordero et al., 2007). Given its presence on late endosomal compartments, Rab13 activity is likely coordinated with the activity of Rab7. However, unlike Rab13 and Rab8 that act sequentially, Rab13 may act to oppose Rab7 activity to prevent the progression of late endosome to lysosomes for degradation.

4.2.3. Rab13 in cell proliferation

In chapter 2 of this thesis, we focused on the role of Rab13 in migration and invasion of cancer cells. However, we unexpectedly discovered that Rab13 affects the proliferation and growth of these cancer cells. This is the first account that Rab13 enhances proliferation rates and that

silencing Rab13 greatly reduced the growth rates of cancer cells. However, the mechanism by which Rab influences cellular growth has never been tested directly. Rab13 could affect cellular growth by recycling EGFR back to the plasma membrane. Upon stimulation, EGFR is internalized onto signaling endosomes and either sorted to the lysosomes for degradation or recycled back to the plasma membrane to enhance EGFR signalling (Lenferink et al., 1998). As described above knockdown of the Rab13 effector MICAL-L1 increase EGFR degradation suggesting that Rab13 and MICAL-L1 promote receptor recycling (Sharma et al., 2009).

EGFR signals cellular growth via the downstream signalling molecule ERK. Consistent with a role for Rab13 activity in enhancing proliferation, expression of DENND2B increases ERK activation following EGF treatment (Majidi et al., 1998). This is particularly interesting because DENND2B was originally identified as a suppressor of tumorigenicity (Oshimura et al., 1990). However, as discussed above DENND2B exists as three isoforms; p70, p82 and p126 (DENND2B). While all three isoforms contain the DENN domain and presumably activate Rab13, only DENND2B could activate ERK signaling downstream of EGFR while p70 inhibits ERK activation. Therefore it only the p70 isoform whose behaviour is consistent with that of a tumor suppressor. Furthermore, DENND2B's ability to enhance ERK activation is lost when its two proline-rich domains are deleted (Majidi et al., 1998). The smaller isoforms, p82 and p70 do not contain the proline-rich domains suggesting that protein interactions within these regions are also important for DENND2Bs ability to promote cell growth (Majidi et al., 1998). It remains elusive whether activation of Rab13 is necessary for this ERK activation and how p70 negatively regulates ERK signalling. As we found localization of DENND2B on actin requires the N-

terminal region that is absent from p70, p70 could fail to activate Rab13 by localizing away from cortical actin or alternatively p70 could directly bind to and inhibit DENND2B.

Another possibility is that Rab13 affects cell growth through its effector PKA. PKA exists as two isozymes with distinct physiochemical properties. The relative ratio of the two isozymes vary throughout the cell cycle as PKA-I promotes proliferation while PKA-II inhibits it (Skalhegg et al., 1998). Both PKA isozymes contain the catalytic subunit but contain distinct regulatory subunits and while active Rab13 binds the catalytic subunit to inhibit PKA activity (Kohler et al., 2004), it is unknown whether the regulatory subunits can influence this interaction. Thus, Rab13 activity could promote proliferation if is it has a preference for and inhibits PKA-II.

4.2.4. Rab13 in neuronal function

In addition to its role in epithelial/endothelial cancer progression, Rab13 could play a role in neuronal development and health. Trafficking of Rab13 influences several polarized cell types and neurons are particularly sensitive to disturbances in polarity. As described above, Rab13 drives neuronal outgrowth in neuronal cultures. This is due to polarized trafficking of Rab13 to the tips of neurites where it promotes actin assembly (Sakane et al., 2010;Di et al., 2006). We found that Rab13 requires activation by DENND2B in order to induce this outgrowth (Supplemental Figure 4.1) and consistently, a breakpoint mutation in DENND2B was discovered in a patient exhibiting several neurological defects such as sensorineural hearing loss and mental retardation (Gohring et al., 2010). Furthermore, expression of DENND2B is increased during development and plateaus into adulthood, consistent with a role for Rab13 and DENND2B in neuritogenesis (Gohring et al., 2010). Thus, Rab13 is proposed to regulate the development of

the nervous system; however this has been largely unexplored and several questions remain. For instance, do Rab13 knockdown mice have neurological defects? And does Rab13 exhibit a polarized distribution in mature neurons? Rab13 localizes to tight junctions in adherent cells and the leading edge of migrating cells, as does the polarity complex Par3/Par6/aPKC (Henrique and Schweisguth, 2003;Kohler et al., 2004;Ioannou et al., 2015). Since Par3/Par6/aPKC is expressed selectively in the axon and growth cone (Shi et al., 2003;Wiggin et al., 2005), perhaps the same is true for Rab13. Certainly axonal growth cones are areas of highly dynamic plasma membrane and actin remodeling where Rab13 is known to function (Wiggin et al., 2005;Ioannou et al., 2015).

Additionally, given Rab13's newly discovered role on Rab7-positive late endosomes, Rab13 could play a passive role in autophagy as Rab7 is required for autophagosome maturation (Gutierrez et al., 2004). Recently, a phosphoproteomics screen identified both Rab8 and Rab13 as indirect targets of PTEN-induced kinase 1 (PINK1) (Lai et al., 2015). PINK1 is often mutated in autosomal-recessive early-onset Parkinson's disease (Valente et al., 2004). PINK1 activation recruits autophagic receptors to mitochondria to initiate mitophagy (Lazarou et al., 2015). Phosphorylation of Rab8 downstream of PINK1 inhibits its activation by its GEF Rabin8 and was suggested to do the same for Rab13 as the residue that is phosphorylated is conserved (Lai et al., 2015). Our studies show the importance of Rab13 activation in associating with the plasma membrane, presumably via fusion. Phosphorylation of Rab13 by PINK1 would likely prevent both Rab13 activation and vesicle fusion with the plasma membrane to increase the availability of vesicles that can instead provide membrane to the growing autophagosomes. Rab13 activity

could conceivably oppose autophagy formation however further studies are required to test this possibility directly.

4.2.5. Cycling inactive Rab13 on membranes

One unexpected finding that came from this study was the trafficking of inactive Rab13 on vesicles. Canonically, Rabs were thought to only associate with membrane upon activation (Goody et al., 2005). However, this does not seem to be the case for all GTPases, as we have previously shown that inactive Rab35 localizes to the plasma membrane and on punctate structures (Allaire et al., 2010). While both inactive and active Rab13 can be found on cytoplasmic vesicles, only the active GTP-bound form associates with the plasma membrane. Thus, one pressing question in the field is how the Rabs are targeted to the correct membrane. Some studies show that the GEF is required for correct membrane targeting (Blumer et al., 2013). Certainly our data supports this idea whereby active Rab13 associates with the plasma membrane where it encounters DENND2B. However this model is incomplete in explaining how inactive Rab13 is targeted to vesicular membranes. Membrane targeting could also be attributed to the hypervariable domain, which is the most distinct region of Rabs (Chavrier et al., 1991;Li et al., 2014a). However, this model is also incomplete as it applies to only a subset of Rabs. The hypervariable domain is required for targeting of Rab7 and Rab35 to the membrane, but is not involved in the targeting of Rab1 or Rab5 (Ali et al., 2004;Li et al., 2014a). Here we show that Rab13 is recruited to vesicles as part of a protein complex. However, the binding partners that recruit Rab13 to these structures and their specificity for active versus inactive Rab13 remain elusive. Perhaps Rab13 associates with distinct motors in its active versus inactive form. This is the case for GTP-bound Rab11 that interacts FIP3 and dynein to induce minus-end microtubule

transport while GDP-bound Rab11 interacts protrudin and KIF5 to induce plus-end microtubule transport (Welz et al., 2014). Thus rather than affect the initial recruitment of Rab13 onto vesicles, the nucleotide status of Rab13 could influence the transport of the vesicles similar to Rab11. Perhaps for certain Rabs, such as Rab11 and Rab13, it is misleading to label the GTP /GDP bound forms as active/inactive, as the GDP-bound form may still function in membrane trafficking albeit playing a different role than the GTP-bound form.

Another unknown question is how is Rab13 recovered from the plasma membrane back to the perinuclear pool? While vesicles that fail to associate with the plasma membrane immediately return to the perinuclear pool, it is unclear what happens to the Rab13 pool that does associate with the plasma membrane. We cannot rule out the possibility that a fraction of Rab13 is solubilized in the cytosol by GDI-like proteins and sequestered on vesicles in the perinuclear region. While Rab13 resists extraction by GDI, PDE-delta was shown to extract Rab13 from particulate fractions in vitro (Marzesco et al., 1998). Another possibility is that active Rab13 is endocytosed onto vesicles carrying its GAP, thus immediately inactivating it. Consistent with this scenario, the Rab13 GAP, AS160 is present on vesicles both throughout the cell and in a perinuclear pool (Gonzalez and McGraw, 2009;Thong et al., 2005). Thus further studies are necessary to uncover the mechanisms of how Rab13 is retrieved back to the perinuclear pool.

4.3 General Conclusion

Rab GTPases are critical regulators of all membrane trafficking pathways in the cell. As such, it is crucial to uncover how Rabs themselves are regulated in order to better understand membrane trafficking pathways. The DENN domain is an evolutionarily conserved domain that functions as

GEFs for Rab GTPases. There are currently 26 known DENN containing proteins, however the function of the majority of these proteins outside of the DENN is largely unknown. In Chapter 2 of this thesis, I have discovered that the DENN domain protein DENND2B harbors enzymatic GEF activity for Rab13 and found that localized activation of Rab13 by DENND2B at the leading edge of migrating cells promotes cancer cell motility as well as the growth and metastasis of tumors. This is the first study to show the contribution of Rab13 to cancer progression in an *in vivo* mouse model. This is a particularly important contribution because as described in Chapter 1, Rab13 is associated with several phenotypes related to cancer, however the mechanisms by which Rab13 activation drives cancer cell progression was largely unknown. Our work not only uncovers the activating GEF for Rab13 in this process, but shows that localized the activation to the leading edge is critical for enhancing the aggressiveness of cancer cells. If Rab13 is specifically activated at the cell periphery, how does it associate with cytoplasmic vesicles the cell? In Chapter 3 of this thesis, we show that Rab13 traffics on endosomes in its inactive form as part of a protein complex. While these findings may seem at odds with the dogma that Rabs are completely cytosolic upon inactivation, other examples of GDP-bound Rabs on endosomal membranes and the cytoskeleton have been reported. Several questions specifically regarding the trafficking of Rab13 remain such as what protein binding partners recruit inactive Rab13 to vesicles and what the function is of having inactive Rab13 on these vesicles? Nonetheless, our findings presented in Chapter 3 corroborated by the work of other groups suggest that the current model of Rab cycling does not adequately describe all Rabs and it will be important to identify whether additional Rabs participate in membrane trafficking in their GDP-bound form. This will not only provide a better understanding of the individual Rab

but a more thorough understanding of how membrane trafficking pathways themselves are regulated.

4.3 Figures

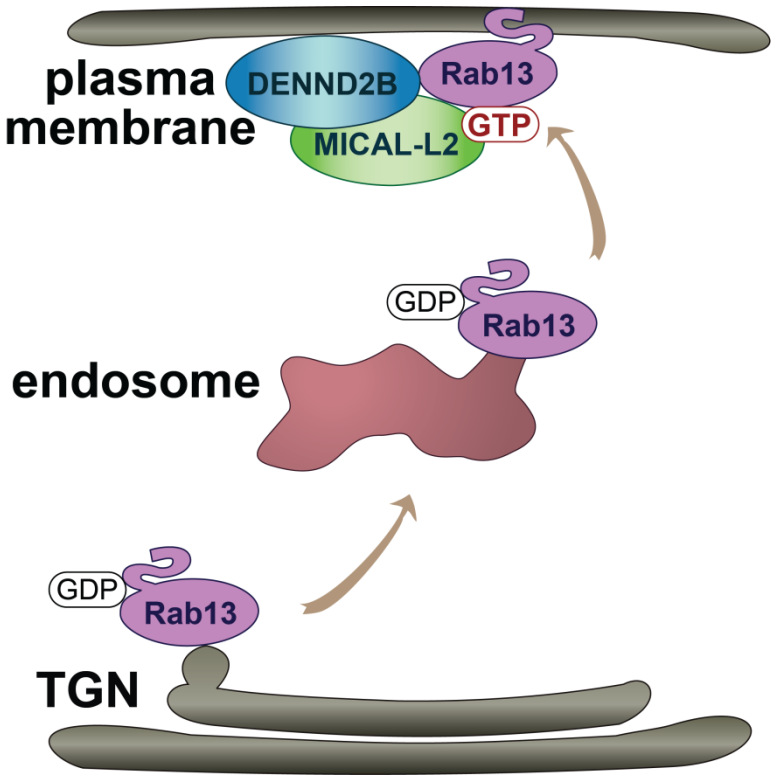

Figure 4.1

Rab13 is activated locally at the plasma membrane. Inactive Rab13 traffics on endosomes from a perinuclear pool to the cell periphery. Upon reaching the cell periphery Rab13 is activated by its GEF DENND2B in a complex with its effector MICAL-L2 and can associate with the plasma membrane.

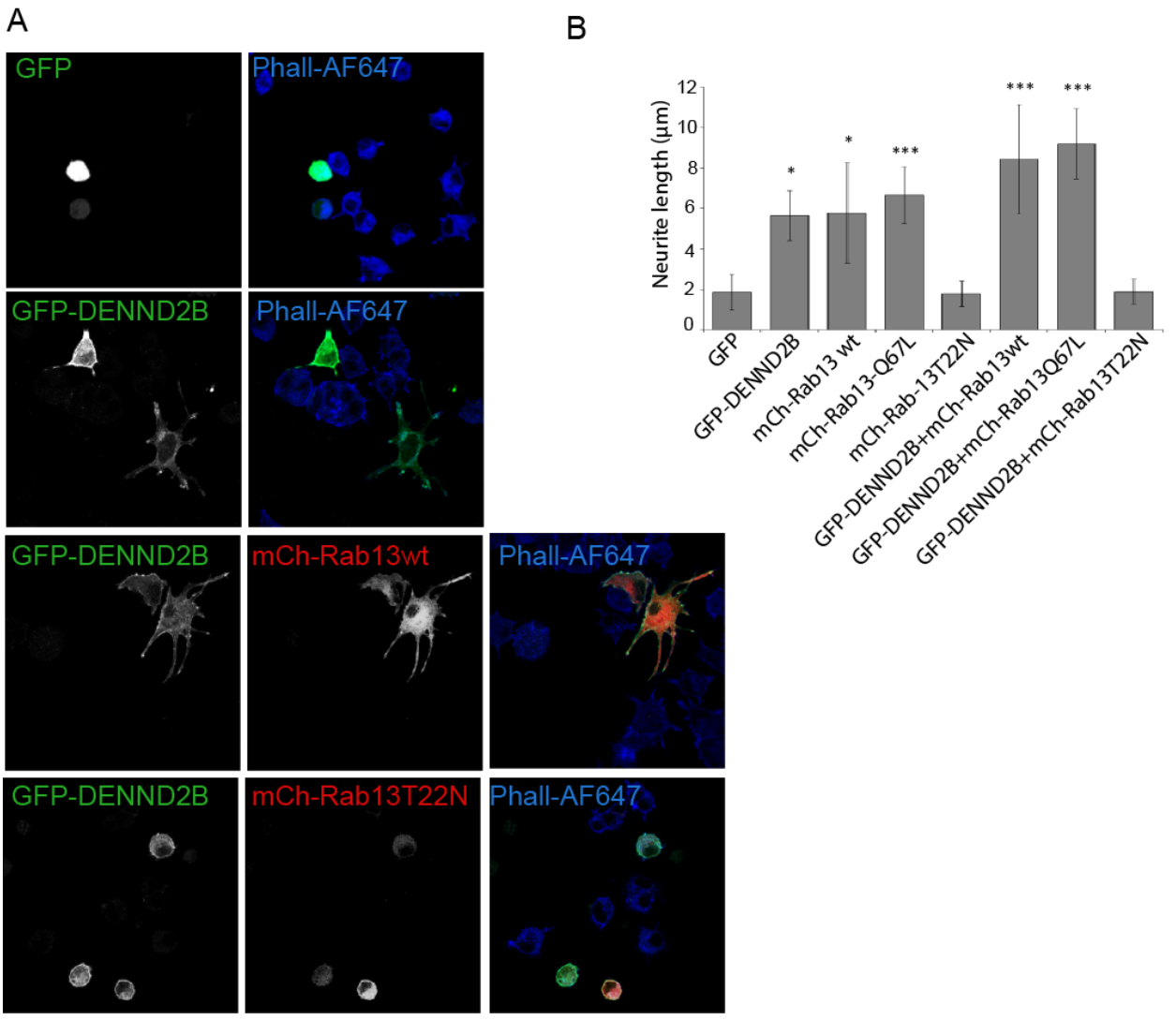

Supplemental Figure 4.1

DENND2B activates Rab13 to induce neurite outgrowth in PC12 cells (A.) PC12 cells were transfected with GFP, GFP-DENND2B with or without mCherry-Rab13 wild type (wt) or mCherry-Rab13T22N for 48 hours, fixed in 3% PFA and stained with Phalloidin-AF647 to label actin. Images were taken on a Zeiss 710 laser scanning confocal microscope. (B.) Quantification of neurite length was performed using imageJ from minimum of 3 experiments. Statistical analysis employed a repeated-measure one-way ANOVA followed by a Dunnett's post-test (*$p<0.05$, ***$p<0.001$).

REFERENCES

Abou-Zeid, N., R.Pandjaitan, L.Sengmanivong, V.David, P.G.Le, J.Salamero, and A.Zahraoui. 2011. MICAL-like1 mediates epidermal growth factor receptor endocytosis. *Mol. Biol. Cell* 22:3431-3441.

Agarwal, R., I.Jurisica, G.B.Mills, and K.W.Cheng. 2009. The emerging role of the RAB25 small GTPase in cancer. *Traffic.* 10:1561-1568.

Alexandrov, K., H.Horiuchi, O.Steele-Mortimer, M.C.Seabra, and M.Zerial. 1994. Rab escort protein-1 is a multifunctional protein that accompanies newly prenylated rab proteins to their target membranes. *EMBO J.* 13:5262-5273.

Ali, B.R., C.Wasmeier, L.Lamoreux, M.Strom, and M.C.Seabra. 2004. Multiple regions contribute to membrane targeting of Rab GTPases. *J. Cell Sci.* 117:6401-6412.

Aligianis, I.A., C.A.Johnson, P.Gissen, D.Chen, D.Hampshire, K.Hoffmann, E.N.Maina, N.V.Morgan, L.Tee, J.Morton, J.R.Ainsworth, D.Horn, E.Rosser, T.R.Cole, I.Stolte-Dijkstra, K.Fieggen, J.Clayton-Smith, A.Megarbane, J.P.Shield, R.Newbury-Ecob, W.B.Dobyns, J.M.Graham, Jr., K.W.Kjaer, M.Warburg, J.Bond, R.C.Trembath, L.W.Harris, Y.Takai, S.Mundlos, D.Tannahill, C.G.Woods, and E.R.Maher. 2005. Mutations of the catalytic subunit of RAB3GAP cause Warburg Micro syndrome. *Nat. Genet.* 37:221-223.

Aligianis, I.A., N.V.Morgan, M.Mione, C.A.Johnson, E.Rosser, R.C.Hennekam, G.Adams, R.C.Trembath, D.T.Pilz, N.Stoodley, A.T.Moore, S.Wilson, and E.R.Maher. 2006. Mutation in Rab3 GTPase-activating protein (RAB3GAP) noncatalytic subunit in a kindred with Martsolf syndrome. *Am. J. Hum. Genet.* 78:702-707.

Allaire, P.D., A.L.Marat, C.Dall'Armi, P.G.Di, P.S.McPherson, and B.Ritter. 2010. The Connecdenn DENN domain: a GEF for Rab35 mediating cargo-specific exit from early endosomes. *Mol. Cell* 37:370-382.

Allaire, P.D., B.Ritter, S.Thomas, J.L.Burman, A.Y.Denisov, V.Legendre-Guillemin, S.Q.Harper, B.L.Davidson, K.Gehring, and P.S.McPherson. 2006. Connecdenn, a novel DENN domain-containing protein of neuronal clathrin-coated vesicles functioning in synaptic vesicle endocytosis. *J. Neurosci.* 26:13202-13212.

Allaire, P.D., S.M.Seyed, M.Chaineau, S.E.Seyed, S.Konefal, M.Fotouhi, D.Maret, B.Ritter, R.F.Del Maestro, and P.S.McPherson. 2013. Interplay between Rab35 and Arf6 controls cargo recycling to coordinate cell adhesion and migration. *J. Cell Sci.* 126:722-731.

Allan, B.B., B.D.Moyer, and W.E.Balch. 2000. Rab1 recruitment of p115 into a cis-SNARE complex: programming budding COPII vesicles for fusion. *Science* 289:444-448.

Alory, C., and W.E.Balch. 2001. Organization of the Rab-GDI/CHM superfamily: the functional basis for choroideremia disease. *Traffic.* 2:532-543.

Anant, J.S., L.Desnoyers, M.Machius, B.Demeler, J.C.Hansen, K.D.Westover, J.Deisenhofer, and M.C.Seabra. 1998. Mechanism of Rab geranylgeranylation: formation of the catalytic ternary complex. *Biochemistry* 37:12559-12568.

Andres, D.A., M.C.Seabra, M.S.Brown, S.A.Armstrong, T.E.Smeland, F.P.Cremers, and J.L.Goldstein. 1993. cDNA cloning of component A of Rab geranylgeranyl transferase and demonstration of its role as a Rab escort protein. *Cell* 73:1091-1099.

Antonin, W., C.Holroyd, R.Tikkanen, S.Honing, and R.Jahn. 2000. The R-SNARE endobrevin/VAMP-8 mediates homotypic fusion of early endosomes and late endosomes. *Mol. Biol. Cell* 11:3289-3298.

Artemenko, Y., P.Batsios, J.Borleis, Z.Gagnon, J.Lee, M.Rohlfs, D.Sanseau, S.S.Willard, M.Schleicher, and P.N.Devreotes. 2012. Tumor suppressor Hippo/MST1 kinase mediates chemotaxis by regulating spreading and adhesion. *Proc. Natl. Acad. Sci. U. S. A* 109:13632-13637.

Attarha, S., S.Andersson, M.Mints, and S.Souchelnytskyi. 2014. Mammalian sterile-like 1 kinase inhibits TGFbeta and EGFdependent regulation of invasiveness, migration and proliferation of HEC-1-A endometrial cancer cells. *Int. J. Oncol.* 45:853-860.

Bailly, E., M.McCaffrey, N.Touchot, A.Zahraoui, B.Goud, and M.Bornens. 1991. Phosphorylation of two small GTP-binding proteins of the Rab family by p34cdc2. *Nature* 350:715-718.

Baldassarre, M., Z.Razinia, C.F.Burande, I.Lamsoul, P.G.Lutz, and D.A.Calderwood. 2009. Filamins regulate cell spreading and initiation of cell migration. *PLoS. One.* 4:e7830.

Bar, J., N.Lukaschuk, A.Zalcenstein, S.Wilder, R.Seger, and M.Oren. 2005. The PI3K inhibitor LY294002 prevents p53 induction by DNA damage and attenuates chemotherapy-induced apoptosis. *Cell Death. Differ.* 12:1578-1587.

Barbero, P., L.Bittova, and S.R.Pfeffer. 2002. Visualization of Rab9-mediated vesicle transport from endosomes to the trans-Golgi in living cells. *J. Cell Biol.* 156:511-518.

Barbieri, M.A., C.Kong, P.I.Chen, B.F.Horazdovsky, and P.D.Stahl. 2003. The SRC homology 2 domain of Rin1 mediates its binding to the epidermal growth factor receptor and regulates receptor endocytosis. *J. Biol. Chem.* 278:32027-32036.

Barr, F., and D.G.Lambright. 2010. Rab GEFs and GAPs. *Curr. Opin. Cell Biol.* 22:461-470.

Basso, A.D., P.Kirschmeier, and W.R.Bishop. 2006. Lipid posttranslational modifications. Farnesyl transferase inhibitors. *J. Lipid Res.* 47:15-31.

Bergo, M.O., G.K.Leung, P.Ambroziak, J.C.Otto, P.J.Casey, A.Q.Gomes, M.C.Seabra, and S.G.Young. 2001. Isoprenylcysteine carboxyl methyltransferase deficiency in mice. *J. Biol. Chem.* 276:5841-5845.

Blumer, J., J.Rey, L.Dehmelt, T.Mazel, Y.W.Wu, P.Bastiaens, R.S.Goody, and A.Itzen. 2013. RabGEFs are a major determinant for specific Rab membrane targeting. *J. Cell Biol.* 200:287-300.

Bock, J.B., H.T.Matern, A.A.Peden, and R.H.Scheller. 2001. A genomic perspective on membrane compartment organization. *Nature* 409:839-841.

Bravo-Cordero, J.J., R.Marrero-Diaz, D.Megias, L.Genis, A.Garcia-Grande, M.A.Garcia, A.G.Arroyo, and M.C.Montoya. 2007. MT1-MMP proinvasive activity is regulated by a novel Rab8-dependent exocytic pathway. *EMBO J.* 26:1499-1510.

Bravo-Cordero, J.J., M.Oser, X.Chen, R.Eddy, L.Hodgson, and J.Condeelis. 2011. A novel spatiotemporal RhoC activation pathway locally regulates cofilin activity at invadopodia. *Curr. Biol.* 21:635-644.

Brown, T.L., and P.H.Howe. 1998. MADD is highly homologous to a Rab3 guanine-nucleotide exchange protein (Rab3-GEP). *Curr. Biol.* 8:R191.

Brumell, J.H., and M.A.Scidmore. 2007. Manipulation of rab GTPase function by intracellular bacterial pathogens. *Microbiol. Mol. Biol. Rev.* 71:636-652.

Bucci, C., M.Chiariello, D.Lattero, M.Maiorano, and C.B.Bruni. 1999. Interaction cloning and characterization of the cDNA encoding the human prenylated rab acceptor (PRA1). *Biochem. Biophys. Res. Commun.* 258:657-662.

Burman, J.L., L.Bourbonniere, J.Philie, T.Stroh, S.Y.Dejgaard, J.F.Presley, and P.S.McPherson. 2008. Scyl1, mutated in a recessive form of spinocerebellar neurodegeneration, regulates COPI-mediated retrograde traffic. *J. Biol. Chem.* 283:22774-22786.

Cairns, R.A., I.S.Harris, and T.W.Mak. 2011. Regulation of cancer cell metabolism. *Nat. Rev. Cancer* 11:85-95.

Calero, M., and R.N.Collins. 2002. Saccharomyces cerevisiae Pra1p/Yip3p interacts with Yip1p and Rab proteins. *Biochem. Biophys. Res. Commun.* 290:676-681.

Calmon, M.F., M.T.Mota, E.Babeto, N.M.Candido, A.P.Girol, C.F.Mendiburu, J.L.Bonilha, R.V.Silvestre, B.M.Rosa, J.A.Thome, G.H.Medeiros, F.A.Soares, G.C.Guimaraes, J.G.de Arruda, S.M.Oliani, L.L.Villa, J.Vassallo, and P.Rahal. 2013. Overexpression of ANXA1 in penile carcinomas positive for high-risk HPVs. *PLoS. One.* 8:e53260.

Carney, D.S., B.A.Davies, and B.F.Horazdovsky. 2006. Vps9 domain-containing proteins: activators of Rab5 GTPases from yeast to neurons. *Trends Cell Biol.* 16:27-35.

Carroll, K.S., J.Hanna, I.Simon, J.Krise, P.Barbero, and S.R.Pfeffer. 2001. Role of Rab9 GTPase in facilitating receptor recruitment by TIP47. *Science* 292:1373-1376.

Casanovas, O., D.J.Hicklin, G.Bergers, and D.Hanahan. 2005. Drug resistance by evasion of antiangiogenic targeting of VEGF signaling in late-stage pancreatic islet tumors. *Cancer Cell* 8:299-309.

Casey, P.J., and M.C.Seabra. 1996. Protein prenyltransferases. *J. Biol. Chem.* 271:5289-5292.

Caswell, P., and J.Norman. 2008. Endocytic transport of integrins during cell migration and invasion. *Trends Cell Biol.* 18:257-263.

Caswell, P.T., and J.C.Norman. 2006. Integrin trafficking and the control of cell migration. *Traffic.* 7:14-21.

Cauvin, C., M.Rosendale, N.Gupta-Rossi, M.Rocancourt, P.Larraufie, R.Salomon, D.Perrais, and A.Echard. 2016. Rab35 GTPase Triggers Switch-like Recruitment of the Lowe Syndrome Lipid Phosphatase OCRL on Newborn Endosomes. *Curr. Biol.* 26:120-128.

Cerami, E., J.Gao, U.Dogrusoz, B.E.Gross, S.O.Sumer, B.A.Aksoy, A.Jacobsen, C.J.Byrne, M.L.Heuer, E.Larsson, Y.Antipin, B.Reva, A.P.Goldberg, C.Sander, and N.Schultz. 2012. The cBio cancer genomics portal: an open platform for exploring multidimensional cancer genomics data. *Cancer Discov.* 2:401-404.

Chaineau, M., L.Danglot, and T.Galli. 2009. Multiple roles of the vesicular-SNARE TI-VAMP in post-Golgi and endosomal trafficking. *FEBS Lett.* 583:3817-3826.

Chaineau, M., M.S.Ioannou, and P.S.McPherson. 2013. Rab35: GEFs, GAPs and effectors. *Traffic.* 14:1109-1117.

Chattopadhyay, D., G.Langsley, M.Carson, R.Recacha, L.DeLucas, and C.Smith. 2000. Structure of the nucleotide-binding domain of Plasmodium falciparum rab6 in the GDP-bound form. *Acta Crystallogr. D. Biol. Crystallogr.* 56:937-944.

Chavrier, P., J.P.Gorvel, E.Stelzer, K.Simons, J.Gruenberg, and M.Zerial. 1991. Hypervariable C-terminal domain of rab proteins acts as a targeting signal. *Nature* 353:769-772.

Chen, Y.A., and R.H.Scheller. 2001. SNARE-mediated membrane fusion. *Nat. Rev. Mol. Cell Biol.* 2:98-106.

Cheng, J.C., S.K.McBrayer, C.Coarfa, S.Dalva-Aydemir, P.H.Gunaratne, J.D.Carpten, J.K.Keats, S.T.Rosen, and M.Shanmugam. 2013. Expression and phosphorylation of the AS160_v2 splice variant supports GLUT4 activation and the Warburg effect in multiple myeloma. *Cancer Metab* 1:14.

Cherry, S., E.J.Jin, M.N.Ozel, Z.Lu, E.Agi, D.Wang, W.H.Jung, D.Epstein, I.A.Meinertzhagen, C.C.Chan, and P.R.Hiesinger. 2013. Charcot-Marie-Tooth 2B mutations in rab7 cause dosage-dependent neurodegeneration due to partial loss of function. *Elife.* 2:e01064.

Chesneau, L., D.Dambournet, M.Machicoane, I.Kouranti, M.Fukuda, B.Goud, and A.Echard. 2012. An ARF6/Rab35 GTPase cascade for endocytic recycling and successful cytokinesis. *Curr. Biol.* 22:147-153.

Chevallier, J., C.Koop, A.Srivastava, R.J.Petrie, N.Lamarche-Vane, and J.F.Presley. 2009. Rab35 regulates neurite outgrowth and cell shape. *FEBS Lett.* 583:1096-1101.

Chotard, L., A.K.Mishra, M.A.Sylvain, S.Tuck, D.G.Lambright, and C.E.Rocheleau. 2010. TBC-2 regulates RAB-5/RAB-7-mediated endosomal trafficking in Caenorhabditis elegans. *Mol. Biol. Cell* 21:2285-2296.

Clabecq, A., J.P.Henry, and F.Darchen. 2000. Biochemical characterization of Rab3-GTPase-activating protein reveals a mechanism similar to that of Ras-GAP. *J. Biol. Chem.* 275:31786-31791.

Clemens, D.L., and M.A.Horwitz. 1995. Characterization of the Mycobacterium tuberculosis phagosome and evidence that phagosomal maturation is inhibited. *J. Exp. Med.* 181:257-270.

Collins, T.J. 2007. ImageJ for microscopy. *Biotechniques* 43:25-30.

D'Angelo, G., J.F.Martini, T.Iiri, W.J.Fantl, J.Martial, and R.I.Weiner. 1999. 16K human prolactin inhibits vascular endothelial growth factor-induced activation of Ras in capillary endothelial cells. *Mol. Endocrinol.* 13:692-704.

Dambournet, D., M.Machicoane, L.Chesneau, M.Sachse, M.Rocancourt, M.A.El, E.Formstecher, R.Salomon, B.Goud, and A.Echard. 2011. Rab35 GTPase and OCRL phosphatase remodel lipids and F-actin for successful cytokinesis. *Nat. Cell Biol.* 13:981-988.

Debnath, J., S.K.Muthuswamy, and J.S.Brugge. 2003. Morphogenesis and oncogenesis of MCF-10A mammary epithelial acini grown in three-dimensional basement membrane cultures. *Methods* 30:256-268.

Deitcher, D.L., A.Ueda, B.A.Stewart, R.W.Burgess, Y.Kidokoro, and T.L.Schwarz. 1998. Distinct requirements for evoked and spontaneous release of neurotransmitter are revealed by mutations in the Drosophila gene neuronal-synaptobrevin. *J. Neurosci.* 18:2028-2039.

Del Conte-Zerial, P., L.Brusch, J.C.Rink, C.Collinet, Y.Kalaidzidis, M.Zerial, and A.Deutsch. 2008. Membrane identity and GTPase cascades regulated by toggle and cut-out switches. *Mol. Syst. Biol.* 4:206.

del Pozo, M.A., W.B.Kiosses, N.B.Alderson, N.Meller, K.M.Hahn, and M.A.Schwartz. 2002. Integrins regulate GTP-Rac localized effector interactions through dissociation of Rho-GDI. *Nat. Cell Biol.* 4:232-239.

Deretic, V., L.E.Via, R.A.Fratti, and D.Deretic. 1997. Mycobacterial phagosome maturation, rab proteins, and intracellular trafficking. *Electrophoresis* 18:2542-2547.

Derre, I., and R.R.Isberg. 2004. Legionella pneumophila replication vacuole formation involves rapid recruitment of proteins of the early secretory system. *Infect. Immun.* 72:3048-3053.

Derre, I., and R.R.Isberg. 2005. LidA, a translocated substrate of the Legionella pneumophila type IV secretion system, interferes with the early secretory pathway. *Infect. Immun.* 73:4370-4380.

Desgrosellier, J.S., and D.A.Cheresh. 2010. Integrins in cancer: biological implications and therapeutic opportunities. *Nat. Rev. Cancer* 10:9-22.

Di, G.S., B.A.De, A.Yakovlev, T.Finn, J.Beers, E.P.Hoffman, and A.I.Faden. 2005. In vivo and in vitro characterization of novel neuronal plasticity factors identified following spinal cord injury. *J. Biol. Chem.* 280:2084-2091.

Di, G.S., C.D.Knights, M.Rao, A.Yakovlev, J.Beers, J.Catania, M.L.Avantaggiati, and A.I.Faden. 2006. The tumor suppressor protein p53 is required for neurite outgrowth and axon regeneration. *EMBO J.* 25:4084-4096.

Diaz, E., and S.R.Pfeffer. 1998. TIP47: a cargo selection device for mannose 6-phosphate receptor trafficking. *Cell* 93:433-443.

Ding, J., G.Soule, J.H.Overmeyer, and W.A.Maltese. 2003. Tyrosine phosphorylation of the Rab24 GTPase in cultured mammalian cells. *Biochem. Biophys. Res. Commun.* 312:670-675.

Dirac-Svejstrup, A.B., T.Sumizawa, and S.R.Pfeffer. 1997. Identification of a GDI displacement factor that releases endosomal Rab GTPases from Rab-GDI. *EMBO J.* 16:465-472.

Doppler, H.R., L.I.Bastea, L.J.Lewis-Tuffin, P.Z.Anastasiadis, and P.Storz. 2013. Protein kinase D1-mediated phosphorylations regulate vasodilator-stimulated phosphoprotein (VASP) localization and cell migration. *J. Biol. Chem.* 288:24382-24393.

Doyle, B., J.P.Morton, D.W.Delaney, R.A.Ridgway, J.A.Wilkins, and O.J.Sansom. 2010. p53 mutation and loss have different effects on tumourigenesis in a novel mouse model of pleomorphic rhabdomyosarcoma. *J. Pathol.* 222:129-137.

Dumas, J.J., Z.Zhu, J.L.Connolly, and D.G.Lambright. 1999. Structural basis of activation and GTP hydrolysis in Rab proteins. *Structure.* 7:413-423.

Dvorak, H.F., L.F.Brown, M.Detmar, and A.M.Dvorak. 1995. Vascular permeability factor/vascular endothelial growth factor, microvascular hyperpermeability, and angiogenesis. *Am. J. Pathol.* 146:1029-1039.

Egami, Y., M.Fukuda, and N.Araki. 2011. Rab35 regulates phagosome formation through recruitment of ACAP2 in macrophages during FcgammaR-mediated phagocytosis. *J. Cell Sci.* 124:3557-3567.

Eom, H.S., H.R.Park, S.K.Jo, Y.S.Kim, C.Moon, and U.Jung. 2015. Ionizing radiation induces neuronal differentiation of Neuro-2a cells via PI3-kinase and p53-dependent pathways. *Int. J. Radiat. Biol.*1-11.

Fanning, A.S., B.J.Jameson, L.A.Jesaitis, and J.M.Anderson. 1998. The tight junction protein ZO-1 establishes a link between the transmembrane protein occludin and the actin cytoskeleton. *J. Biol. Chem.* 273:29745-29753.

Farnsworth, C.L., and L.A.Feig. 1991. Dominant inhibitory mutations in the Mg(2+)-binding site of RasH prevent its activation by GTP. *Mol. Cell Biol.* 11:4822-4829.

Faux, M.C., J.L.Ross, C.Meeker, T.Johns, H.Ji, R.J.Simpson, M.J.Layton, and A.W.Burgess. 2004. Restoration of full-length adenomatous polyposis coli (APC) protein in a colon cancer cell line enhances cell adhesion. *J. Cell Sci.* 117:427-439.

Filippini, F., V.Rossi, T.Galli, A.Budillon, M.D'Urso, and M.D'Esposito. 2001. Longins: a new evolutionary conserved VAMP family sharing a novel SNARE domain. *Trends Biochem. Sci.* 26:407-409.

Fitzgerald, M.L., and G.L.Reed. 1999. Rab6 is phosphorylated in thrombin-activated platelets by a protein kinase C-dependent mechanism: effects on GTP/GDP binding and cellular distribution. *Biochem. J.* 342 (Pt 2):353-360.

Foster, L.J., B.Yeung, M.Mohtashami, K.Ross, W.S.Trimble, and A.Klip. 1998. Binary interactions of the SNARE proteins syntaxin-4, SNAP23, and VAMP-2 and their regulation by phosphorylation. *Biochemistry* 37:11089-11096.

Frasa, M.A., K.T.Koessmeier, M.R.Ahmadian, and V.M.Braga. 2012. Illuminating the functional and structural repertoire of human TBC/RABGAPs. *Nat. Rev. Mol. Cell Biol.* 13:67-73.

Fukuda, M. 2011. TBC proteins: GAPs for mammalian small GTPase Rab? *Biosci. Rep.* 31:159-168.

Fukuda, M., E.Kanno, K.Ishibashi, and T.Itoh. 2008. Large scale screening for novel rab effectors reveals unexpected broad Rab binding specificity. *Mol. Cell Proteomics.* 7:1031-1042.

Fukuda, M., T.S.Kuroda, and K.Mikoshiba. 2002. Slac2-a/melanophilin, the missing link between Rab27 and myosin Va: implications of a tripartite protein complex for melanosome transport. *J. Biol. Chem.* 277:12432-12436.

Gabernet-Castello, C., A.J.O'Reilly, J.B.Dacks, and M.C.Field. 2013. Evolution of Tre-2/Bub2/Cdc16 (TBC) Rab GTPase-activating proteins. *Mol. Biol. Cell*.

Galli, T., T.Chilcote, O.Mundigl, T.Binz, H.Niemann, and C.P.De. 1994. Tetanus toxin-mediated cleavage of cellubrevin impairs exocytosis of transferrin receptor-containing vesicles in CHO cells. *J. Cell Biol.* 125:1015-1024.

Ganley, I.G., and S.R.Pfeffer. 2006. Cholesterol accumulation sequesters Rab9 and disrupts late endosome function in NPC1-deficient cells. *J. Biol. Chem.* 281:17890-17899.

Gao, J., B.A.Aksoy, U.Dogrusoz, G.Dresdner, B.Gross, S.O.Sumer, Y.Sun, A.Jacobsen, R.Sinha, E.Larsson, E.Cerami, C.Sander, and N.Schultz. 2013. Integrative analysis of complex cancer genomics and clinical profiles using the cBioPortal. *Sci. Signal.* 6:l1.

Gerez, L., K.Mohrmann, R.M.van, M.Jongeneelen, X.Z.Zhou, K.P.Lu, and S.P.van Der. 2000. Accumulation of rab4GTP in the cytoplasm and association with the peptidyl-prolyl isomerase pin1 during mitosis. *Mol. Biol. Cell* 11:2201-2211.

Gerondopoulos, A., L.Langemeyer, J.R.Liang, A.Linford, and F.A.Barr. 2012. BLOC-3 mutated in Hermansky-Pudlak syndrome is a Rab32/38 guanine nucleotide exchange factor. *Curr. Biol.* 22:2135-2139.

Girard, M., P.D.Allaire, P.S.McPherson, and F.Blondeau. 2005a. Non-stoichiometric relationship between clathrin heavy and light chains revealed by quantitative comparative proteomics of clathrin-coated vesicles from brain and liver. *Mol. Cell Proteomics.* 4:1145-1154.

Girard, M., V.Poupon, F.Blondeau, and P.S.McPherson. 2005b. The DnaJ-domain protein RME-8 functions in endosomal trafficking. *J. Biol. Chem.* 280:40135-40143.

Gluck, U., and A.Ben-Ze'ev. 1994. Modulation of alpha-actinin levels affects cell motility and confers tumorigenicity on 3T3 cells. *J. Cell Sci.* 107 (Pt 7):1773-1782.

Gohring, I., A.Tagariello, S.Endele, C.C.Stolt, M.Ghassibe, M.Fisher, C.T.Thiel, U.Trautmann, M.Vikkula, A.Winterpacht, D.R.FitzPatrick, and A.Rauch. 2010. Disruption of ST5 is associated with mental retardation and multiple congenital anomalies. *J. Med. Genet.* 47:91-98.

Goldenring, J.R. 2013. A central role for vesicle trafficking in epithelial neoplasia: intracellular highways to carcinogenesis. *Nat. Rev. Cancer* 13:813-820.

Gomes, A.Q., B.R.Ali, J.S.Ramalho, R.F.Godfrey, D.C.Barral, A.N.Hume, and M.C.Seabra. 2003. Membrane targeting of Rab GTPases is influenced by the prenylation motif. *Mol. Biol. Cell* 14:1882-1899.

Gonzalez, E., and T.E.McGraw. 2009. Insulin-modulated Akt subcellular localization determines Akt isoform-specific signaling. *Proc. Natl. Acad. Sci. U. S. A* 106:7004-7009.

Goody, P.R., K.Heller, L.K.Oesterlin, M.P.Muller, A.Itzen, and R.S.Goody. 2012. Reversible phosphocholination of Rab proteins by Legionella pneumophila effector proteins. *EMBO J.* 31:1774-1784.

Goody, R.S., A.Rak, and K.Alexandrov. 2005. The structural and mechanistic basis for recycling of Rab proteins between membrane compartments. *Cell Mol. Life Sci.* 62:1657-1670.

Grosshans, B.L., D.Ortiz, and P.Novick. 2006. Rabs and their effectors: achieving specificity in membrane traffic. *Proc. Natl. Acad. Sci. U. S. A* 103:11821-11827.

Guo, W., D.Roth, C.Walch-Solimena, and P.Novick. 1999. The exocyst is an effector for Sec4p, targeting secretory vesicles to sites of exocytosis. *EMBO J.* 18:1071-1080.

Gutierrez, M.G., D.B.Munafo, W.Beron, and M.I.Colombo. 2004. Rab7 is required for the normal progression of the autophagic pathway in mammalian cells. *J. Cell Sci.* 117:2687-2697.

Gyorffy, B., A.Lanczky, A.C.Eklund, C.Denkert, J.Budczies, Q.Li, and Z.Szallasi. 2010. An online survival analysis tool to rapidly assess the effect of 22,277 genes on breast cancer prognosis using microarray data of 1,809 patients. *Breast Cancer Res. Treat.* 123:725-731.

Han, L., and J.Colicelli. 1995. A human protein selected for interference with Ras function interacts directly with Ras and competes with Raf1. *Mol. Cell Biol.* 15:1318-1323.

Hanna, S., V.Miskolci, D.Cox, and L.Hodgson. 2014. A new genetically encoded single-chain biosensor for Cdc42 based on FRET, useful for live-cell imaging. *PLoS. One.* 9:e96469.

Harbeck, B., S.Huttelmaier, K.Schluter, B.M.Jockusch, and S.Illenberger. 2000. Phosphorylation of the vasodilator-stimulated phosphoprotein regulates its interaction with actin. *J. Biol. Chem.* 275:30817-30825.

Harsay, E., and R.Schekman. 2007. Avl9p, a member of a novel protein superfamily, functions in the late secretory pathway. *Mol. Biol. Cell* 18:1203-1219.

Hattula, K., J.Furuhjelm, J.Tikkanen, K.Tanhuanpaa, P.Laakkonen, and J.Peranen. 2006. Characterization of the Rab8-specific membrane traffic route linked to protrusion formation. *J. Cell Sci.* 119:4866-4877.

Henrique, D., and F.Schweisguth. 2003. Cell polarity: the ups and downs of the Par6/aPKC complex. *Curr. Opin. Genet. Dev.* 13:341-350.

Hodgson, L., P.Nalbant, F.Shen, and K.Hahn. 2006. Imaging and photobleach correction of Mero-CBD, sensor of endogenous Cdc42 activation. *Methods Enzymol.* 406:140-156.

Hodgson, L., O.Pertz, and K.M.Hahn. 2008. Design and optimization of genetically encoded fluorescent biosensors: GTPase biosensors. *Methods Cell Biol.* 85:63-81.

Hodgson, L., F.Shen, and K.Hahn. 2010. Biosensors for characterizing the dynamics of rho family GTPases in living cells. *Curr. Protoc. Cell Biol.* Chapter 14:Unit-26.

Honda, K., T.Yamada, R.Endo, Y.Ino, M.Gotoh, H.Tsuda, Y.Yamada, H.Chiba, and S.Hirohashi. 1998. Actinin-4, a novel actin-bundling protein associated with cell motility and cancer invasion. *J. Cell Biol.* 140:1383-1393.

Horiuchi, H., R.Lippe, H.M.McBride, M.Rubino, P.Woodman, H.Stenmark, V.Rybin, M.Wilm, K.Ashman, M.Mann, and M.Zerial. 1997. A novel Rab5 GDP/GTP exchange factor complexed to Rabaptin-5 links nucleotide exchange to effector recruitment and function. *Cell* 90:1149-1159.

Hsu, J., Y.Shi, S.Krajewski, S.Renner, M.Fisher, J.C.Reed, T.F.Franke, and A.Lichtenstein. 2001. The AKT kinase is activated in multiple myeloma tumor cells. *Blood* 98:2853-2855.

Hu, P., J.Yang, Y.Hou, H.Zhang, Z.Zeng, L.Zhao, T.Yu, X.Tang, G.Tu, X.Cui, and M.Liu. 2014. LncRNA expression signatures of twist-induced epithelial-to-mesenchymal transition in MCF10A cells. *Cell Signal.* 26:83-93.

Hubbs, A.E., M.Majidi, and J.H.Lichy. 1999. Expression of an isoform of the novel signal transduction protein ST5 is linked to cell morphology. *Oncogene* 18:2519-2525.

Hussain, N.K., S.Jenna, M.Glogauer, C.C.Quinn, S.Wasiak, M.Guipponi, S.E.Antonarakis, B.K.Kay, T.P.Stossel, N.Lamarche-Vane, and P.S.McPherson. 2001. Endocytic protein intersectin-l regulates actin assembly via Cdc42 and N-WASP. *Nat. Cell Biol.* 3:927-932.

Imamura, H., K.Takaishi, K.Nakano, A.Kodama, H.Oishi, H.Shiozaki, M.Monden, T.Sasaki, and Y.Takai. 1998. Rho and Rab small G proteins coordinately reorganize stress fibers and focal adhesions in MDCK cells. *Mol. Biol. Cell* 9:2561-2575.

Ioannou, M.S., E.S.Bell, M.Girard, M.Chaineau, J.N.Hamlin, M.Daubaras, A.Monast, M.Park, L.Hodgson, and P.S.McPherson. 2015. DENND2B activates Rab13 at the leading edge of migrating cells and promotes metastatic behavior. *J. Cell Biol.*

Itzen, A., W.Blankenfeldt, and R.S.Goody. 2011. Adenylylation: renaissance of a forgotten post-translational modification. *Trends Biochem. Sci.* 36:221-228.

Jahn, R., and T.C.Sudhof. 1999. Membrane fusion and exocytosis. *Annu. Rev. Biochem.* 68:863-911.

Jakobsen, K.R., E.Sorensen, K.K.Brondum, T.F.Daugaard, R.Thomsen, and A.L.Nielsen. 2013. Direct RNA sequencing mediated identification of mRNA localized in protrusions of human MDA-MB-231 metastatic breast cancer cells. *J. Mol. Signal.* 8:9.

Jiang, X.H., J.W.Sun, M.Xu, X.F.Jiang, C.F.Liu, and Y.Lu. 2010. Frequent hyperphosphorylation of AS160 in breast cancer. *Cancer Biol. Ther.* 10:362-367.

Joberty, G., A.Tavitian, and A.Zahraoui. 1993. Isoprenylation of Rab proteins possessing a C-terminal CaaX motif. *FEBS Lett.* 330:323-328.

Jones, S., C.Newman, F.Liu, and N.Segev. 2000. The TRAPP complex is a nucleotide exchanger for Ypt1 and Ypt31/32. *Mol. Biol. Cell* 11:4403-4411.

Kanda, I., N.Nishimura, H.Nakatsuji, R.Yamamura, H.Nakanishi, and T.Sasaki. 2008. Involvement of Rab13 and JRAB/MICAL-L2 in epithelial cell scattering. *Oncogene* 27:1687-1695.

Kandoth, C., M.D.McLellan, F.Vandin, K.Ye, B.Niu, C.Lu, M.Xie, Q.Zhang, J.F.McMichael, M.A.Wyczalkowski, M.D.Leiserson, C.A.Miller, J.S.Welch, M.J.Walter, M.C.Wendl, T.J.Ley, R.K.Wilson, B.J.Raphael, and L.Ding. 2013. Mutational landscape and significance across 12 major cancer types. *Nature* 502:333-339.

Kang, Y., P.M.Siegel, W.Shu, M.Drobnjak, S.M.Kakonen, C.Cordon-Cardo, T.A.Guise, and J.Massague. 2003. A multigenic program mediating breast cancer metastasis to bone. *Cancer Cell* 3:537-549.

Karniguian, A., A.Zahraoui, and A.Tavitian. 1993. Identification of small GTP-binding rab proteins in human platelets: thrombin-induced phosphorylation of rab3B, rab6, and rab8 proteins. *Proc. Natl. Acad. Sci. U. S. A* 90:7647-7651.

Katagiri, K., T.Katakai, Y.Ebisuno, Y.Ueda, T.Okada, and T.Kinashi. 2009. Mst1 controls lymphocyte trafficking and interstitial motility within lymph nodes. *EMBO J.* 28:1319-1331.

Kelley, V.A., and J.S.Schorey. 2004. Modulation of cellular phosphatidylinositol 3-phosphate levels in primary macrophages affects heat-killed but not viable Mycobacterium avium's transport through the phagosome maturation process. *Cell Microbiol.* 6:973-985.

Kim, H.S., S.C.Kim, S.J.Kim, C.H.Park, H.C.Jeung, Y.B.Kim, J.B.Ahn, H.C.Chung, and S.Y.Rha. 2012. Identification of a radiosensitivity signature using integrative metaanalysis of published microarray data for NCI-60 cancer cells. *BMC. Genomics* 13:348.

Kim, Y.G., S.Raunser, C.Munger, J.Wagner, Y.L.Song, M.Cygler, T.Walz, B.H.Oh, and M.Sacher. 2006. The architecture of the multisubunit TRAPP I complex suggests a model for vesicle tethering. *Cell* 127:817-830.

Kitano, M., M.Nakaya, T.Nakamura, S.Nagata, and M.Matsuda. 2008. Imaging of Rab5 activity identifies essential regulators for phagosome maturation. *Nature* 453:241-245.

Klopper, T.H., N.Kienle, D.Fasshauer, and S.Munro. 2012. Untangling the evolution of Rab G proteins: implications of a comprehensive genomic analysis. *BMC. Biol.* 10:71.

Knight, J.F., R.Lesurf, H.Zhao, D.Pinnaduwage, R.R.Davis, S.M.Saleh, D.Zuo, M.A.Naujokas, N.Chughtai, J.I.Herschkowitz, A.Prat, A.M.Mulligan, W.J.Muller, R.D.Cardiff, J.P.Gregg, I.L.Andrulis, M.T.Hallett, and M.Park. 2013. Met synergizes with p53 loss to induce mammary tumors that possess features of claudin-low breast cancer. *Proc. Natl. Acad. Sci. U. S. A* 110:E1301-E1310.

Kobayashi, H., K.Etoh, N.Ohbayashi, and M.Fukuda. 2014. Rab35 promotes the recruitment of Rab8, Rab13 and Rab36 to recycling endosomes through MICAL-L1 during neurite outgrowth. *Biol. Open.* 3:803-814.

Kobayashi, H., and M.Fukuda. 2012. Rab35 regulates Arf6 activity through centaurin-beta2 (ACAP2) during neurite outgrowth. *J. Cell Sci.* 125:2235-2243.

Kohler, K., D.Louvard, and A.Zahraoui. 2004. Rab13 regulates PKA signaling during tight junction assembly. *J. Cell Biol.* 165:175-180.

Kohler, K., and A.Zahraoui. 2005. Tight junction: a co-ordinator of cell signalling and membrane trafficking. *Biol. Cell* 97:659-665.

Kumari, R., and A.Francesconi. 2011. Identification of GPCR localization in detergent resistant membranes. *Methods Mol. Biol.* 746:411-423.

Kuper, H., H.O.Adami, and D.Trichopoulos. 2000. Infections as a major preventable cause of human cancer. *J. Intern. Med.* 248:171-183.

Lai, Y.C., C.Kondapalli, R.Lehneck, J.B.Procter, B.D.Dill, H.I.Woodroof, R.Gourlay, M.Peggie, T.J.Macartney, O.Corti, J.C.Corvol, D.G.Campbell, A.Itzen, M.Trost, and M.M.Muqit. 2015. Phosphoproteomic screening identifies Rab GTPases as novel downstream targets of PINK1. *EMBO J.* 34:2840-2861.

Lamalice, L., B.F.Le, and J.Huot. 2007. Endothelial cell migration during angiogenesis. *Circ. Res.* 100:782-794.

Lane, K.T., and L.S.Beese. 2006. Thematic review series: lipid posttranslational modifications. Structural biology of protein farnesyltransferase and geranylgeranyltransferase type I. *J. Lipid Res.* 47:681-699.

Lawrence, D.W., K.M.Comerford, and S.P.Colgan. 2002. Role of VASP in reestablishment of epithelial tight junction assembly after Ca2+ switch. *Am. J. Physiol Cell Physiol* 282:C1235-C1245.

Lazarou, M., D.A.Sliter, L.A.Kane, S.A.Sarraf, C.Wang, J.L.Burman, D.P.Sideris, A.I.Fogel, and R.J.Youle. 2015. The ubiquitin kinase PINK1 recruits autophagy receptors to induce mitophagy. *Nature* 524:309-314.

Lebrand, C., M.Corti, H.Goodson, P.Cosson, V.Cavalli, N.Mayran, J.Faure, and J.Gruenberg. 2002. Late endosome motility depends on lipids via the small GTPase Rab7. *EMBO J.* 21:1289-1300.

Lee, M.T., A.Mishra, and D.G.Lambright. 2009. Structural mechanisms for regulation of membrane traffic by rab GTPases. *Traffic.* 10:1377-1389.

Lenferink, A.E., R.Pinkas-Kramarski, M.L.van de Poll, M.J.van Vugt, L.N.Klapper, E.Tzahar, H.Waterman, M.Sela, E.J.van Zoelen, and Y.Yarden. 1998. Differential endocytic routing of homo- and hetero-dimeric ErbB tyrosine kinases confers signaling superiority to receptor heterodimers. *EMBO J.* 17:3385-3397.

Leoni, C., A.Menegon, F.Benfenati, D.Toniolo, M.Pennuto, and F.Valtorta. 1999. Neurite extension occurs in the absence of regulated exocytosis in PC12 subclones. *Mol. Biol. Cell* 10:2919-2931.

Leung, K.F., R.Baron, and M.C.Seabra. 2006. Thematic review series: lipid posttranslational modifications. geranylgeranylation of Rab GTPases. *J. Lipid Res.* 47:467-475.

Levine, T.P., R.D.Daniels, A.T.Gatta, L.H.Wong, and M.J.Hayes. 2013. The product of C9orf72, a gene strongly implicated in neurodegeneration, is structurally related to DENN Rab-GEFs. *Bioinformatics.* 29:499-503.

Levivier, E., B.Goud, M.Souchet, T.P.Calmels, J.P.Mornon, and I.Callebaut. 2001. uDENN, DENN, and dDENN: indissociable domains in Rab and MAP kinases signaling pathways. *Biochem. Biophys. Res. Commun.* 287:688-695.

Li, F., L.Yi, L.Zhao, A.Itzen, R.S.Goody, and Y.W.Wu. 2014a. The role of the hypervariable C-terminal domain in Rab GTPases membrane targeting. *Proc. Natl. Acad. Sci. U. S. A* 111:2572-2577.

Li, W., K.Li, L.Zhao, and H.Zou. 2014b. Bioinformatics analysis reveals disturbance mechanism of MAPK signaling pathway and cell cycle in Glioblastoma multiforme. *Gene*.

Li, W., L.Xie, X.He, J.Li, K.Tu, L.Wei, J.Wu, Y.Guo, X.Ma, P.Zhang, Z.Pan, X.Hu, Y.Zhao, H.Xie, G.Jiang, T.Chen, J.Wang, S.Zheng, J.Cheng, D.Wan, S.Yang, Y.Li, and J.Gu. 2008. Diagnostic and prognostic implications of microRNAs in human hepatocellular carcinoma. *Int. J. Cancer* 123:1616-1622.

Lichy, J.H., M.Majidi, J.Elbaum, and M.M.Tsai. 1996. Differential expression of the human ST5 gene in HeLa-fibroblast hybrid cell lines mediated by YY1: evidence that YY1 plays a part in tumor suppression. *Nucleic Acids Res.* 24:4700-4708.

Lichy, J.H., W.S.Modi, H.N.Seuanez, and P.M.Howley. 1992. Identification of a human chromosome 11 gene which is differentially regulated in tumorigenic and nontumorigenic somatic cell hybrids of HeLa cells. *Cell Growth Differ.* 3:541-548.

Lippe, R., M.Miaczynska, V.Rybin, A.Runge, and M.Zerial. 2001. Functional synergy between Rab5 effector Rabaptin-5 and exchange factor Rabex-5 when physically associated in a complex. *Mol. Biol. Cell* 12:2219-2228.

Liu, K., L.Li, P.E.Nisson, C.Gruber, J.Jessee, and S.N.Cohen. 1999. Reversible tumorigenesis induced by deficiency of vasodilator-stimulated phosphoprotein. *Mol. Cell Biol.* 19:3696-3703.

Ma, X., E.Fei, C.Fu, H.Ren, and G.Wang. 2011. Dysbindin-1, a schizophrenia-related protein, facilitates neurite outgrowth by promoting the transcriptional activity of p53. *Mol. Psychiatry* 16:1105-1116.

Mahadevan, D., C.Spier, C.K.Della, S.Miller, B.George, C.Riley, S.Warner, T.M.Grogan, and T.P.Miller. 2005. Transcript profiling in peripheral T-cell lymphoma, not otherwise specified, and diffuse large B-cell lymphoma identifies distinct tumor profile signatures. *Mol. Cancer Ther.* 4:1867-1879.

Majidi, M., J.S.Gutkind, and J.H.Lichy. 2000. Deletion of the COOH terminus converts the ST5 p70 protein from an inhibitor of RAS signaling to an activator with transforming activity in NIH-3T3 cells. *J. Biol. Chem.* 275:6560-6565.

Majidi, M., A.E.Hubbs, and J.H.Lichy. 1998. Activation of extracellular signal-regulated kinase 2 by a novel Abl-binding protein, ST5. *J. Biol. Chem.* 273:16608-16614.

Mantovani, A., P.Allavena, A.Sica, and F.Balkwill. 2008. Cancer-related inflammation. *Nature* 454:436-444.

Marat, A.L., H.Dokainish, and P.S.McPherson. 2011. DENN domain proteins: regulators of Rab GTPases. *J. Biol. Chem.* 286:13791-13800.

Marat, A.L., M.S.Ioannou, and P.S.McPherson. 2012. Connecdenn 3/DENND1C binds actin linking Rab35 activation to the actin cytoskeleton. *Mol. Biol. Cell* 23:163-175.

Marat, A.L., and P.S.McPherson. 2010. The connecdenn family, Rab35 guanine nucleotide exchange factors interfacing with the clathrin machinery. *J. Biol. Chem.* 285:10627-10637.

Martincic, I., M.E.Peralta, and J.K.Ngsee. 1997. Isolation and characterization of a dual prenylated Rab and VAMP2 receptor. *J. Biol. Chem.* 272:26991-26998.

Martinez-Arca, S., P.Alberts, A.Zahraoui, D.Louvard, and T.Galli. 2000. Role of tetanus neurotoxin insensitive vesicle-associated membrane protein (TI-VAMP) in vesicular transport mediating neurite outgrowth. *J. Cell Biol.* 149:889-900.

Martinez-Arca, S., S.Coco, G.Mainguy, U.Schenk, P.Alberts, P.Bouille, M.Mezzina, A.Prochiantz, M.Matteoli, D.Louvard, and T.Galli. 2001. A common exocytotic mechanism mediates axonal and dendritic outgrowth. *J. Neurosci.* 21:3830-3838.

Martinez-Arca, S., R.Rudge, M.Vacca, G.Raposo, J.Camonis, V.Proux-Gillardeaux, L.Daviet, E.Formstecher, A.Hamburger, F.Filippini, M.D'Esposito, and T.Galli. 2003. A dual mechanism controlling the localization and function of exocytic v-SNAREs. *Proc. Natl. Acad. Sci. U. S. A* 100:9011-9016.

Marzesco, A.M., I.Dunia, R.Pandjaitan, M.Recouvreur, D.Dauzonne, E.L.Benedetti, D.Louvard, and A.Zahraoui. 2002. The small GTPase Rab13 regulates assembly of functional tight junctions in epithelial cells. *Mol. Biol. Cell* 13:1819-1831.

Marzesco, A.M., T.Galli, D.Louvard, and A.Zahraoui. 1998. The rod cGMP phosphodiesterase delta subunit dissociates the small GTPase Rab13 from membranes. *J. Biol. Chem.* 273:22340-22345.

McBrayer, S.K., J.C.Cheng, S.Singhal, N.L.Krett, S.T.Rosen, and M.Shanmugam. 2012. Multiple myeloma exhibits novel dependence on GLUT4, GLUT8, and GLUT11: implications for glucose transporter-directed therapy. *Blood* 119:4686-4697.

McBride, H.M., V.Rybin, C.Murphy, A.Giner, R.Teasdale, and M.Zerial. 1999. Oligomeric complexes link Rab5 effectors with NSF and drive membrane fusion via interactions between EEA1 and syntaxin 13. *Cell* 98:377-386.

Medkova, M., Y.E.France, J.Coleman, and P.Novick. 2006. The rab exchange factor Sec2p reversibly associates with the exocyst. *Mol. Biol. Cell* 17:2757-2769.

Mellman, I., and Y.Yarden. 2013. Endocytosis and cancer. *Cold Spring Harb. Perspect. Biol.* 5:a016949.

Miinea, C.P., H.Sano, S.Kane, E.Sano, M.Fukuda, J.Peranen, W.S.Lane, and G.E.Lienhard. 2005. AS160, the Akt substrate regulating GLUT4 translocation, has a functional Rab GTPase-activating protein domain. *Biochem. J.* 391:87-93.

Milburn, M.V., L.Tong, A.M.deVos, A.Brunger, Z.Yamaizumi, S.Nishimura, and S.H.Kim. 1990. Molecular switch for signal transduction: structural differences between active and inactive forms of protooncogenic ras proteins. *Science* 247:939-945.

Mili, S., K.Moissoglu, and I.G.Macara. 2008. Genome-wide screen reveals APC-associated RNAs enriched in cell protrusions. *Nature* 453:115-119.

Militello, R.D., D.B.Munafo, W.Beron, L.A.Lopez, S.Monier, B.Goud, and M.I.Colombo. 2013. Rab24 is required for normal cell division. *Traffic.* 14:502-518.

Miserey-Lenkei, S., F.Waharte, A.Boulet, M.H.Cuif, D.Tenza, M.A.El, G.Raposo, J.Salamero, L.Heliot, B.Goud, and S.Monier. 2007. Rab6-interacting protein 1 links Rab6 and Rab11 function. *Traffic.* 8:1385-1403.

Mizuno-Yamasaki, E., M.Medkova, J.Coleman, and P.Novick. 2010. Phosphatidylinositol 4-phosphate controls both membrane recruitment and a regulatory switch of the Rab GEF Sec2p. *Dev. Cell* 18:828-840.

Mo, W., J.Zhang, X.Li, D.Meng, Y.Gao, S.Yang, X.Wan, C.Zhou, F.Guo, Y.Huang, S.Amente, E.V.Avvedimento, Y.Xie, and Y.Li. 2013. Identification of novel AR-targeted microRNAs mediating androgen signalling through critical pathways to regulate cell viability in prostate cancer. *PLoS. One.* 8:e56592.

Mochizuki, N., S.Yamashita, K.Kurokawa, Y.Ohba, T.Nagai, A.Miyawaki, and M.Matsuda. 2001. Spatio-temporal images of growth-factor-induced activation of Ras and Rap1. *Nature* 411:1065-1068.

Mochizuki, Y., R.Ohashi, T.Kawamura, H.Iwanari, T.Kodama, M.Naito, and T.Hamakubo. 2013. Phosphatidylinositol 3-phosphatase myotubularin-related protein 6 (MTMR6) is regulated by small GTPase Rab1B in the early secretory and autophagic pathways. *J. Biol. Chem.* 288:1009-1021.

Moore, I., J.Schell, and K.Palme. 1995. Subclass-specific sequence motifs identified in Rab GTPases. *Trends Biochem. Sci.* 20:10-12.

Morimoto, S., N.Nishimura, T.Terai, S.Manabe, Y.Yamamoto, W.Shinahara, H.Miyake, S.Tashiro, M.Shimada, and T.Sasaki. 2005. Rab13 mediates the continuous endocytic recycling of occludin to the cell surface. *J. Biol. Chem.* 280:2220-2228.

Morozova, N., Y.Liang, A.A.Tokarev, S.H.Chen, R.Cox, J.Andrejic, Z.Lipatova, V.A.Sciorra, S.D.Emr, and N.Segev. 2006. TRAPPII subunits are required for the specificity switch of a Ypt-Rab GEF. *Nat. Cell Biol.* 8:1263-1269.

Morton, J.P., P.Timpson, S.A.Karim, R.A.Ridgway, D.Athineos, B.Doyle, N.B.Jamieson, K.A.Oien, A.M.Lowy, V.G.Brunton, M.C.Frame, T.R.Evans, and O.J.Sansom. 2010. Mutant p53 drives metastasis and overcomes growth arrest/senescence in pancreatic cancer. *Proc. Natl. Acad. Sci. U. S. A* 107:246-251.

Moshfegh, Y., J.J.Bravo-Cordero, V.Miskolci, J.Condeelis, and L.Hodgson. 2014. A Trio-Rac1-Pak1 signalling axis drives invadopodia disassembly. *Nat. Cell Biol.* 16:574-586.

Mourskaia, A.A., E.Amir, Z.Dong, K.Tiedemann, S.Cory, A.Omeroglu, N.Bertos, V.Ouellet, M.Clemons, G.L.Scheffer, M.Park, M.Hallett, S.V.Komarova, and P.M.Siegel. 2012. ABCC5 supports osteoclast formation and promotes breast cancer metastasis to bone. *Breast Cancer Res.* 14:R149.

Moyer, B.D., B.B.Allan, and W.E.Balch. 2001. Rab1 interaction with a GM130 effector complex regulates COPII vesicle cis--Golgi tethering. *Traffic.* 2:268-276.

Mukherjee, S., X.Liu, K.Arasaki, J.McDonough, J.E.Galan, and C.R.Roy. 2011. Modulation of Rab GTPase function by a protein phosphocholine transferase. *Nature* 477:103-106.

Muller, M.P., H.Peters, J.Blumer, W.Blankenfeldt, R.S.Goody, and A.Itzen. 2010. The Legionella effector protein DrrA AMPylates the membrane traffic regulator Rab1b. *Science* 329:946-949.

Muller, M.P., A.V.Shkumatov, L.K.Oesterlin, S.Schoebel, P.R.Goody, R.S.Goody, and A.Itzen. 2012. Characterization of enzymes from Legionella pneumophila involved in reversible adenylylation of Rab1 protein. *J. Biol. Chem.* 287:35036-35046.

Muller, P.A., P.T.Caswell, B.Doyle, M.P.Iwanicki, E.H.Tan, S.Karim, N.Lukashchuk, D.A.Gillespie, R.L.Ludwig, P.Gosselin, A.Cromer, J.S.Brugge, O.J.Sansom, J.C.Norman, and K.H.Vousden. 2009. Mutant p53 drives invasion by promoting integrin recycling. *Cell* 139:1327-1341.

Muller, P.A., and K.H.Vousden. 2014. Mutant p53 in cancer: new functions and therapeutic opportunities. *Cancer Cell* 25:304-317.

Nagai, T., S.Yamada, T.Tominaga, M.Ichikawa, and A.Miyawaki. 2004. Expanded dynamic range of fluorescent indicators for Ca(2+) by circularly permuted yellow fluorescent proteins. *Proc. Natl. Acad. Sci. U. S. A* 101:10554-10559.

Nagano, F., T.Sasaki, K.Fukui, T.Asakura, K.Imazumi, and Y.Takai. 1998. Molecular cloning and characterization of the noncatalytic subunit of the Rab3 subfamily-specific GTPase-activating protein. *J. Biol. Chem.* 273:24781-24785.

Nagy, G., K.Reim, U.Matti, N.Brose, T.Binz, J.Rettig, E.Neher, and J.B.Sorensen. 2004. Regulation of releasable vesicle pool sizes by protein kinase A-dependent phosphorylation of SNAP-25. *Neuron* 41:417-429.

Nakatsuji, H., N.Nishimura, R.Yamamura, H.O.Kanayama, and T.Sasaki. 2008. Involvement of actinin-4 in the recruitment of JRAB/MICAL-L2 to cell-cell junctions and the formation of functional tight junctions. *Mol. Cell Biol.* 28:3324-3335.

Nalbant, P., L.Hodgson, V.Kraynov, A.Toutchkine, and K.M.Hahn. 2004. Activation of endogenous Cdc42 visualized in living cells. *Science* 305:1615-1619.

Narita, K., A.Choudhury, K.Dobrenis, D.K.Sharma, E.L.Holicky, D.L.Marks, S.U.Walkley, and R.E.Pagano. 2005. Protein transduction of Rab9 in Niemann-Pick C cells reduces cholesterol storage. *FASEB J.* 19:1558-1560.

Neary, C.L., M.Nesterova, Y.S.Cho, C.Cheadle, K.G.Becker, and Y.S.Cho-Chung. 2004. Protein kinase A isozyme switching: eliciting differential cAMP signaling and tumor reversion. *Oncogene* 23:8847-8856.

Nichols, B.J., A.K.Kenworthy, R.S.Polishchuk, R.Lodge, T.H.Roberts, K.Hirschberg, R.D.Phair, and J.Lippincott-Schwartz. 2001. Rapid cycling of lipid raft markers between the cell surface and Golgi complex. *J. Cell Biol.* 153:529-541.

Nishikimi, A., S.Ishihara, M.Ozawa, K.Etoh, M.Fukuda, T.Kinashi, and K.Katagiri. 2014. Rab13 acts downstream of the kinase Mst1 to deliver the integrin LFA-1 to the cell surface for lymphocyte trafficking. *Sci. Signal.* 7:ra72.

Nishimura, N., H.Nakamura, Y.Takai, and K.Sano. 1994. Molecular cloning and characterization of two rab GDI species from rat brain: brain-specific and ubiquitous types. *J. Biol. Chem.* 269:14191-14198.

Nishimura, N., and T.Sasaki. 2008a. Identification and characterization of JRAB/MICAL-L2, a junctional Rab13-binding protein. *Methods Enzymol.* 438:141-153.

Nishimura, N., and T.Sasaki. 2008b. Regulation of epithelial cell adhesion and repulsion: role of endocytic recycling. *J. Med. Invest* 55:9-16.

Nokes, R.L., I.C.Fields, R.N.Collins, and H.Folsch. 2008. Rab13 regulates membrane trafficking between TGN and recycling endosomes in polarized epithelial cells. *J. Cell Biol.* 182:845-853.

Nookala, R.K., L.Langemeyer, A.Pacitto, B.Ochoa-Montano, J.C.Donaldson, B.K.Blaszczyk, D.Y.Chirgadze, F.A.Barr, J.F.Bazan, and T.L.Blundell. 2012. Crystal structure of folliculin reveals a hidDENN function in genetically inherited renal cancer. *Open. Biol.* 2:120071.

Normanno, N., L.A.De, C.Bianco, L.Strizzi, M.Mancino, M.R.Maiello, A.Carotenuto, F.G.De, F.Caponigro, and D.S.Salomon. 2006. Epidermal growth factor receptor (EGFR) signaling in cancer. *Gene* 366:2-16.

Nuoffer, C., H.W.Davidson, J.Matteson, J.Meinkoth, and W.E.Balch. 1994. A GDP-bound of rab1 inhibits protein export from the endoplasmic reticulum and transport between Golgi compartments. *J. Cell Biol.* 125:225-237.

Oshimura, M., H.Kugoh, M.Koi, M.Shimizu, H.Yamada, H.Satoh, and J.C.Barrett. 1990. Transfer of a normal human chromosome 11 suppresses tumorigenicity of some but not all tumor cell lines. *J. Cell Biochem.* 42:135-142.

Ostermeier, C., and A.T.Brunger. 1999. Structural basis of Rab effector specificity: crystal structure of the small G protein Rab3A complexed with the effector domain of rabphilin-3A. *Cell* 96:363-374.

Overmeyer, J.H., and W.A.Maltese. 2005. Tyrosine phosphorylation of Rab proteins. *Methods Enzymol.* 403:194-202.

Pan, X., S.Eathiraj, M.Munson, and D.G.Lambright. 2006. TBC-domain GAPs for Rab GTPases accelerate GTP hydrolysis by a dual-finger mechanism. *Nature* 442:303-306.

Parangi, S., M.O'Reilly, G.Christofori, L.Holmgren, J.Grosfeld, J.Folkman, and D.Hanahan. 1996. Antiangiogenic therapy of transgenic mice impairs de novo tumor growth. *Proc. Natl. Acad. Sci. U. S. A* 93:2002-2007.

Pereira-Leal, J.B., A.N.Hume, and M.C.Seabra. 2001. Prenylation of Rab GTPases: molecular mechanisms and involvement in genetic disease. *FEBS Lett.* 498:197-200.

Pereira-Leal, J.B., and M.C.Seabra. 2000. The mammalian Rab family of small GTPases: definition of family and subfamily sequence motifs suggests a mechanism for functional specificity in the Ras superfamily. *J. Mol. Biol.* 301:1077-1087.

Pertz, O., L.Hodgson, R.L.Klemke, and K.M.Hahn. 2006. Spatiotemporal dynamics of RhoA activity in migrating cells. *Nature* 440:1069-1072.

Pfeffer, S., and D.Aivazian. 2004. Targeting Rab GTPases to distinct membrane compartments. *Nat. Rev. Mol. Cell Biol.* 5:886-896.

Pfeffer, S.R., A.B.Dirac-Svejstrup, and T.Soldati. 1995. Rab GDP dissociation inhibitor: putting rab GTPases in the right place. *J. Biol. Chem.* 270:17057-17059.

Pignatelli, J., D.A.Tumbarello, R.P.Schmidt, and C.E.Turner. 2012. Hic-5 promotes invadopodia formation and invasion during TGF-beta-induced epithelial-mesenchymal transition. *J. Cell Biol.* 197:421-437.

Prates, J., G.B.Franco-Salla, A.R.Dinarte Dos Santos, W.A.J.da Silva, B.R.da Cunha, E.H.da Silva, S.M.Oliani, and F.C.Rodrigues-Lisoni. 2015. ANXA1 peptide reduces ID1 expression in cervical carcinoma cultures. *Gene*.

Proux-Gillardeaux, V., J.Gavard, T.Irinopoulou, R.M.Mege, and T.Galli. 2005a. Tetanus neurotoxin-mediated cleavage of cellubrevin impairs epithelial cell migration and integrin-dependent cell adhesion. *Proc. Natl. Acad. Sci. U. S. A* 102:6362-6367.

Proux-Gillardeaux, V., G.Raposo, T.Irinopoulou, and T.Galli. 2007. Expression of the Longin domain of TI-VAMP impairs lysosomal secretion and epithelial cell migration. *Biol. Cell* 99:261-271.

Proux-Gillardeaux, V., R.Rudge, and T.Galli. 2005b. The tetanus neurotoxin-sensitive and insensitive routes to and from the plasma membrane: fast and slow pathways? *Traffic.* 6:366-373.

Rainero, E., P.T.Caswell, P.A.Muller, J.Grindlay, M.W.McCaffrey, Q.Zhang, M.J.Wakelam, K.H.Vousden, A.Graziani, and J.C.Norman. 2012. Diacylglycerol kinase alpha controls RCP-dependent integrin trafficking to promote invasive migration. *J. Cell Biol.* 196:277-295.

Rak, A., R.Fedorov, K.Alexandrov, S.Albert, R.S.Goody, D.Gallwitz, and A.J.Scheidig. 2000. Crystal structure of the GAP domain of Gyp1p: first insights into interaction with Ypt/Rab proteins. *EMBO J.* 19:5105-5113.

Rawat, S.J., and J.Chernoff. 2015. Regulation of mammalian Ste20 (Mst) kinases. *Trends Biochem. Sci.* 40:149-156.

Ren, J., J.Hamada, N.Takeichi, S.Fujikawa, and H.Kobayashi. 1990. Ultrastructural differences in junctional intercellular communication between highly and weakly metastatic clones derived from rat mammary carcinoma. *Cancer Res.* 50:358-362.

Ridley, A.J. 2011. Life at the leading edge. *Cell* 145:1012-1022.

Rink, J., E.Ghigo, Y.Kalaidzidis, and M.Zerial. 2005. Rab conversion as a mechanism of progression from early to late endosomes. *Cell* 122:735-749.

Ritter, B., S.Murphy, H.Dokainish, M.Girard, M.V.Gudheti, G.Kozlov, M.Halin, J.Philie, E.M.Jorgensen, K.Gehring, and P.S.McPherson. 2013. NECAP 1 regulates AP-2 interactions to control vesicle size, number, and cargo during clathrin-mediated endocytosis. *PLoS. Biol.* 11:e1001670.

Rossi, V., D.K.Banfield, M.Vacca, L.E.Dietrich, C.Ungermann, M.D'Esposito, T.Galli, and F.Filippini. 2004. Longins and their longin domains: regulated SNAREs and multifunctional SNARE regulators. *Trends Biochem. Sci.* 29:682-688.

Sacher, M., Y.G.Kim, A.Lavie, B.H.Oh, and N.Segev. 2008. The TRAPP complex: insights into its architecture and function. *Traffic.* 9:2032-2042.

Sakane, A., A.A.Abdallah, K.Nakano, K.Honda, W.Ikeda, Y.Nishikawa, M.Matsumoto, N.Matsushita, T.Kitamura, and T.Sasaki. 2012. Rab13 small G protein and junctional Rab13-binding protein (JRAB) orchestrate actin cytoskeletal organization during epithelial junctional development. *J. Biol. Chem.* 287:42455-42468.

Sakane, A., A.A.Alamir Mahmoud, K.Nakano, K.Honda, T.Kitamura, I.Imoto, N.Matsushita, and T.Sasaki. 2013. Junctional Rab13-binding protein (JRAB) regulates cell spreading via filamins. *Genes Cells* 18:810-822.

Sakane, A., K.Honda, and T.Sasaki. 2010. Rab13 regulates neurite outgrowth in PC12 cells through its effector protein, JRAB/MICAL-L2. *Mol. Cell Biol.* 30:1077-1087.

Salomon, D.S., R.Brandt, F.Ciardiello, and N.Normanno. 1995. Epidermal growth factor-related peptides and their receptors in human malignancies. *Crit Rev. Oncol. Hematol.* 19:183-232.

Sano, H., S.Kane, E.Sano, C.P.Miinea, J.M.Asara, W.S.Lane, C.W.Garner, and G.E.Lienhard. 2003. Insulin-stimulated phosphorylation of a Rab GTPase-activating protein regulates GLUT4 translocation. *J. Biol. Chem.* 278:14599-14602.

Sato, M., K.Sato, W.Liou, S.Pant, A.Harada, and B.D.Grant. 2008. Regulation of endocytic recycling by C. elegans Rab35 and its regulator RME-4, a coated-pit protein. *EMBO J.* 27:1183-1196.

Satoh, H., Y.Zhong, H.Isomura, M.Saitoh, K.Enomoto, N.Sawada, and M.Mori. 1996. Localization of 7H6 tight junction-associated antigen along the cell border of vascular endothelial cells correlates with paracellular barrier function against ions, large molecules, and cancer cells. *Exp. Cell Res.* 222:269-274.

Savina, A., M.Vidal, and M.I.Colombo. 2002. The exosome pathway in K562 cells is regulated by Rab11. *J. Cell Sci.* 115:2505-2515.

Scales, S.J., Y.A.Chen, B.Y.Yoo, S.M.Patel, Y.C.Doung, and R.H.Scheller. 2000. SNAREs contribute to the specificity of membrane fusion. *Neuron* 26:457-464.

Scheper, W., R.Zwart, and F.Baas. 2004. Rab6 membrane association is dependent of Presenilin 1 and cellular phosphorylation events. *Brain Res. Mol. Brain Res.* 122:17-23.

Schlichting, I., S.C.Almo, G.Rapp, K.Wilson, K.Petratos, A.Lentfer, A.Wittinghofer, W.Kabsch, E.F.Pai, G.A.Petsko, and . 1990. Time-resolved X-ray crystallographic study of the conformational change in Ha-Ras p21 protein on GTP hydrolysis. *Nature* 345:309-315.

Seabra, M.C., J.L.Goldstein, T.C.Sudhof, and M.S.Brown. 1992. Rab geranylgeranyl transferase. A multisubunit enzyme that prenylates GTP-binding proteins terminating in Cys-X-Cys or Cys-Cys. *J. Biol. Chem.* 267:14497-14503.

Shahinian, S., and J.R.Silvius. 1995. Doubly-lipid-modified protein sequence motifs exhibit long-lived anchorage to lipid bilayer membranes. *Biochemistry* 34:3813-3822.

Sharma, M., S.S.Giridharan, J.Rahajeng, N.Naslavsky, and S.Caplan. 2009. MICAL-L1 links EHD1 to tubular recycling endosomes and regulates receptor recycling. *Mol. Biol. Cell* 20:5181-5194.

Shaw, L.M. 2005. Tumor cell invasion assays. *Methods Mol. Biol.* 294:97-105.

Sheff, D., Pelletier, L., O'Connell, C.B., Warren, G., Mellman, I. (2002) Transferrin receptor recycling in the absence of perinuclear recycling endosomes. *J Cell Biol*. 156: 797-804.

Shen, F., L.Hodgson, A.Rabinovich, O.Pertz, K.Hahn, and J.H.Price. 2006. Functional proteometrics for cell migration. *Cytometry A* 69:563-572.

Shi, S.H., L.Y.Jan, and Y.N.Jan. 2003. Hippocampal neuronal polarity specified by spatially localized mPar3/mPar6 and PI 3-kinase activity. *Cell* 112:63-75.

Shirane, M., and K.I.Nakayama. 2006. Protrudin induces neurite formation by directional membrane trafficking. *Science* 314:818-821.

Simons, K., and E.Ikonen. 1997. Functional rafts in cell membranes. *Nature* 387:569-572.

Simonsen, A., R.Lippe, S.Christoforidis, J.M.Gaullier, A.Brech, J.Callaghan, B.H.Toh, C.Murphy, M.Zerial, and H.Stenmark. 1998. EEA1 links PI(3)K function to Rab5 regulation of endosome fusion. *Nature* 394:494-498.

Sivars, U., D.Aivazian, and S.R.Pfeffer. 2003. Yip3 catalyses the dissociation of endosomal Rab-GDI complexes. *Nature* 425:856-859.

Skalhegg, B.S., A.K.Johansen, F.O.Levy, K.B.Andersson, E.M.Aandahl, H.K.Blomhoff, V.Hansson, and K.Tasken. 1998. Isozymes of cyclic AMP-dependent protein kinases (PKA) in human lymphoid cell lines: levels of endogenous cAMP influence levels of PKA subunits and growth in lymphoid cell lines. *J. Cell Physiol* 177:85-93.

Smeland, T.E., M.C.Seabra, J.L.Goldstein, and M.S.Brown. 1994. Geranylgeranylated Rab proteins terminating in Cys-Ala-Cys, but not Cys-Cys, are carboxyl-methylated by bovine brain membranes in vitro. *Proc. Natl. Acad. Sci. U. S. A* 91:10712-10716.

Soldati, T., M.A.Riederer, and S.R.Pfeffer. 1993. Rab GDI: a solubilizing and recycling factor for rab9 protein. *Mol. Biol. Cell* 4:425-434.

Spiering, D., J.J.Bravo-Cordero, Y.Moshfegh, V.Miskolci, and L.Hodgson. 2013. Quantitative ratiometric imaging of FRET-biosensors in living cells. *Methods Cell Biol.* 114:593-609.

Steegmaier, M., K.C.Lee, R.Prekeris, and R.H.Scheller. 2000. SNARE protein trafficking in polarized MDCK cells. *Traffic.* 1:553-560.

Stenmark, H. 2009. Rab GTPases as coordinators of vesicle traffic. *Nat. Rev. Mol. Cell Biol.* 10:513-525.

Stenmark, H., and V.M.Olkkonen. 2001. The Rab GTPase family. *Genome Biol.* 2:REVIEWS3007.

Stenmark, H., R.G.Parton, O.Steele-Mortimer, A.Lutcke, J.Gruenberg, and M.Zerial. 1994. Inhibition of rab5 GTPase activity stimulates membrane fusion in endocytosis. *EMBO J.* 13:1287-1296.

Stroupe, C., and A.T.Brunger. 2000. Crystal structures of a Rab protein in its inactive and active conformations. *J. Mol. Biol.* 304:585-598.

Sturgill-Koszycki, S., P.H.Schlesinger, P.Chakraborty, P.L.Haddix, H.L.Collins, A.K.Fok, R.D.Allen, S.L.Gluck, J.Heuser, and D.G.Russell. 1994. Lack of acidification in Mycobacterium phagosomes produced by exclusion of the vesicular proton-ATPase. *Science* 263:678-681.

Sun, Y., P.J.Bilan, Z.Liu, and A.Klip. 2010. Rab8A and Rab13 are activated by insulin and regulate GLUT4 translocation in muscle cells. *Proc. Natl. Acad. Sci. U. S. A* 107:19909-19914.

Sztul, E., and V.Lupashin. 2006. Role of tethering factors in secretory membrane traffic. *Am. J. Physiol Cell Physiol* 290:C11-C26.

Tall, G.G., M.A.Barbieri, P.D.Stahl, and B.F.Horazdovsky. 2001. Ras-activated endocytosis is mediated by the Rab5 guanine nucleotide exchange activity of RIN1. *Dev. Cell* 1:73-82.

Tan, Y.H., R.J.Arnold, and Z.Q.Luo. Legionella pneumophila regulates the small GTPase Rab1 activity by reversible phosphorylcholination. Proc.Natl.Acad.Sci.U.S.A 108, 21212-21217. 2011.

Ref Type: Journal (Full)

Terai, T., N.Nishimura, I.Kanda, N.Yasui, and T.Sasaki. 2006. JRAB/MICAL-L2 is a junctional Rab13-binding protein mediating the endocytic recycling of occludin. *Mol. Biol. Cell* 17:2465-2475.

Thoma, N.H., A.Iakovenko, A.Kalinin, H.Waldmann, R.S.Goody, and K.Alexandrov. 2001a. Allosteric regulation of substrate binding and product release in geranylgeranyltransferase type II. *Biochemistry* 40:268-274.

Thoma, N.H., A.Niculae, R.S.Goody, and K.Alexandrov. 2001b. Double prenylation by RabGGTase can proceed without dissociation of the mono-prenylated intermediate. *J. Biol. Chem.* 276:48631-48636.

Thomann, D., D.R.Rines, P.K.Sorger, and G.Danuser. 2002. Automatic fluorescent tag detection in 3D with super-resolution: application to the analysis of chromosome movement. *J. Microsc.* 208:49-64.

Thomas, S., B.Ritter, D.Verbich, C.Sanson, L.Bourbonniere, R.A.McKinney, and P.S.McPherson. 2009. Intersectin regulates dendritic spine development and somatodendritic

endocytosis but not synaptic vesicle recycling in hippocampal neurons. *J. Biol. Chem.* 284:12410-12419.

Thong, F.S., C.B.Dugani, and A.Klip. 2005. Turning signals on and off: GLUT4 traffic in the insulin-signaling highway. *Physiology. (Bethesda.)* 20:271-284.

Tochio, H., M.M.Tsui, D.K.Banfield, and M.Zhang. 2001. An autoinhibitory mechanism for nonsyntaxin SNARE proteins revealed by the structure of Ykt6p. *Science* 293:698-702.

Ullrich, O., H.Horiuchi, C.Bucci, and M.Zerial. 1994. Membrane association of Rab5 mediated by GDP-dissociation inhibitor and accompanied by GDP/GTP exchange. *Nature* 368:157-160.

Ullrich, O., H.Stenmark, K.Alexandrov, L.A.Huber, K.Kaibuchi, T.Sasaki, Y.Takai, and M.Zerial. 1993. Rab GDP dissociation inhibitor as a general regulator for the membrane association of rab proteins. *J. Biol. Chem.* 268:18143-18150.

Uytterhoeven, V., S.Kuenen, J.Kasprowicz, K.Miskiewicz, and P.Verstreken. 2011. Loss of skywalker reveals synaptic endosomes as sorting stations for synaptic vesicle proteins. *Cell* 145:117-132.

Valente, E.M., P.M.Abou-Sleiman, V.Caputo, M.M.Muqit, K.Harvey, S.Gispert, Z.Ali, T.D.Del, A.R.Bentivoglio, D.G.Healy, A.Albanese, R.Nussbaum, R.Gonzalez-Maldonado, T.Deller, S.Salvi, P.Cortelli, W.P.Gilks, D.S.Latchman, R.J.Harvey, B.Dallapiccola, G.Auburger, and N.W.Wood. 2004. Hereditary early-onset Parkinson's disease caused by mutations in PINK1. *Science* 304:1158-1160.

van, Z.F., G.Krupitza, and W.Mikulits. 2011. Initial steps of metastasis: cell invasion and endothelial transmigration. *Mutat. Res.* 728:23-34.

Verhoeven, K., J.P.De, K.Coen, N.Verpoorten, M.Auer-Grumbach, J.M.Kwon, D.FitzPatrick, E.Schmedding, V.E.De, A.Jacobs, G.Van, V, K.Wagner, H.P.Hartung, and V.Timmerman. 2003. Mutations in the small GTP-ase late endosomal protein RAB7 cause Charcot-Marie-Tooth type 2B neuropathy. *Am. J. Hum. Genet.* 72:722-727.

Vetter, I.R., and A.Wittinghofer. 2001. The guanine nucleotide-binding switch in three dimensions. *Science* 294:1299-1304.

Wada, M., H.Nakanishi, A.Satoh, H.Hirano, H.Obaishi, Y.Matsuura, and Y.Takai. 1997. Isolation and characterization of a GDP/GTP exchange protein specific for the Rab3 subfamily small G proteins. *J. Biol. Chem.* 272:3875-3878.

Walch-Solimena, C., R.N.Collins, and P.J.Novick. 1997. Sec2p mediates nucleotide exchange on Sec4p and is involved in polarized delivery of post-Golgi vesicles. *J. Cell Biol.* 137:1495-1509.

Wang, W., M.Sacher, and S.Ferro-Novick. 2000. TRAPP stimulates guanine nucleotide exchange on Ypt1p. *J. Cell Biol.* 151:289-296.

Weisz, L., M.Oren, and V.Rotter. 2007. Transcription regulation by mutant p53. *Oncogene* 26:2202-2211.

Welz, T., J.Wellbourne-Wood, and E.Kerkhoff. 2014. Orchestration of cell surface proteins by Rab11. *Trends Cell Biol.* 24:407-415.

Whitlow, M., B.A.Bell, S.L.Feng, D.Filpula, K.D.Hardman, S.L.Hubert, M.L.Rollence, J.F.Wood, M.E.Schott, D.E.Milenic, and . 1993. An improved linker for single-chain Fv with reduced aggregation and enhanced proteolytic stability. *Protein Eng* 6:989-995.

Wiggin, G.R., J.P.Fawcett, and T.Pawson. 2005. Polarity proteins in axon specification and synaptogenesis. *Dev. Cell* 8:803-816.

Willumsen, B.M., A.Christensen, N.L.Hubbert, A.G.Papageorge, and D.R.Lowy. 1984. The p21 ras C-terminus is required for transformation and membrane association. *Nature* 310:583-586.

Wilson, A.L., R.A.Erdman, F.Castellano, and W.A.Maltese. 1998. Prenylation of Rab8 GTPase by type I and type II geranylgeranyl transferases. *Biochem. J.* 333 (Pt 3):497-504.

Wu, C., S.Agrawal, A.Vasanji, J.Drazba, S.Sarkaria, J.Xie, C.M.Welch, M.Liu, B.Anand-Apte, and A.Horowitz. 2011a. Rab13-dependent trafficking of RhoA is required for directional migration and angiogenesis. *J. Biol. Chem.* 286:23511-23520.

Wu, X., M.J.Bradley, Y.Cai, D.Kummel, E.M.De La Cruz, F.A.Barr, and K.M.Reinisch. 2011b. Insights regarding guanine nucleotide exchange from the structure of a DENN-domain protein complexed with its Rab GTPase substrate. *Proc. Natl. Acad. Sci. U. S. A* 108:18672-18677.

Yamamoto, Y., N.Nishimura, S.Morimoto, H.Kitamura, S.Manabe, H.O.Kanayama, S.Kagawa, and T.Sasaki. 2003. Distinct roles of Rab3B and Rab13 in the polarized transport of apical, basolateral, and tight junctional membrane proteins to the plasma membrane. *Biochem. Biophys. Res. Commun.* 308:270-275.

Yamamura, R., N.Nishimura, H.Nakatsuji, S.Arase, and T.Sasaki. 2008. The interaction of JRAB/MICAL-L2 with Rab8 and Rab13 coordinates the assembly of tight junctions and adherens junctions. *Mol. Biol. Cell* 19:971-983.

Yamasaki, A., S.Menon, S.Yu, J.Barrowman, T.Meerloo, V.Oorschot, J.Klumperman, A.Satoh, and S.Ferro-Novick. 2009. mTrs130 is a component of a mammalian TRAPPII complex, a Rab1 GEF that binds to COPI-coated vesicles. *Mol. Biol. Cell* 20:4205-4215.

Yamashiro, D.J., B.Tycko, S.R.Fluss, and F.R.Maxfield. 1984. Segregation of transferrin to a mildly acidic (pH 6.5) para-Golgi compartment in the recycling pathway. *Cell* 37:789-800.

Yang, P.S., P.H.Yin, L.M.Tseng, C.H.Yang, C.Y.Hsu, M.Y.Lee, C.F.Horng, and C.W.Chi. 2011. Rab5A is associated with axillary lymph node metastasis in breast cancer patients. *Cancer Sci.* 102:2172-2178.

Yang, X., H.T.Matern, and D.Gallwitz. 1998. Specific binding to a novel and essential Golgi membrane protein (Yip1p) functionally links the transport GTPases Ypt1p and Ypt31p. *EMBO J.* 17:4954-4963.

Yoshimura, S., A.Gerondopoulos, A.Linford, D.J.Rigden, and F.A.Barr. 2010. Family-wide characterization of the DENN domain Rab GDP-GTP exchange factors. *J. Cell Biol.* 191:367-381.

Zeng, Q., and W.Hong. 2008. The emerging role of the hippo pathway in cell contact inhibition, organ size control, and cancer development in mammals. *Cancer Cell* 13:188-192.

Zerial, M., and H.McBride. 2001. Rab proteins as membrane organizers. *Nat. Rev. Mol. Cell Biol.* 2:107-117.

Zhang, D., L.M.Iyer, F.He, and L.Aravind. 2012. Discovery of Novel DENN Proteins: Implications for the Evolution of Eukaryotic Intracellular Membrane Structures and Human Disease. *Front Genet.* 3:283.

Zhang, J., M.Fonovic, K.Suyama, M.Bogyo, and M.P.Scott. 2009. Rab35 controls actin bundling by recruiting fascin as an effector protein. *Science* 325:1250-1254.

Zhang, K., T.Zhu, D.Gao, Y.Zhang, Q.Zhao, S.Liu, T.Su, M.Bernier, and R.Zhao. 2014. Filamin A expression correlates with proliferation and invasive properties of human metastatic melanoma tumors: implications for survival in patients. *J. Cancer Res. Clin. Oncol.* 140:1913-1926.

Zhou, D., C.Conrad, F.Xia, J.S.Park, B.Payer, Y.Yin, G.Y.Lauwers, W.Thasler, J.T.Lee, J.Avruch, and N.Bardeesy. 2009. Mst1 and Mst2 maintain hepatocyte quiescence and suppress hepatocellular carcinoma development through inactivation of the Yap1 oncogene. *Cancer Cell* 16:425-438.

Zhou, G., J.Wang, M.Zhao, T.X.Xie, N.Tanaka, D.Sano, A.A.Patel, A.M.Ward, V.C.Sandulache, S.A.Jasser, H.D.Skinner, A.L.Fitzgerald, A.A.Osman, Y.Wei, X.Xia, Z.Songyang, G.B.Mills, M.C.Hung, C.Caulin, J.Liang, and J.N.Myers. 2014. Gain-of-function mutant p53 promotes cell growth and cancer cell metabolism via inhibition of AMPK activation. *Mol. Cell* 54:960-974.

Zhou, K., A.Muroyama, J.Underwood, R.Leylek, S.Ray, S.H.Soderling, and T.Lechler. 2013. Actin-related protein2/3 complex regulates tight junctions and terminal differentiation to promote epidermal barrier formation. *Proc. Natl. Acad. Sci. U. S. A* 110:E3820-E3829.

Zhu, L.Y., W.M.Zhang, X.M.Yang, L.Cui, J.Li, Y.L.Zhang, Y.H.Wang, J.P.Ao, M.Z.Ma, H.Lu, Y.Ren, S.H.Xu, G.D.Yang, W.W.Song, J.H.Wang, X.D.Zhang, R.Zhang, and Z.G.Zhang. 2015. Silencing of MICAL-L2 suppresses malignancy of ovarian cancer by inducing mesenchymal-epithelial transition. *Cancer Lett.* 363:71-82.